Fabrication of Ultrathin Palladium Composite Membranes by a New Technique and Their Application in the Ethanol Steam Reforming Reaction for H_2 Production

Samhun Yun

Dissertation submitted to the faculty of the Virginia Polytechnic Institute and State University in partial fulfillment of the requirements for the degree of

Doctor of Philosophy
In
Chemical Engineering

S. Ted Oyama, Committee Chair
Luke E. K. Achenie
John Y. Walz
David F. Cox

March 21, 2011
Blacksburg, VA

Keywords: Pd membrane, Pd-Cu membrane, electric-field assisted activation, electroless plating, hydrogen separation, ethanol steam reforming, membrane reactor

Fabrication of Ultrathin Palladium Composite Membranes by a New Technique and Their Application in the Ethanol Steam Reforming Reaction for H_2 Production

Samhun Yun

ABSTRACT

This thesis describes a new technique for the preparation of ultrathin Pd based membranes supported on a hollow-fiber α-alumina substrate for H_2 separation. The effectiveness of the membranes is demonstrated in the ethanol steam reforming (EtOH SR) reaction in a membrane reactor (MR) for H_2 production.

The membrane preparation technique uses an electric-field to uniformly deposit Pd nanoparticle seeds on a substrate followed by deposition of Pd or Pd-Cu layers on the activated surface by electroless plating (ELP). The well distributed Pd nanoparticles allow for enhanced bonding between the selective layer and the substrate and the formation of gas tight and thermally stable Pd or Pd-Cu layers as thin as 1μm, which is a record in the field. The best Pd membrane showed H_2 permeance as high as 5.0×10^{-6} mol $m^{-2}s^{-1}Pa^{-1}$ and stable H_2/N_2 selectivity of 9000 - 7000 at 733 K for 5days. The Pd-Cu alloy membrane showed H_2 permeance of 2.5×10^{-6} mol $m^{-2}s^{-1}Pa^{-1}$ and H_2/N_2 selectivity of 970 at the same conditions.

The reaction studies were carried out with a Co-Na/ZnO catalyst both in a packed bed reactor (PBR) and in a MR equipped with the Pd or Pd-Cu membrane to evaluate the benefits of employing membranes. For all studies, ethanol conversion and hydrogen product yields were significantly higher in the MRs compared to the PBR. Average

ethanol conversion enhancement and hydrogen molar flow enhancement were measured to be 12 % and 11 % in the Pd MR and 22 % and 19 % in the Pd-Cu MR, respectively. These enhancements of the conversion and product yield can be attributed to the shift in reaction equilibria by continuous hydrogen removal by the Pd based membranes. The comparative low enhancement in the Pd MR was found to be the result of significant contamination of Pd layer by CO or carbon compounds deposition during the reaction.

A one-dimensional modeling of the MR and the PBR was conducted using identical conditions and their performances were compared with the values obtained from the experimental study. The model was developed using a simplified power law and the predicted values matched experimental data with only minor deviations indicating that the model was capturing the essential physicochemical behavior of the system. Enhancements of ethanol conversion and hydrogen yield were observed to increase with rise in space velocity (SV), which could be explained by the increase in H_2 flux through the membranes with SV in the MRs.

Acknowledgements

For the past four years, there were many people who made my long journey enjoyable, beneficial, and smooth in many ways. Without them, it would have been very hard for me to arrive at the finish line of my PhD studies. With the conclusion of my dissertation, this is a great opportunity to deliver my thanks to them.

I would first like to express my sincere gratitude to my advisor, Dr. S. Ted Oyama for his excellent guidance and invaluable support through the period. He showed me the attitude and quality that a research scientist ought to have and encouraged me to challenge myself in every step of the way. I would like to thank my committee members, Dr. Walz, Dr. Achenie, and Dr. Cox for their valuable time and continuous support of my research.

I would like to thank all current and previous group members of the Environmental Catalysis and Nanomaterials Laboratory, Dr. Haiyan Zhao, Dr. Jason Gaudet, Dr. Travis Gott, Dr. Makarand R. Gogate, Dr Katia De Souza, Dr. Sheima J. Khatib, Phuong Bui, Dmitri Iarikov, and Dan Li for their help. Special thanks to goes to Dr. Hankwon Lim and Dr. Pelin Hacarlioglu for their generous help and useful advice. I also thank Dr. Joon Ho Ko who gave me a lot of helpful ideas for this study. I would like to give my appreciation to all staff in the Department of Chemical Engineering at Virginia Tech for their help, specially to Riley Chan and Michael Vaught for their help in constructing and fixing equipment, and Diane Cannaday for her assistance with documents.

I would like thank to my mother, Chansoon Kim, my brothers, Jinhun Yun and Sunghun Yun, my sister, Soochang Yun, sister-in law, Changmi Lee, and brother- in-law, Changwon Choi for their trust and strong belief in me. I also thank my mother-in-law, Hwasun Ahn, brothers- in-law, Sungwon Kim and Jaegoo Lee, sisters-in-law, Hyunok Kim and Haejin Kim for their continuous support.

Finally, I would like to express my deep love and special thanks to my wife, Eunkyoung Kim who has been always beside me and has encouraged me to reach this point by her endless love and support. Special thoughts go to my lovely sons, Junseok and Junwon.

This dissertation is dedicated to my father, Kwangsik Yun who would have delighted me more than anyone else if he could have seen this small achievement.

Table of Contents

List of Tables

List of Figures

List of Abbreviations

PEM	-	proton exchange membrane
EtOH SR	-	ethanol steam reforming
MR	-	membrane reactor
NETL	-	national energy technology laboratory
WGS	-	water gas shift
ELP	-	electroless plating
CVD	-	chemical vapor deposition
PVD	-	physical vapor deposition
EPD	-	electrodeposition
MOCVD	-	metal organic chemical vapor deposition
APS	-	atmospheric plasma spray
SEM	-	scanning electron microscope
EDS	-	energy dispersive spectroscopy
OD	-	outside diameter
ID	-	inside diameter

Me SR	-	methane steam reforming
MeOH SR	-	methanol steam reforming
GHSV	-	gas hourly space velocity
SV	-	space velocity
Me DR	-	methane dry reforming
PBR	-	packed bed reactor
OLC	-	operability level coefficient
ICP	-	inductively coupled plasma
AES	-	atomic emission spectroscopy
XRD	-	X-ray diffraction
NTP	-	normal temperature pressure
GC	-	gas chromatography
FID	-	flame ionization detector
TCD	-	thermal conductivity detector
PDF	-	powder diffraction file
TOF	-	turnover frequency

Chapter 1 . Introduction

Hydrogen has been a valuable material since it was first artificially produced by Hohenheim via mixing of metals and strong acids [1] and is consumed on the order of billions of cubic meters per day in various industrial fields [2,3,4]. Hydrogen is widely used in the petroleum industry especially in hydrodealkylation, hydrodesulfurization and hydrocracking [5] and has recently attracted attention as a possible alternative energy carrier to relieve environmental problems derived from fossil fuel use [6]. Particularly, hydrogen use in proton exchange membrane (PEM) fuel cells is attractive because of the efficiency of the energy conversion and the lack of release of greenhouse gases [7,8,9]. Currently, hydrogen is produced in several different ways, such as electrolysis of water, steam reforming of methane, gasification of coal or partial oxidation of oil or natural gas, and the total production has increased annually at a considerable pace (Fig. 1.1) [10].

Common technologies employed for hydrogen separation include solvent adsorption, pressure swing adsorption, cryogenic recovery and membrane separation. Compared with other methods, membrane separation technologies have economic potential in reducing operating costs, minimizing unit operations and lowering energy consumption [5]. For these reasons and because of the increasing demand for high purity hydrogen, the development for effective hydrogen membranes has engendered considerable interest in academia and industry.

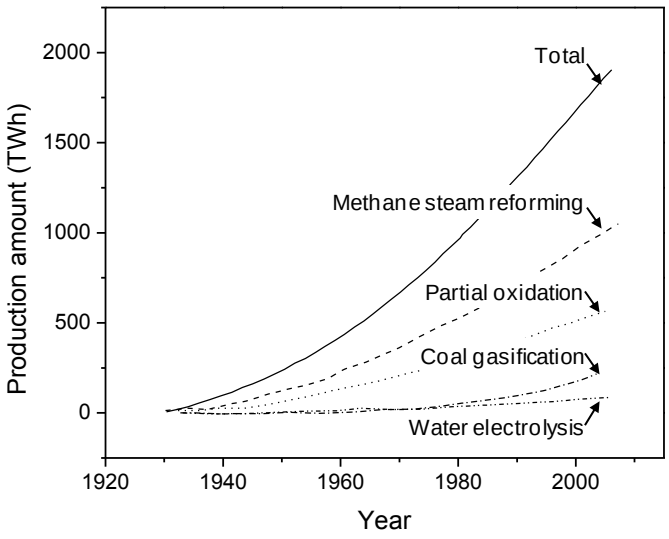

Figure 1.1. Annual global amount of hydrogen produced.

Recently, ethanol steam reforming (EtOH SR) reaction has been considered as an important route to produce hydrogen using bio-ethanol because this bio-ethanol, which contains around 12 wt% of ethanol in aqueous solution, can be directly used in steam reforming without separation of water [11]. This method is also attractive because ethanol is a CO_2-neutral energy source and has less toxicity than methanol.

Membrane reactors (MRs) are devices, in which reaction and separation can be carried out simultaneously. Membrane reactors have attracted attention due to their compactness and possible cost-savings over conventional reactors [12]. They also enhance product yield by shifting equilibrium through the removal of one of the products of reaction. To realize the benefits of using MRs, it is important to develop highly selective membranes with high flux for a particular species.

1.1. Palladium membranes for hydrogen separation

The subject of palladium membranes for hydrogen separation and membrane reactors for hydrogen production have been covered extensively since the early work of Gryaznov [13], and has been covered in a number of reviews [5,6,14,15,16]. This paper covers recent developments with a concentration on the presentation of structural and performance correlations.

Membranes made of nickel, palladium, and platinum which belong to group 10, and some metallic elements in groups 3-5 of the periodic table have the ability to dissociate and dissolve hydrogen, but only palladium membranes show an outstanding ability to transport hydrogen through the metal due to a much higher solubility of hydrogen in its bulk over a wide temperature range (Fig. 1.2) [17]. This property has given rise to numerous studies of palladium based membranes for the separation and purification of hydrogen. In addition, there have been many applications of palladium in catalytic membrane reactors for reactions involving hydrogen, such as hydrogenation and dehydrogenation [18,19], methoxymethane reforming [20], methane steam reforming [21], water-gas shift [22,23], hydroxylation of benzene [24], and hydrogen peroxide synthesis [25]. General results in membrane reactor science have also been described recently. Examples are correlation of conversion enhancement versus permeance [26], identification of the regions for the use of 1-D versus 2-D models [27], and the distinction between primary and secondary products [28].

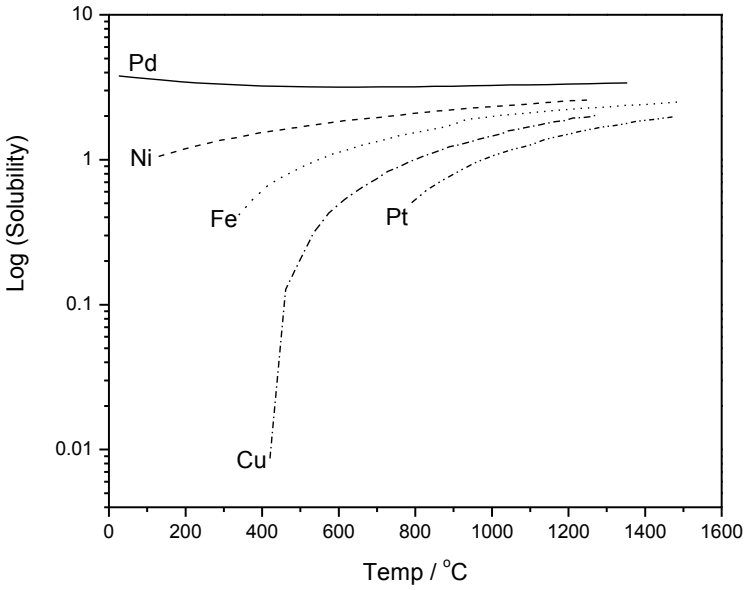

Figure 1.2. Comparison of hydrogen solubility in several metals at a pressure of 1 atm. Solubility is given units of standard cm^3 of H_2 per 100 g of metal.

Requirements for commercial applications of palladium-based membranes include a reasonable membrane cost, high hydrogen permeance, high hydrogen selectivity versus other gases, and steady, predictable performance over a long period of time under harsh conditions [29,30], resistance to poisoning by hydrogen sulfide, chlorine, carbon monoxide, and hydrocarbons and thermal stability under thermal cycling [31]. Much effort has been expended to improve these important aspects, and various palladium based membranes supported on ceramic and metallic materials with high hydrogen permeance and hydrogen selectivity have been reported. Concerning durability, several Pd or Pd-alloy membranes were reported to be stable for several months under H_2 flow in the temperature range of 623-773 K [31,32,33]. Pd-based metallic or composite

membranes are currently known to be stable for up to 10 months according to a National Energy Technology Laboratory (NETL) report [34].

1.1.1. General properties of palladium

Despite palladium's unique ability to permeate hydrogen, the metal suffers from several limitations. A first problem is that the absorption of hydrogen below its critical point of 571 K (298 ^{o}C) and 2 MPa produces two different phases (α and β) (Fig. 1.3) [17], both of which retain the pure palladium face-centered cubic (fcc) lattice but with the crystal unit cell lattice parameter increasing from 0.3890 nm for hydrogen-free palladium to 0.3895 nm for the α-phase and up to 0.410 nm for the β-phase at room temperature [17,35] The α-phase is obtained at low H/Pd atomic ratios and becomes the dominant phase at high temperature. The β-phase is formed at high H/Pd atomic ratios and coexists with the α-phase at low temperature (Fig. 1.3). The hydrogen vapor pressure is constant in the region of phase coexistence and is bounded by an envelope defining α_{max} and β_{min}, the compositions of maximum and minimum H/Pd ratio for pure palladium. The change in volume accompanying the phase transformation can give rise to strain and recrystallization which lead to bulk and grain boundary defects.

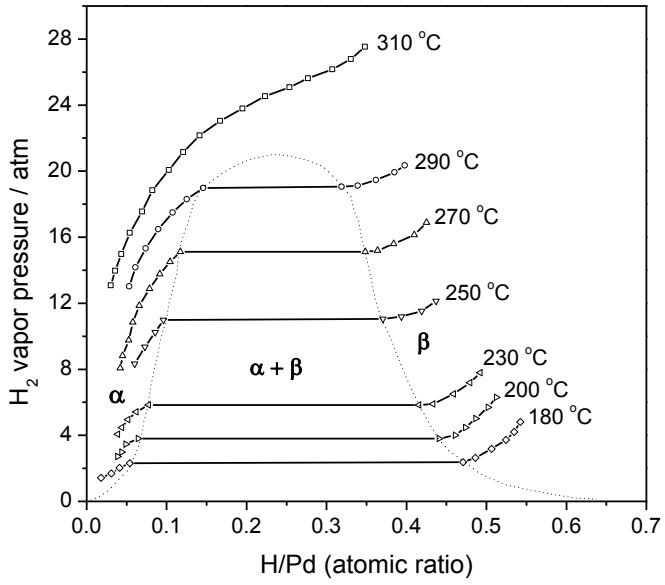

Figure 1.3. P-C-T phase diagram of the palladium-hydrogen system.

A second problem is that metals can lose ductility from exposure to hydrogen, a process called hydrogen embrittlement, which causes cracking of the metal [36]. Finally, the metallic nature of palladium gives rise to interactions with carbon containing species which deactivates the surface [37], especially by exposure to unsaturated hydrocarbons, sulfur, or carbon monoxide [5].

In order to prevent phase transition and alleviate embrittlement and poisoning problems, palladium can be alloyed with other metallic elements such as Ag, Cu, Fe, Ni, Pt and Y [38,39,40,41,42,43]. In general, the critical temperature for the α/β-phase transformation can be lowered considerably by alloying palladium with those metals. For example, the critical temperature of Pd-Ag (Ag 23%) and Pd-Pt (Pt 19%) were reported to be lowered from 571 K (298 ^{o}C) to around room temperature [44,45]. The difference in lattice size between the α- and β-phases also decreases in palladium-alloys so that less

distortion occurs during hydrogen absorption-desorption cycles (Fig. 1.4) [35,46,47.48,49] In several studies, the hydrogen permeance of palladium-alloys was also reported to be higher than that of pure palladium when yttrium, cerium, silver, copper and gold were used as the alloying metal. This interesting behavior was observed in some tertiary palladium alloys such as Pd-Ru-In, Pd-Ag-Ru and Pd-Ag-Rh (Table 1.1) [50,51].

The use of nanometer-sized palladium grains was reported as an alternative method for minimizing the lattice distortion from the α/β-phase transition. This occurs because the concentration of hydrogen on the grain surface and subsurface significantly increases compared with that in the interior sites for the case of nanometer particles [52].

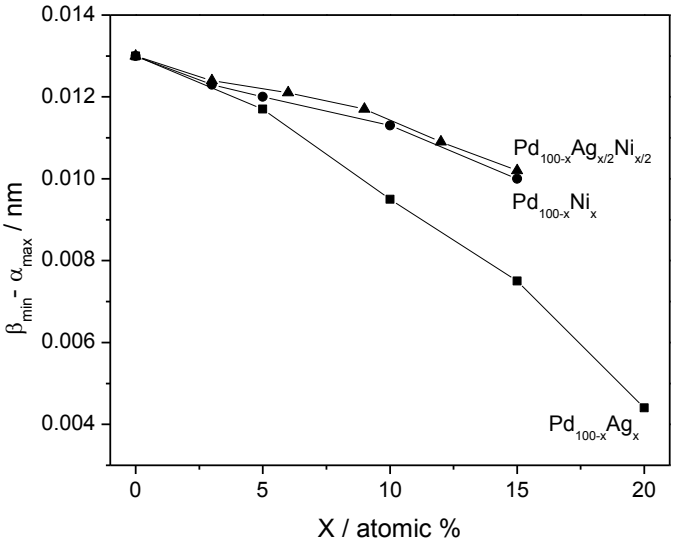

Figure 1.4. Correlation between the lattice parameter differences of palladium and palladium alloys and composition (room temperature).

Table 1.1. Higher hydrogen permeance of various palladium-alloys compared with pure palladium

Pd-alloy	Wt% of alloy metal	Average bond distance [a,b] / nm	Permeance ratio Pd-alloy / Pd
Pd	0	0.275	1.0
Pd-Y	6.6	0.281	3.5
Pd-Y	10	0.284	3.8
Pd-Ag	23	0.278	1.7
Pd-Ce	7.7	0.280	1.6
Pd-Cu	10	0.272	0.48
Pd-Au	5	0.275	1.1
Pd-Ru-In	0.5, 6	0.278	2.8
Pd-Ag-Ru	30, 2	0.279	2
Pd-Ag-Ru	19,1	0.278	2.6

[a] bond distance of each metal: Pd (0.275), Y (0.355), Ag (0.289), Ce (0.365), Cu (0.256), Au (0.288), Ru (0.265), In (0.325)

[b] average bond distance: $\sum_i$ bond distance of $M_i \cdot n_i$, M: metal, n: mole fraction.

In the case of binary palladium-alloys, it is observed that H_2 permeance is generally proportional to the average bond distance of the alloys (Fig. 1.5). This result is reasonable because hydrogen permeation is controlled by the diffusion of atomic hydrogen through the metal lattice [53] and the larger atomic distance facilitates this process. In the case of Pd-Ru careful studies by the group of Way show that permeance is not improved over pure Pd [54], and this can be understood from the shorter bond distance in Ru (0.265 nm) than in Pd (0.275 nm). However, the Pd-Ru material shows 80% higher hardness, which is an improvement. On the other hand for Pd-Ag permeance is enhanced [55,56,57], and this fits with the larger bond distance in Ag (0.289 nm).

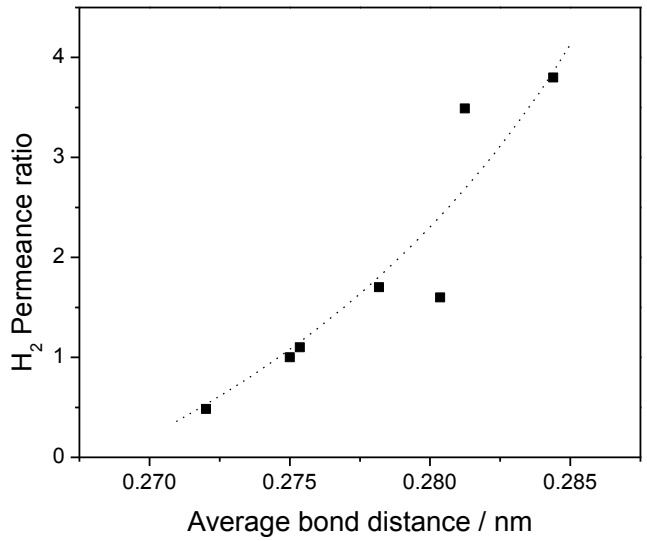

Figure 1.5. H_2 permeance ratio as a function of average bond distance.

Permeability is given by the product of diffusivity and solubility. Investigation of diffusion and H_2 solubility of Pd-alloy membranes are therefore of interest for the understanding and improvement of H_2 permeance. In the literature, the product of diffusivity and solubility is found to be proportional to the H_2 permeance in Pd-alloys [58,59,60].

Rare-earth palladium alloys such as Pd-Y or Pd-Ce can achieve a higher H_2 solubility because the rare-earth elements are 30% larger than Pd in atomic size, thus increasing the hydrogen permeation rate, even though the diffusion coefficients in the alloys are relatively smaller than that of pure Pd [58]. In the case of Pd-Ag alloys, the H_2 solubility increased with Ag content up to the 20-40 wt % of Ag while the H_2 diffusivity decreased with increasing Ag content. The simultaneous changes in solubility and diffusivity result in a 1.7 times higher H_2 permeability than pure Pd at 23 wt% of Ag and

at 623 K [59]. The estimated solubility for Pd-Ag (30% Ag) and for Pd-Au (20% Au) are 10 times and 12 times higher, respectively, than that of pure Pd at 456 K, while the solubility of Pd-Cu (20% Cu) is 5 times less than that of pure Pd [60], which corresponds to the permeability behavior.

Sulfur poisoning is a significant problem in some feedstocks, for examples those derived from coal. An advantage of alloys is that they are sometimes more resistant to poisoning by sulfur [61]. Considerable work has been done with Pd-Cu membranes because they do not show embrittlement even at low temperatures [62,63]. Studies by Morreale et al. have shown that the face-centered cubic (fcc) phase is more resistant to sulfur than the body-centered cubic (bcc) phase [64]. In transient experiments the fcc Pd-Cu composition showed a decline of 0-10% when exposed to 1000 ppm of sulfur, while a bcc Pd-Cu composition had a decline of 99%. Studies by Pomerantz and Ma [65] confirm these results for Pd-Cu compositions of 8, 18, and 19 wt% Cu, with permeance losses of 80% at 500 ^{o}C (773 K). They further showed that the loss was partially reversible by hydrogen treatment. A recent study by Howard and coworkers [66] shows that Pd exposed to 1000 ppm sulfur at 350 ^{o}C (623 K) corrodes over a period of hours to form a thick (6.6 μm) PdS_4 layer, probably by an autocatalytic process. In contrast a $Pd_{47}Cu_{53}$ alloy forms a thin (~3 nm) Pd-Cu-S layer. Although this layer cannot dissociate hydrogen or is impermeable to hydrogen, it does protect the bulk from sulfidation, and could be removed by a hydrogen treatment.

Pd-Au alloy composite membranes are of interest because the presence of gold reduces the embrittlement problem resulting from the hydride phase transition and improves resistance to catalytic poisoning and corrosive degradation by sulfur

compounds while giving rise to higher hydrogen permeability than pure Pd up to 15% Au content [16, 67]. In early work, Pd-Au alloys were prepared by metallurgical processes with thickness range of 25 to 100 μm [51,67]. This method requires substantial capital investment, but can produce homogeneous films with precisely controlled composition [68]. Recent production of thin Pd-Au alloy membranes by electroless plating or electroplating has been reported [68,69]. The group of Way [68] prepared self-supporting Pd-Au alloy films with thickness of 5 - 13 mm by electroless plating on mirror-finished 304 stainless steel sheeting. They reported that heterogeneous Pd-Au films can be homogeneous after heat treatment at greater than 1023K. A recent patent reported by Way et al [70]. described the fabrication of Pd or Pd-alloy membranes by sequential electroless plating on a metal or ceramic substrate and demonstrated that their Pd-Au membranes had an enhanced resistance to the poisoning by sulfur compounds. Their Pd-Au alloy membranes with the thickness of 5 to 7 μm plated on α-alumina tubes showed about 10 % reduction (from 0.2 to 0.18 mol m^{-2}) in H_2 flux during a permeation test for 20 days under a WGS (water gas shift) mixture with 1 ppm H_2S at 673 K. Shi et al. [69] prepared 3-5 μm Pd-Au layers via sequential electroless plating of Pd and Au onto porous ceramic surfaces followed by heat treatment at 823 K for 300 h under H_2 flow to obtain homogeneous alloy structure. Their best membrane showed a hydrogen permeance of 1.7 x 10^{-5} mol $m^{-2}s^{-1}Pa^{-1}$ at 673K, which is the highest value disclosed so far, but is of questionable validity because hydrogen selectivity against other gases was not reported. The group of Ma [71] prepared a Pd-Au alloy (8 wt% Au) membrane by a sequential electroless plating method on an Inconel tube followed by H_2 flow at 773 K for 48 h. Their Pd-Au alloy membrane showed a 40 % reduction of H_2 permeance during

exposure to a mixture of 54.8 ppm H_2S in H_2 at 673 K and 100 % recovery of H_2 permeance with pure H_2 treatment at 773 K for 24 h, which indicated that sulfur was reversibly adsorbed only on the surface in the case of this Pd-Au alloy layer. However, the H_2 permeance of their alloy membrane (18 µm layer) was unexpectedly three times lower than their pure Pd membrane (14 µm layer), which was attributed to the intermetallic diffusion of the support elements into the selective layer.

1.1.2. Hydrogen permeation through palladium membranes

The mechanism of hydrogen permeation through palladium membranes has been studied extensively and it is well known that it generally follows a solution-diffusion mechanism. The steps involved in hydrogen transport from a high to a low pressure gas region are the following (Fig. 1.6): a) diffusion of molecular hydrogen to the surface of the palladium membrane, b) reversible dissociative adsorption on the palladium surface, c) dissolution of atomic hydrogen into the bulk metal, d) diffusion of atomic hydrogen through the bulk metal, e) association of hydrogen atom on the palladium surface f) desorption of molecular hydrogen from the surface g) diffusion of molecular hydrogen away from the surface [31].

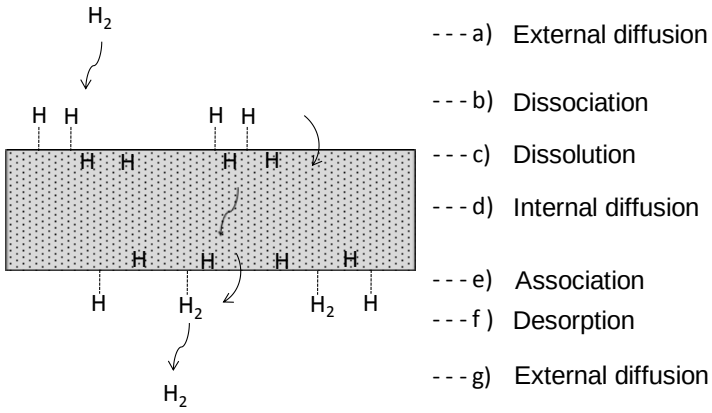

Figure 1.6. Solution diffusion mechanism of hydrogen permeation through a palladium membrane.

Generally, hydrogen permeation is described by the following equation:

$$J=\frac{P(p_h^n-p_l^n)}{L} \qquad (1.1)$$

In this equation, J is the hydrogen flux, P is the permeability, L is the thickness of the palladium layer, p_h and p_l are the partial pressures of hydrogen on the high pressure (feed) side and the low pressure (permeate) side, respectively, and n is the pressure exponent. The latter generally ranges from 0.5 to 1 depending on what step (a – g) is the rate-determining step. According to Sievert's law [72,73], when the rate controlling step is bulk diffusion through the palladium layer which is step (d), the value of n is 0.5 because the diffusion rate is proportional to the concentration of hydrogen atoms on opposite sides of the metal surface and this hydrogen concentration is proportional to the square root of the hydrogen pressure. When mass transport to or from the surface (a, g) or dissociative adsorption (b) or associative desorption (e) become rate determining, the expected value of n is 1 since there processes depend linearly on the concentration of

molecular hydrogen. A detailed description is given in Appendix A. An exponent of unity suggests that permeation through the palladium is very fast and usually indicates that the palladium layer is thin, less than 5 μm (Fig. 1.7). However, *n*-values of 0.5 - 0.8 have been reported for thin (< 5 μm) palladium membranes [38,74,75]. In the case of thick (> 5 μm) Pd layers, *n*-values of greater than 0.5 can be attributed to defects or pin-holes through which a substantial portion of the hydrogen permeates [7,76]. This can be by the Knudsen or Pouiselle flow mechanisms, and gives rise to exponents higher than 0.5 (Appendix A). Guazzone et al. [76] described the contribution of different transport mechanisms such as solution-diffusion (giving rise to Sievert's law), Knudsen diffusion or viscous flow to the total flux. Measurement of the helium flux was used to calculate the portion of Knudsen and viscous flows and the total flux was assumed to be the sum of these flows and the solution-diffusion contribution.

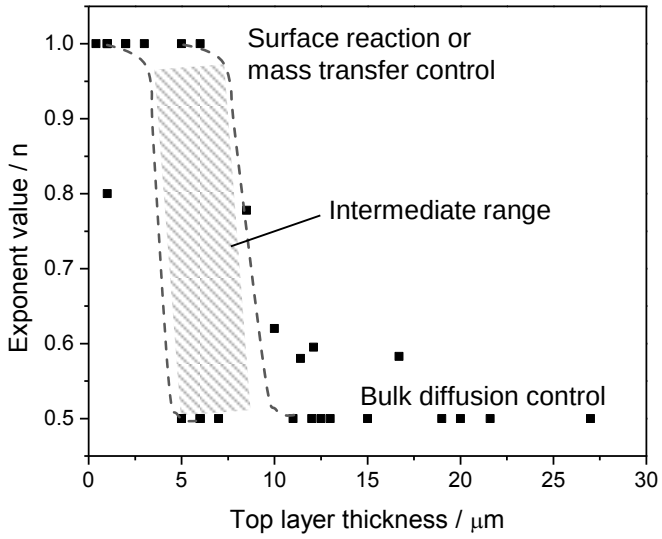

Figure 1.7. Usual range of n as a function of palladium thickness at the temperature of 623-773 K.

A recent detailed analysis by Barbieri and coworkers [77] considers cases where there is no single rate-determining step, and it is found that pressure differences and temperature can affect the exponent, particularly when adsorption and desorption are important. For the particular case of low temperatures and thin membranes the exponent can be lower than 0.5. When membrane transport is fast as with thin membranes it is expected that external transport limitations will become important, giving rise to concentration gradients in a narrow region (external film) around the membrane. The presence of these gradients is known as concentration polarization, and maps have been developed that indicate when they will be important [78]. However, even with thick membranes where the expected exponent is $n = 0.5$ deviations can be found [79]. As pointed out by Barbieri and coworkers [77] experiments to measure n should use materials where the selectivity is infinite to discount the influence of mechanisms such as Knudsen diffusion on the exponent. In addition, they point out that the activation energy can give an indication of the limiting process. Diffusion through bulk Pd has a low activation energy (< 30 kJ mol^{-1}), whereas adsorption and desorption steps have much higher activation energy (54-146 kJ mol^{-1}). The flow pattern around the membranes is also important, particularly for large scale units, and computational fluid mechanics studies have been carried out to analyze the situation for different operating conditions [80].

A microkinetic model of the surface activation and internal diffusion steps has been carried out for a Pd-Ag membrane and good agreement with experimental results were obtained [81]. Although useful transport parameters were obtained, unfortunately, no general conclusions could be made about the mechanism of transport.

In a study of transient permeation [82] it is claimed that a minimum pressure difference of about 30 kPa is necessary to overcome the membrane internal resistance and that the optimal pressure exponent is n = 0.5-0.7. These results seem to be particular to the specific membrane studied.

1.2. Fabrication methods of palladium membranes

A variety of methods have been employed in the preparation of Pd or Pd alloy membranes. The most common methods are electroless plating (ELP), chemical vapor deposition (CVD), physical vapor deposition (PVD), and electrodeposition (EPD), and these are described below.

1.2.1. Electroless plating (ELP)

Electroless plating (ELP) is a method for plating metallic films on a substrate by the reduction of metal complex ions in solution with the aid of a reducing agent without the application of an external electric field, but using the metal formed as a catalyst. This technique is the most common preparation method for Pd membranes and was first applied for the preparation of Pd or Pd alloy composite membranes by Kikuchi et al. and Uemiya et al. [83,84]. A brief history is given by Ayturk and Ma [85].

The mechanism of ELP involves the reduction of metallic salt complexes on the surface of a support material and thus an activation step is needed to initiate the reaction

because the plated metal on the surface acts as a catalyst for further reaction [86]. Conventional electroless plating involves a) seeding a support surface with Pd precursor particles by sensitization and activation and b) plating of the Pd layer on top of the activated surface. If the initial support surface is rough, it may be smoothed by the deposition of intermediate layers (Fig. 1.8). The process of sensitization is usually accomplished by dipping the smoothed support into acidic tin ($SnCl_2$ or $SnCl_4$) solutions to bond the Pd particles on the surface in the following activation step. The method has positive and negative aspects. The advantages of ELP over other preparation methods include ease of coating on materials having any shape, low cost, and use of very simple equipment [87]. The drawback of ELP is the complicated and time-consuming nature of the method due to the requirement of a number of pre-treatment steps such as activation and sensitization before final plating of the desired metal can be carried out. A particular challenge in the formation of Pd alloys is the unequal reduction potential of the metallic ions which results in uneven deposition. This was observed for the case of Pd-Ag alloys where dendritic growth occurred [88]. This could be overcome by adjusting reactant concentrations (metal/hydrazine ratios) so as to lower the reduction over potential of Ag to make it closer to Pd. However, considerable effort is needed to find the right conditions for preparation.

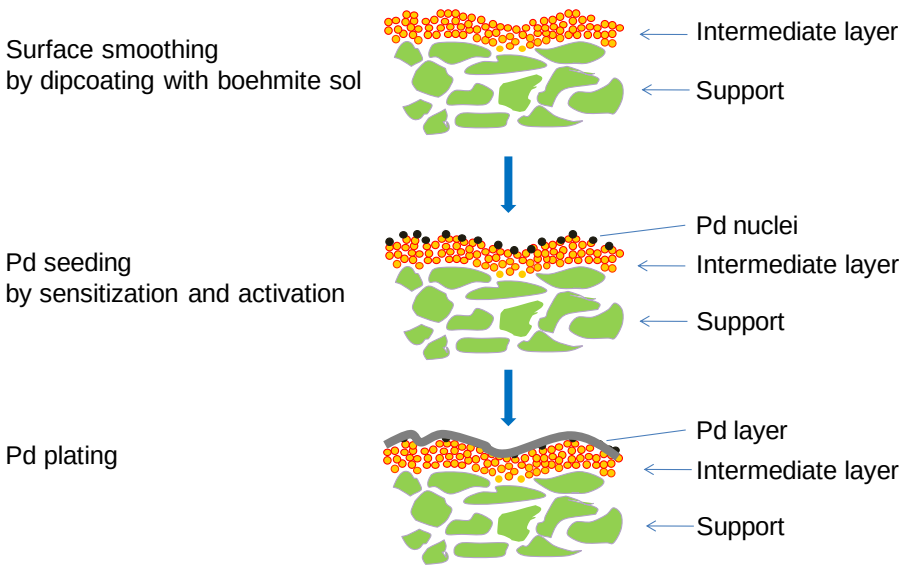

Figure 1.8. Conventional electroless plating procedure.

1.2.2. Chemical vapor deposition (CVD)

Chemical vapor deposition (CVD) is a method for obtaining thin films on a substrate by the thermal decomposition of one or several volatile precursors on the near surface of the substrate. This method is an attractive technique for obtaining Pd layers of controlled thicknesses [86]. It was first reported as a method for the formation of a Pd composite membranes using $PdCl_2$ as the metal source by Ye et al. [89] who used an α-Al_2O_3 disk as a support. Itoh et al. [90] suggested an apparatus for preparing tubular Pd composite membranes by means of forced-flow CVD (Fig. 1.9). The obtained Pd membrane had a selective layer of 2-4 μm of Pd with a H_2/N_2 selectivity of 5000.

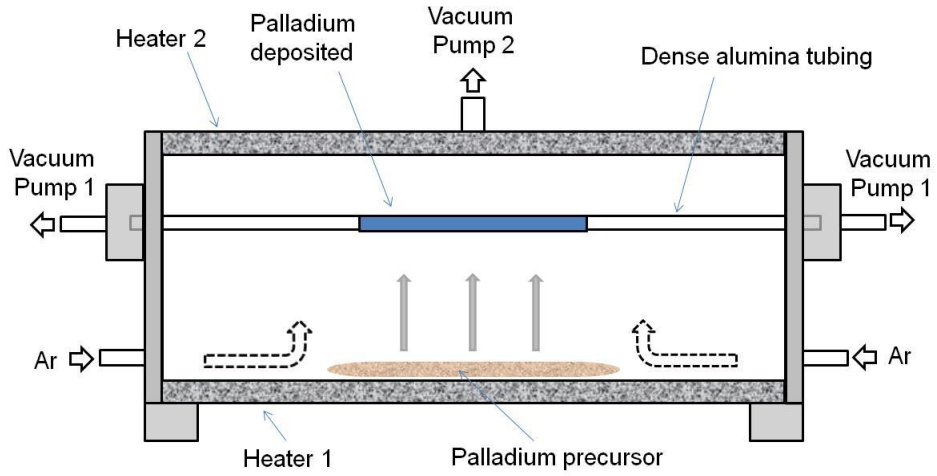

Figure 1.9. Apparatus for preparing tubular Pd composite membranes by means of forced-flow chemical vapor deposition.

Compared with ELP, the CVD technique often results in better film quality control in the film thickness so that very thin (< 2 μm) Pd or Pd alloy films can be obtained. The kinetics of hydrogen permeation on CVD films usually have n values much greater than 0.5 and close to 1 because external transport or surface hydrogen dissociation become rate-determining due to fast passage through the thin palladium layer [86,91]. Although the CVD method can be used to manufacture thin and highly selective layers, it requires Pd precursors of high volatility and good thermal stability which are necessary for short processing time and high yield [89,91]. In addition, high purity constituents and strict process conditions are needed, which limit the general use of this technique. Even though highly volatile organometallic Pd precursors such as $Pd(C_3H_5)_2$, $Pd(C_3H_5)(C_5H_5)$ and $Pd(C_5H_5)_2$ are available for the fabrication of Pd films by MOCVD (metal organic CVD), high-vacuum (< 0.1 mmHg) conditions are required [41] and the

precursors have high cost. In addition, residual carbon may contaminate the palladium membranes.

1.2.3. Physical vapor deposition (PVD)

Physical vapor deposition (PVD) is a vaporization coating technique involving transfer of material at an atomic level by bombardment of a solid precursor, denoted as a target, with the aid of a high energy source such as a beam of electrons or ions in a vacuum [92]. The process is similar to CVD except that chemical decomposition reactions are generally not involved in the surface reactions. This is because the precursors are usually pure metals in the elemental state, whereas in CVD, the precursors are chemical compounds in a vaporized state. A representative technique in PVD is the magnetron sputtering method (Fig. 1.10) [93]. The target is atomized by collisions of Ar ions excited by the action of a plasma, delivered to a substrate, and deposited on its surface.

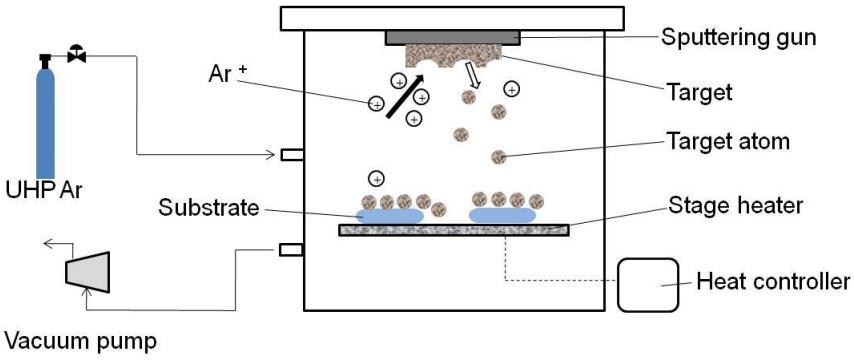

Figure 1.10. Schematic diagram of magnetron sputtering deposition apparatus.

In comparison to electroless plating, the sputtering technique allows better control of the film composition, phase and thickness, for example for the preparation of composite Pd/$Nb_{40}Ti_{30}Ni_{30}$/Pd material on a porous nickel support by a multilayer magnetron sputtering method [94]. Drawbacks are that the equipment used is usually expensive due to the need for a high vacuum and a very high power density to evaporate the target material [95]. The geometry of a support is also limited to a flat substrate, and this severely restricts practical applications.

1.2.4. Electroplating deposition (EPD)

Electroplating deposition (EPD) is a liquid-phase electrochemical method in which metal ions are transported by the action of an electric potential and deposited on a substrate, which also acts as an electrode. The substrate is a cathode and the positive metallic ions are reduced to metal and deposited on the substrate. Pd composite membranes using EPD were described extensively by Shu et al. [16] and Hsieh et al. [96]. The advantages of this technique are that it can be conducted with simple equipment and can easily deposit films of desired thickness by controlling electroplating time or current density (Fig. 1.11) [97]. However this method is limited to use of conducting support materials such as stainless steel, and cannot be generally applied.

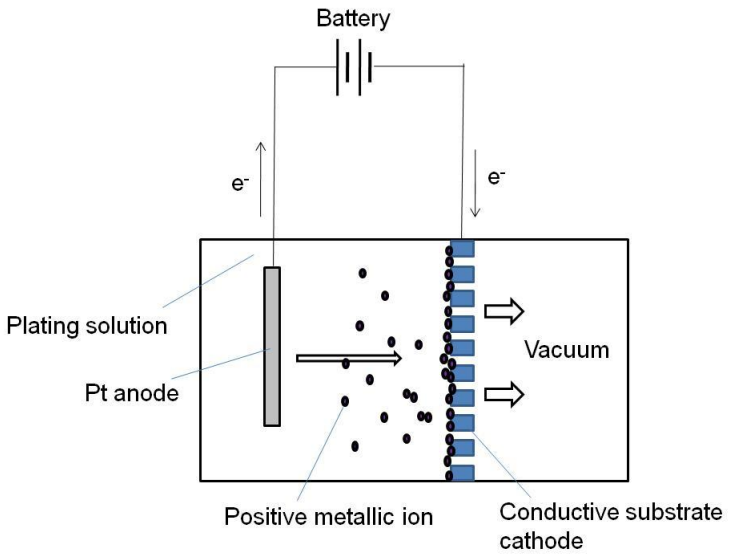

Figure 1.11. Schematic diagram of vacuum electrodeposition system.

1.3. Overview of this study

Chapter 1 describes backgrounds of this study including interests of palladium based membranes for practical applications and preparation methods of the membranes.

Chapter 2 reviews Pd and Pd alloy membranes reported in the lasted literature prepared by different fabrication methods and using different membrane supports. Several correlations of structure and function for those membranes are also provided based on mechanistic considerations of permeance along with structural properties and membrane morphologies. Particular attraction is placed in analysis of the hydrogen permeance and selectivity of membranes reported in recent papers. Composite palladium membranes prepared by electroless plating technique deposited on alumina substrates are found to be the most promising for practical applications.

Chapter 3 presents a novel method to fabricate thin, defect-less, and thermally stable Pd membranes using an electric-field assisted activation technique on a hollow-fiber α-alumina support. The membranes prepared by this new method were compared with a Pd membrane prepared by a classic method in terms of hydrogen permeance, hydrogen over nitrogen selectivity and membrane durability. The formation of the thin, defect-less and robust Pd layer is described by the evenly distributed Pd seeds on the support layer and the enhanced bonding between the Pd layer and the support layer resulting from the strong anchoring of the Pd seeds onto the support in the new activation step.

Chapter 4 describes the studies of ethanol steam reforming (EtOH SR) reaction over a Co-Na/ZnO catalyst in a packed bed reactor (PBR) and membrane reactors (MRs) equipped with Pd and Pd-Cu membranes. The advantages of use of the membranes in the reaction are provided by showing a higher ethanol conversion and hydrogen yield in MRs compared to in the PBR under identical conditions. One dimensional model developed by a power law model for the EtOH SR both in a MR and a PBR is also carried out to investigate the effects of various parameters such as temperature and space velocity.

Chapter 5 presents the conclusions of this study.

References

[1] A.C. Andrews, Oxygen, in: C.A. Hampel (Ed.), The Encyclopedia of the Chemical Elements, Reinhold Book Corporation, New York, 1968.

[2] R. G. Lemus, J. M. Martínez Duart, Updated hydrogen production costs and parities for conventional and renewable technologies, Int. J. Hydrogen Energy 35 (2010) 3929-3936.

[3] Z. Al-Hamamre, S. Voss, and D. Trimis, Hydrogen production by thermal partial oxidation of hydrocarbon fuels in porous media based reformer, Int. J. of Hydrogen Energy 34 (2009) 827-823.

[4] C.-J. Winter, Hydrogen energy - Abundant, efficient, clean: A debate over the energy-system-of-change, Int. J. Hydrogen Energy 34 (2009) S1-S52.

[5] S.N. Paglieri, J.D. Way, Innovations in palladium membrane research, Sep. Pur. Rev. 31 (2002) 1-169.

[6] J.D. Holladay, J. Hu, D.L. King, Y. Wang, An overview of hydrogen production technologies, Catal. Today 139 (2009) 244-260.

[7] S.K. Gade, P.M. Thoen, J.D. Way, Unsupported palladium alloy foil membranes fabricated by electroless plating, J. Mem. Sci. 316 (2008) 112-118.

[8] W.C. Lattin, V.P. Utgikar, Transition to hydrogen energy in the United States: A 2006 status report. Int J Hydrogen Energy 32 (2007) 3230-3237.

[9] J.B. Pearlman, A. Bhargav, E. B. Shields, G. S. Jackson, P. L. Hearn, Modeling efficiency and water balance in PEM fuel cell systems with liquid fuel processing and hydrogen membranes. J Power Sources 185 (2008) 1056-1065.

[10] K. Schoots, F. Ferioli, G.J. Kramer, B.C.C. van der Zwaan, Learning curves for hydrogen production technology: An assessment of observed cost reductions, Int. J. Hydrogen Energy 33 (2008) 2630-2645.

[11] P. D. Vaidya, A. E. Rodrigues, Insight into steam reforming of ethanol to produce hydrogen for fuel cells, Chem. Eng. J. 117 (2006) 39.

[12] K. Li, Ceramic Membranes for Separation and Reaction, Wiley, New York, 2008.

[13] V. Gryaznov, Membrane catalysis, Catalysis Today 51 (1999) 391-395.

[14] A. Basile, F. Gallucci, S. Tosti, Synthesis, characterization and applications of palladium membranes, in: R. Mallada, M. Menéndez (Eds.), Membrane Science and Technology, Elsevier, 2008, pp. 255-323.

[15] S. Tennison, Current hurdles in the commercial development of inorganicmembrane reactors, Membr. Technol. 2000 (2000) 4-9.

[16] J. Shu, B.P.A. Grandjean, A.V. Neste, S. Kaliaguine, Catalytic Pd-based membrane reactors: A Review, Can. J. Chem. Eng. 69 (1991) 1036-1060.

[17] F.A. Lewis, The Palladium Hydrogen system, Academic press, New York, 1967.

[18] R. Dittmeyer, V. Höllein, K. Daub, Membrane reactors for hydrogenation and dehydro-genation processes based on supported palladium, J. Mol. Catal. A: Chem. 173 (2001) 135-184.

[19] M.P. Gimeno, Z.T.Wu, J. Soler, J. Herguido, K. Li, M. Menéndez, Combination of a two-zone fluidized bed reactor with a Pd hollow fiber membrane for catalytic alkane dehydrogenation, Chem. Eng. J. 155 (2009) 298-303.

[20] D. Feng, Y. Wang, D. Wang, J. Wang, Pd-Ag-Au-Ni membrane reactor for ethoxymethane steam reforming, J. Chem. Eng. Data 54 (2009) 2444-2451.

[21] J. Tong, Y. Matsumura, H. Suda, K. Haraya, Experimental study of steam reforming of methane in a thin (6 μm) Pd-based membrane reactor, Ind. Eng. Chem. Res. 44 (2005) 1454-1465.

[22] Y. Bi, H. Xu, W.Li, A. Goldbach, Water–gas shift reaction in a Pd membrane reactor over $Pt/Ce_{0.6}Zr_{0.4}O_2$ catalyst, Int. J. Hydrogen Energy 34 (2009) 2965-2971.

[23] A. Brunettia, G.Barbieria, E.Drioli, Upgrading of a syngas mixture for pure hydrogen production in a Pd–Ag membrane reactor, Chem. Eng. Sci. 64 (2009) 3448-3454.

[24] Y. Guo, X. Zhang, H. Zou, H. Liu, J. Wang, K. L. Yeung, Pd–silicalite-1 composite membrane for direct hydroxylation of benzene, Chem. Commun. (2009) 5898-5900.

[25] L. Shi, A. Goldbach, G. Zeng, H. Xu, Direct H_2O_2 synthesis over Pd membranes at elevated temperatures, J. Membr. Sci. 348 (2010) 160-166.

[26] S.T. Oyama, H. Lim, An Operability Level Coefficient (*OLC*) as a Useful Tool for Correlating the Performance of Membrane Reactors, Chem. Eng. Sci. 151 (2009) 351-358.

[27] S.T. Oyama, P. Hacarlioglu, The boundary between simple and complex descriptions of membrane reactors: The transition between 1-D and 2-D analysis, J. Membr. Sci 337 (2009) 188-199.

[28] H. Lim, Y. Gu, S.T. Oyama, Reaction of primary and secondary products in a membrane reactor: Studies of ethanol steam reforming with a silica-alumina composite membrane, J. Membr. Sci. 351 (2010) 149-159.

[29] K. Aasberg-Petersen, C.S. Nielsen, S.L. Jørgensen, Membrane reforming for hydrogen, Catal. Today 46 (1998) 193-201.

[30] A.J. DeRosset, Diffusion of hydrogen through palladium membranes, Ind. Eng. Chem. 52 (1960) 525-528.

[31] X. Zhang, G. Xiong, W. Yang, A modified electroless plating technique for thin dense palladium composite membranes with enhanced stability, J. Membr. Sci. 314 (2008) 226-237.

[32] R.S. Souleimanova, A.S. Mukasyan, A. Varma, Effects of osmosis on microstructure of Pd-composite membranes synthesized by electroless plating technique, J. Membr. Sci. 166 (2000) 249-257.

[33] H. Chen, C. Chu, T. Huang, Comprehensive characterization and permeation analysis of thin Pd/Al2O3 composite membranes prepared by suction-assisted electroless deposition, Sep. Sci. Technol. 39 (2004) 1461-1483.

[34] Hydrogen from Coal Program, RD&D Plan, External Draft, U.S. Department of Energy, Office of Fossil Energy, NETL, September 2010.

[35] K. Ohira, Y. Sakamoto, T.B. Flanagan, Thermodynamic properties for solution of hydrogen in Pd-Ag-Ni ternary alloys. J. Alloys Compd. 236 (1996) 42-49.

[36] H.C. Rogers, Hydrogen embrittlement of metals: Atomic hydrogen from a variety of sources reduces the ductility of many metals, Science, 159 (1968) 1057-1064.

[37] J.P. Collins, R.W. Schwartz, R. Sehgal, T.L. Ward, C.J. Brinker, G.P. Hagen, C.A. Udovich, Catalytic dehydrogenation of propane in hydrogen permselective membrane reactors, Ind. Eng. Chem. Res. 35 (1996) 4398-4405.

[38] Y. Cheng, K. Yeung, Palladium-silver composite membranes by electroless plating technique, J. Membr. Sci. 158 (1999) 127-141.

[39] K.J. Bryden, J.Y. Ying, Nanostructured palladium-iron membranes for hydrogen separation and membrane hydrogenation reactions, J. Membr. Sci. 203 (2002) 29-42.

[40] D. Fort, J. Farr, I. Harris, A comparison of palladium-silver and palladium-yttrium alloys as hydrogen separation membranes, J. Less-Common Met. 39 (1975) 293-308.

[41] C.-S. Jun, K.-H. Lee, Palladium and palladium alloy composite membranes prepared by metal-organic chemical vapor deposition method (cold-wall), J. Membr. Sci. 176 (2000) 121-130.

[42] S. Uemiya, T. Endo, R. Yoshiie, W. Katoh, T. Kojima, Fabrication of thin palladium-silver alloy film by using electroplating technique. Mater Trans 48 (2007) 1119-1123.

[43] M. Katoh, A. Sondoh, T. Horikawa ,T, Tomida, Characterization of palladium and palladium-silver alloy layers on stainless steel support. Intl. J Mod Phys B 20 (2006) 3866-3871.

[44] N.I. Timofeev, F.N. Berseneva, V.I. Gromov, Influence of preliminary hydrogen impregnation on the mechanical properties of palladium and its alloys with silver, Mater. Sci. 17 (1982) 417-419.

[45] H. Yoshida, K. Okuno, Y. Naruse, T. Kashiwai, Metallurgical considerations on Pd, Pd-alloy and their metal-hydrogen systems, Fusion Technol. 8 (1985) 2388-2394.

[46] A.L. Cabrera, E. Morales, J.N. Armor, Kinetics of hydrogen desorption from palladium and ruthenium-palladium foils, J. Mater. Res. 10 (1995) 779-785.

[47] Y. Sakamoto, K. Ohira, N. Ishimaru, F.L. Chen, M. Kokubu, T.B. Flanagan, Absorption of hydrogen by palladium-nickel-rhodium ternary alloys, J. Alloys Compd. 217 (1995) 226-234.

[48] Y. Sakamoto, K. Yuwasa, K. Hirayama, X-ray investigation of the absorption of hydrogen by several palladium and nickel solid solution alloys, J. Less-Comm. Met. 88 (1992) 115-124.

[49] Y. Sakamoto, F.L. Chen, M. Furukawa, K. Mine, The ($\alpha + \beta$) hydrogen miscibility gaps in hydrogenated palladium-rich Pd-Y(Gd)-Ag ternary alloys, J. Less-Comm. Met. 166 (1990) 45-56.

[50] A.G. Knapton, Palladium Alloys for Hydrogen Diffusion Membranes, Platinum Met. Rev. 21 (1977**)** 44-50.

[51] V. Gryaznov, Metal containing membranes for the production of ultrapure hydrogen and the recovery of hydrogen isotopes, Sep. Purif. Methods 29 (2000**)** 171-187.

[52] A. Pundt, C. Sachs, M. Winter, M.T. Reetz, D. Fritsch, R. Kirchheim, Hydrogen sorption in elastically soft stabilized Pd-clusters, J. Alloys Compd. 293-295 (1999) 480-483.

[53] G.L. Holleck, Diffusion and solubility of hydrogen in palladium and palladium–silver alloys, J. Phys. Chem. 74 (1970) 503-511.

[54] S.K. Gade, M.K. Keeling, A.P. Davidson, O. Hatlevik, J.D. Way, Palladium–ruthenium membranes for hydrogen separation fabricated by electroless co-deposition, Int. J. Hydrogen Energy 34 (2009) 6484-6491.

[55] T.A. Peters, M. Stange, H. Klette, R. Bredesen, High pressure performance of thin Pd-23% Ag/stainless steel composite membranes in water gas shift gas mixtures; influence of dilution, mass transfer and surface effects on the hydrogen flux. J. Membr. Sci.316 (2008) 119-127.

[56] A.L. Mejdell, H. Klette, A. Ramachandran, A. Borg, R. Bredesen, Hydrogen permeation of thin, free-standing Pd/Ag 23% membranes before and after heat treatment in air. J. Membr. Sci. 307 (2008) 96-104.

[57] G. Barbieri, F. Scura, F. Lentini, G. De Luca, E. Drioli, A novel model equation for the permeation of hydrogen in mixture with carbon monoxide through Pd-Ag membranes, Sep. Purif. Technol. 61 (2008) 217-224.

[58] M.L. Doyle, I.R. Harris, Palladium-rare earth alloys: their order-disorder transformations and behavior with hydrogen, Platinum Metals Rev. 32 (1988) 130-140.

[59] Y.H. Ma, E.E. Engwall, I.P. Mardilovich, Composite palladium and palladium-alloy membranes for high temperature hydrogen separation, Fuel Chemistry Division Preprints 48 (2003) 333-334.

[60] Y.H. Ma, I.P. Mardilovich, E.E. Engwall, Thin composite palladium and palladium/alloy membranes for hydrogen separation, Adv. Membr. Technol. 984 (2003) 346-360.

[61] V. Gryaznov, Hydrogen permeable palladium membrane catalysts, Platinum Met. Rev. 30 (1986) 68-79.

[62] A. Kulprathipanja, G.O. Alptekin, J. L. Falconer, J. D. Way, Pd and Pd-Cu Membranes: Inhibition of H_2 Permeation by H_2S. J. Membr. Sci. 254 (2005) 49-62.

[63] J.B. Miller, B.D. Morreale, A.J. Gellman, The effect of adsorbed sulfur on surface segregation in a polycrystalline $Pd_{70}Cu_{30}$ alloy, Surf. Sci. 602 (2008) 1819-1825.

[64] B.D. Morreale, M.V. Ciocco, B.H. Howard, R.P. Killmeyer, A.V. Cugini, R.M. Enick, Effect of hydrogen-sulfide on the hydrogen permeance of palladium-copper alloys at elevated temperatures. J. Membr.Sci. 241 (2004) 219-224.

[65] N. Pomerantz, Y.H. Ma, Effect of H_2S on the Performance and long-term stability of Pd/Cu membranes, Ind. Eng. Chem. Res. 48 (2009) 4030-4039.

[66] C.P. O'Brien, B.H. Howarda, J.B. Miller, B.D. Morreale, A.J. Gellman, Inhibition of hydrogen transport through Pd and $Pd_{47}Cu_{53}$ membranes by H_2S at 350 ◦C, J. Membr. Sci. 349 (2010) 380–384.

[67] D.L. McKinley, Method for hydrogen separation and purification, US Patent 3,439,474, Apr 22, 1969, Assigned to Union Carbide Corp.

[68] S.K. Gade, E.A. Payzant, H.J. Park, P.M. Thoen, J.D. Way, The effects of fabrication and annealing on the structure and hydrogen permeation of Pd-Au binary alloy membranes, J. Membr. Sci.340 (2009) 227-233.

[69] L. Shi, A. Goldbach, G. Zeng, H. Xu, Preparation and performance of thin-layer PdAu/ceramic composite membranes, Int. J. Hydrogen Energy 35 (2010) 4201-4208.

[70] J.D. Way, M. Lusk, P. Thoen, Sulfur-resistant composite metal membranes, US Patent 2008/0038567, Feb. 14, 2008.

[71] C.-H. Chen, Y.H. Ma, The effect of H_2S on the performance of Pd and Pd/Au composite membrane, J. Membr. Sci. 362 (2010) 535-544.

[72] R.C. Hurlbert, J.O. Konecny, Diffusion of hydrogen through palladium, J. Chem. Phys. 34 (1961) 655-658.

[73] A. Caravella, G. Barbieri, E. Drioli, Modelling and simulation of hydrogen permeation through supported Pd-based membranes with a multicomponent approach. Chem. Eng. Sci.63 (2008) 2149-2160.

[74] R.S. Souleimanova, A.S. Mukastan, A. Varma, Pd membranes formed by electroless plating with osmosis: H_2 permeation studies, AIChE J. 48 (2002) 262-268.

[75] X. Li, T.M.Liu, D. Huang, Y.Q. Fan, N.P. Xu, Preparation and characterization of ultrathin palladium membranes, Ind. Eng. Chem. Res. 48 (2009) 2061-2065.

[76] F. Guazzone, E.E. Engwall, Y.H. Ma, Effects of surface activity, defects and mass transfer on hydrogen permeance and n-values in composite palladium-porous, Catal. Today 118 (2006) 24-31.

[77] A. Caravella, F. Scura, G. Barbieri, E. Drioli, Sieverts law empirical exponent for Pd-based membranes: Critical analysis in pure H_2 permeation, J. Phys. Chem. B 114 (2010) 6033-6047.

[78] A. Caravella, G. Barbieri, E. Drioli, Concentration polarization analysis in self-supported Pd-based membranes, Sep. Purf. Technol. 66 (2009) 613-624.

[79] S. Hara, M. Ishitsuka, H. Suda, M. Mukaida, K. Haraya, Pressure dependent hydrogen permeability extended for metal membranes not obeying the square-root law, J. Phys. Chem. B 117 (2009) 9795-9801.

[80] M. Coroneo, G. Montante, J. Catalano, A. Paglianti, Modelling the effect of operating conditions on hydrodynamics and mass transfer in a Pd–Ag membrane module for H2 purification, J. Membr. Sci. 343 (2009) 34-41.

[81] A. Bhargav, G.S. Jackson, Thermokinetic modeling and parameter estimation for hydrogen permeation through $Pd_{0.77}Ag_{0.23}$ membranes, Inter. J. Hydrogen Energy 34 (2009) 6164-5173.

[82] W.-H. Chen, P.-C. Hsu, B.-J. Lin, Hydrogen permeation dynamics across a palladium membrane in a varying pressure environment, Int. J. Hydrogen Energy 35 (2010) 5410-5418.

[83] S. Uemiya, Y. Kude, K. Sugino, N. Sato, T. Matsuda, E. Kikuchi, A palladium /porous-glass composite membrane for hydrogen separation, Chem. Lett. (1988) 1687-1690.

[84] H. Kikuchi, Medium for separating hydrogen, JP Patent 62-273,029, 1987, Assigned to ISE Chem Ind.

[85] M.E. Ayturk, Y.H. Ma, Electroless Pd and Ag deposition kinetics of the composite Pd and Pd/Ag membranes synthesized from agitated plating baths, J. Membr. Sci. 330 (2009) 233-245.

[86] G. Xomeritakis, Y. Lin, CVD synthesis and gas permeation properties of thin Pd /alumina membranes, AIChE J. 44 (1998) 174-183.

[87] O. Altinisik, M. Dogan, G. Dogu, Preparation and characterization of Pd-plated porous glass for hydrogen enrichment, Catal. Today 105 (2005) 641-646.

[88] R. Bhandari, Y.H. Ma, Pd–Ag membrane synthesis: The electroless and electro-plating conditions and their effect on the deposits morphology, J. Membr. Sci. 334 (2009) 50-63.

[89] J. Ye, G. Dan, Q. Yuan, The preparation of ultrathin palladium membranes, Key Eng. Mater. 61 (1991) 437-442.

[90] N. Itoh, T. Akiha, T. Sato, Preparation of thin palladium composite membrane tube by a CVD technique and its hydrogen permselectivity, Catal. Today 104 (2005) 231-237.

[91] G. Xomeritakis, Y.S. Lin, Fabrication of a thin palladium membrane supported in a porous ceramic substrate by chemical vapor deposition, J. Membr. Sci. 120 (1996) 261-272.

[92] D.M. Mattox, Handbook of Physical Vapor Deposition (PVD) Process, Noyes Publications, Park Ridge, NJ, 1998.

[93] G. Xomeritakis, Y.S. Lin, Fabrication of thin metallic membranes by MOCVD and sputtering, J. Membr. Sci. 133 (1997) 217-230.

[94] L. Xiong, S.Liu, L. Rong, Fabrication and characterization of Pd/$Nb_{40}Ti_{30}Ni_{30}$/Pd/porous nickel support composite membrane for hydrogen separation and purification, Int. J. Hydr. Energy 35 (2010) 1643-1649.

[95] Z. Hongbin, X. Guoxing, Preparation and characterization of Pd-Ag alloy composite membrane with magnetron sputtering, Sci. China, Ser. B Chem. 42 (1999) 581-588.

[96] H.P. Hsieh, Inorganic Membranes for Separation and Reaction, Elservier, Amsterdam, 1996.

[97] S.-E. Nam, K.-H. Lee, A study on the Pd/nickel composite membrane by vacuum electrodeposition, J. Membr. Sci. 170 (2000) 163.

Chapter 2 . Literature Review

Palladium-based membrane systems surveyed in this chapter can be broadly divided into two categories: unsupported Pd membranes and supported Pd membranes, both of which include pure Pd and Pd alloy materials. Unsupported Pd membranes are used in a stand-alone form, usually as foils or tubes without any auxiliary component to give structure or strength for sustaining the top metal layer. Supported Pd membranes utilize porous materials such as Vycor glass, ceramics, or stainless steel to provide a structural scaffold for holding the metallic component.

2.1. Unsupported membranes

As reported in a 2002 review by Paglieri and Way early research in the United States and the former Soviet Union employed Pd or Pd alloy membranes with a tubular geometry with thickness in the range of 20-100 μm for structural integrity [1]. This type of membranes produced ultra high purity H_2 for use in the semiconductor manufacturing industry or in the recovery of H_2 isotopes. Unfortunately, the high cost of the Pd material imposed limits on economic practicality in comparison with other separation methods [2]. Nevertheless, the method remains of importance for small scale production and for research applications to evaluate the intrinsic material properties of pure Pd or Pd alloys. Generally in this type of membranes, the rate-determining step in H_2 permeation is bulk diffusion, so the partial pressure exponent value is 0.5. The permeance of theses

membranes is rather low, with values around $1.4\times10^{-8} – 9.3\times10^{-7}$ mol $m^{-2}s^{-1}Pa^{-1}$ due to the high membrane thickness of at least 20 μm required for mechanical stability [3]. In early work Mckinley [4] described a diffusion barrier formed by a Pd-alloy, which had an improved practical permeability and physical strength in hydrogen diffusion system compared with pure Pd. He reported that a diffusion layer with 25 μm thickness, composed of 60 wt% of Pd and 40% of Cu showed H_2 permeance of 6.69×10^{-7} mol $m^{-2}s^{-1}Pa^{-1}$ at 623 K, which is 1.5 times higher than pure Pd.

A summary of the properties of bulk Pd membranes is provided in Table 2.1. In this review the permeance and permeability values from various studies have been converted into units of mol m^{-2} s^{-1} Pa^{-1} and Barrer, respectively using the thickness of the separation layer and partial pressure difference of hydrogen so that reported values can be compared. Reported values of n in the literature are indicated in Tables 2-4,6. In most studies, the permeate side (downstream) was at atmospheric pressure, but actual reported values were used in the calculations of permeance.

Recently, Way and coworkers [5] reported the preparation of a defect-free unsupported Pd film as thin as 7.2 μm with H_2 permeance of 1.56×10^{-6} mol $m^{-2}s^{-1}Pa^{-1}$ and H_2/N_2 selectivity of 40,000 at 673 K. They prepared a Pd disk by an ELP technique on a mirror-finished stainless steel support followed by mechanical removal of the membrane. Morreale et al. [6] reported the permeability of H_2 in bulk Pd membranes at conditions of elevated temperature in the range of 623 to 1173 K and high H_2 pressure up to 2.8 MPa. They found that the fitted exponent value of n is 0.62 instead of 0.5 at high pressure and proposed that the increase may be because either the bulk diffusion-limited

mechanism is not operating or because the Sievert's constant and diffusion coefficient changes with increasing pressure. It is likely that gas-phase mass transfer resistance is the cause of the result, as it is expected to grow with pressure. The evaluated activation energy (E_a) of bulk Pd was in the range of 12 – 20 kJ/mol and was affected by such factors as the thickness of the Pd layer, the preparation method in the bulk Pd membranes, the grain microstructure of the layers, and experimental conditions such as temperature and pressure [7]. The apparent activation energy is low because it reflects the temperature dependence of the entire transport process, including mass transport.

Table 2.1. Bulk Pd or Pd-alloy membranes for H_2 separation

Membrane type	L μm	T K	Δp kPa	n	P [a]	*P* [b]	$\alpha_{H2/N2}$	Ref
Pd disk by ELP	7.2	673	120	0.5	15.6	33500	40000	[5]
Pd disk by ELP	12.1	673	120	0.5	9.30	33600	172	[5]
$Pd_{59}Cu_{41}$ disk by ELP	16.7	673	120	0.5	10.1	50600	105	[5]
Pd disk	25	623	517	0.5	4.58	34200	-	[4]
$Pd_{60}Cu_{40}$ disk	25	623	517	0.5	6.69	49900	-	[4]
$Pd_{60}Cu_{40}$ disk	25	673	517	0.5	7.56	56400	-	[4]
Pd disk from Pd sheet	1000	623	91	0.5	0.76	230000	∞	[6]

[a] P is H_2 permeance in the unit of 10^{-7}mol $m^{-2}s^{-1}Pa^{-1}$

[b] *P* is permeability in the unit of Barrer, 1Barrer = 3.35×10^{-16} mol $m^{-1}s^{-1}Pa^{-1}$

2.2. Supported membranes

As mentioned earlier, self-supporting palladium membranes need to be thick for a sufficient mechanical strength, so such membranes have not only a high intrinsic material cost but also a low hydrogen flux. Supported membranes can be prepared with much thinner palladium layers leading to lower expense, so considerable efforts have been expended to develop methods of preparation using supports. Different supports and deposition methods have been tried so as to obtain thin palladium films with good membrane integrity along with high hydrogen permeance and selectivity [8,9,10]. Supported palladium membranes reviewed in this chapter can be divided into three broad categories based on the supporting materials used: Vycor glass, ceramics and stainless steel.

2.2.1. Porous Vycor glass supports

Vycor glass is a borosilicate glass whose typical starting composition is 63% SiO_2, 27% B_2O_3, 7% Na_2O_3, and 3.5% Al_2O_3, from which the boron has been leached out by a treatment of a hot dilute acid solution to leave a regular porous network with pores generally 4-300 nm [11] and a final composition of 75-80 % SiO_2, 4-6% Al_2O_3 and 10-12% B_2O_3 [12]. This support material has high temperature and thermal shock resistance, and about 28% of porosity, but is mechanically fragile. Porous Vycor glass was one of the first support materials used in the fabrication of composite Pd membranes [13,14]. A

summary of the properties of Pd membranes using Vycor glass supports is given in Table 2.2.

Uemiya et al. [12] first proposed a composite membrane consisting of a thin Pd film deposited on a porous glass tube in 1991. The Uemiya group examined thin Pd membranes supported on porous glass tubes using an ELP method and studied the effect of copper or silver addition to suppress the problem of H_2 embrittlement. The H_2 permeance of the pure Pd membrane, the Pd-Ag alloy, and the Pd-Cu alloy at 673 K with a pressure difference of 0.2 MPa were 4.44×10^{-7} mol $m^{-2}s^{-1}Pa^{-1}$, 3.57×10^{-7} mol $m^{-2}s^{-1}Pa^{-1}$, and 2.04×10^{-7} mol $m^{-2}s^{-1}Pa^{-1}$ respectively. Although, the H_2 permeance of the Pd alloy membranes was lower compared with the pure Pd membranes, the H_2/N_2 selectivity remained high at 473 K, much lower than the critical temperature of 571 K, which indicates that the addition of Cu or Ag inhibited the formation of the β-phase Pd hydride. Kuraoka et al. [15] prepared Pd composite membranes using Vycor glass as a supporting material by inserting Pd into the glass pores under vacuum to increase the adhesion between the support and the top Pd layer. The H_2 permeance of their Pd-glass composite membrane at 723 K was 0.50×10^{-7} mol $m^{-2}s^{-1}Pa^{-1}$, which was almost the same as that of the substrate, and the H_2/N_2 selectivity was ~ 500. Altinisik et al. [16] prepared Pd composite membranes using porous glass tablets as substrates by ELP. The H_2 permeance of their membrane was very high ~ 2.2×10^{-5} mol $m^{-2}s^{-1}Pa^{-1}$ at 473 K but the H_2/N_2 selectivity was 7, just slightly higher than the Knudsen selectivity of 3.7, which could be explained by the presence of large pore defects.

Table 2.2. Palladium or Palladium-alloy membranes supported on Vycor for hydrogen separation

Layers on support	Method	L μm	T K	Δp kPa	n	P [a]	*P* [b]	$\alpha_{H2/N2}$	Ref
Pd	ELP	15	473	10	1	220	985000	7	[16]
Pd	ELP	13	773	194	0.5	9.64	37400	high[c]	[12]
Pd	ELP	27	673	194	0.5	4.44	38500	high	[12]
$Pd_{94}Cu_6$	ELP	19	673	194	0.5	2.04	11600	high	[12]
$Pd_{93}Ag_7$	ELP	22	673	194	0.5	3.57	23000	high	[12]
Pd/glass layer with pore-filled Pd	ELP	-	723	100	1	0.49	-	520	[15]

[a] P is H_2 permeance in the unit of 10^{-7}mol $m^{-2}s^{-1}Pa^{-1}$
[b] *P* is permeability in the unit of Barrer, 1Barrer = 3.35×10^{-16} mol $m^{-1}s^{-1}Pa^{-1}$
[c] reported as a high value in the literature

2.2.2. Porous ceramic supports

Porous ceramic supports are a broad class of non-metallic substrates which can be formed into a variety of shapes with controllable pore sizes of 5 – 200 nm. Alumina is the most common ceramic materials used for Pd composite membrane preparation because it is widely available in different compositions, has good mechanical and thermal stability, and can be modified through the use of intermediate layers. Tubular geometry is popular, but disks are often used as well. The simplest form has a symmetric structure and is composed of a single and uniform wall of a material with nano-sized pores. To

obtain sufficient mechanical strength, the single-walled symmetric structure usually needs a considerable thickness which reduces gas permeation. More advanced alumina supports have an asymmetric structure [17], composed of a thin selective layer with a small and narrow pore size distribution placed on the surface of a bulk layer with larger particles. These asymmetric supports are good substrates for Pd membranes due to their smooth outer surface and low gas flow resistance, but the multi-step fabricating process makes them relatively expensive [1].

Defects and roughness in the support usually produce defects or pinholes in the deposited top layer [17]. Consequently, proper supports should have homogeneous surface characteristics, a narrow pore size distribution, and a particle size range smaller than the top layer thickness. To suppress pinholes and to obtain a narrow pore size distribution on the supports while preventing a decrease of permeance, Oyama et al. proposed the use of very thin multiple graded layers of alumina deposited on various porous substrates (Fig. 2.1) [18].

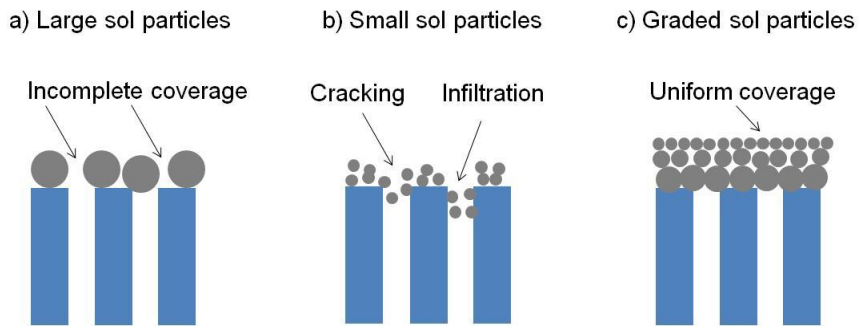

Figure 2.1. Demonstration of the effect of graded layers.

On the other hand, Abate et al. [19] reported that surface roughness of the underlying alumina support is required for good mechanical stability of the Pd alloy membrane and prevent the peeling or formation of cracks during use. They prepared Pd-Ag alloy membranes by an ELP method directly on alumina substrate with average pore size of 70 nm and surface roughness of several microns. The H_2 permeance of their membrane at 623 K was 1.2×10^{-6} mol $m^{-2}s^{-1}Pa^{-1}$ with a H_2/N_2 selectivity of 450. The gas separation properties of recently published Pd and Pd alloy composite membranes supported on α-alumina are summarized in Table 2.3.

Wang et al. [20] prepared Pd-Ag-Ru composite membranes supported on porous α-alumina using a simultaneous ELP method. The hydrogen permeance of their ternary alloy membranes was 3 to 4 times higher than that of pure palladium membranes of similar thickness. Although this composition has higher permeance than pure Pd (Table 1.1), the permeance is too high. Since the hydrogen selectivity was not reported, the result could be due to defects. Xomeritakis et al. [21] prepared thin palladium/alumina membranes by CVD using palladium acetylacetonate and palladium chloride as Pd precursors. They reported that the H_2 permeance was dependent on the crystallinity and morphology of the Pd metal deposited. The highest H_2 permeance and H_2/He selectivity of their membranes were 2.0×10^{-7} mol $m^{-2}s^{-1}Pa^{-1}$ and 200 at 573 K, respectively. Zhang et al. [7] fabricated thin and dense palladium composite membranes with defect free selective layers using a vacuum assisted electroless plating (VELP) method. They claimed the vacuum was effective because the nitrogen gas produced during the plating procedure could be removed from the surface of the membrane and where it could cause defects in the palladium film (Fig. 2.2). The hydrogen permeance of their membrane

prepared by VELP was ~ 2.6×10^{-6} mol $m^{-2}s^{-1}Pa^{-1}$ and a high H_2/Ar selectivity of over 2000 at 753 K.

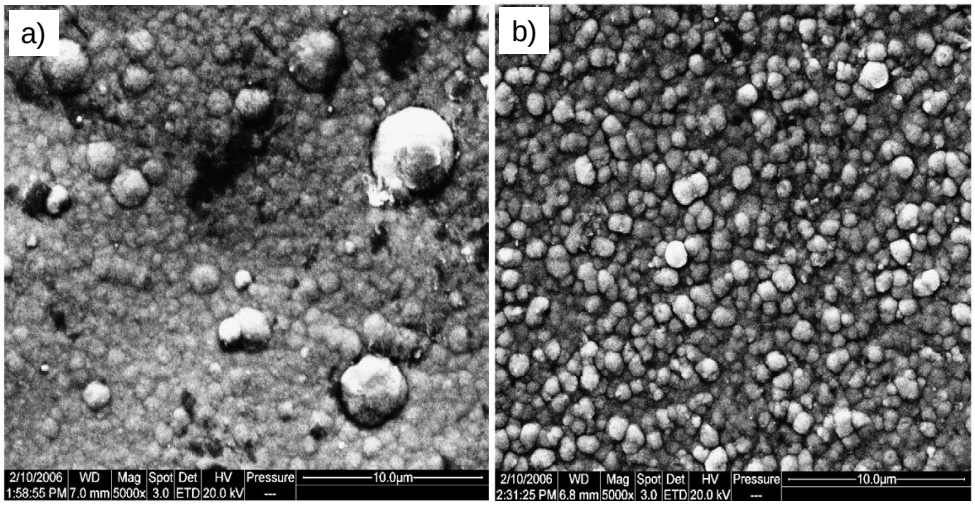

Figure 2.2. SEM photos of top surface of Pd membranes prepared: a) by ELP, b) by VELP.

Tong et al. [22] produced dense Pd membranes without intermediate layers by pre- depositing Pd by ELP on a polymer layer which was dip-coated on an alumina substrate and then removing the organic layer with a high temperature (873-1273 K) treatment under stagnant air atmosphere followed by ELP to obtain a selective layer (Fig. 2.3). They proposed that Pd nuclei could be thus uniformly distributed on the non-porous polymer layer, which is required for forming a defect-free Pd layer. After removal of the organic layer, the presence of adequate space between the Pd layer and the support was reported as a key factor for durability of the Pd layer because it provide room for the Pd

to expand during thermal cycles without stress. The H_2 permeance of their membrane at 773 K was 3.3×10^{-6} mol $m^{-2}s^{-1}Pa^{-1}$ and it was impermeable to N_2.

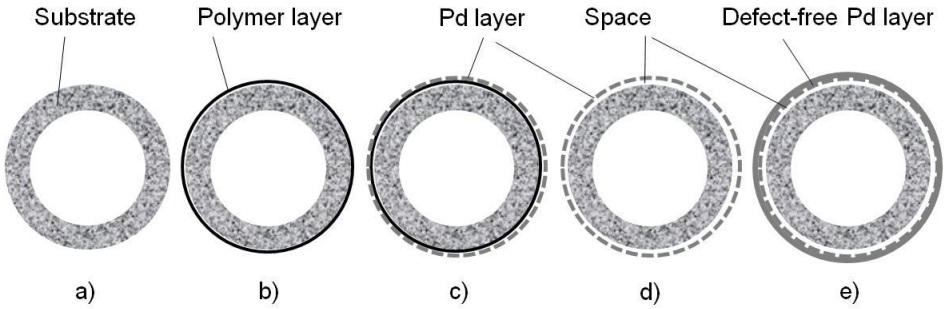

Figure 2.3. Schematic of a polymer - inorganic process for preparing a Pd membrane on a porous substrate. Cross sections: a) substrate, b) polymer layer + substrate, c) Pd layer + polymer layer + substrate, d) Pd layer + space + substrate, and e) Pd separation layer + space + substrate.

Nair et al. [23] prepared Pd or Pd-Ag alloy membranes of controlled thickness by monitoring the amount of deposited metal by a quartz crystal microbalance with a resolution of 0.01μg/cm^2 metal loading (Fig. 2.4). Their apparatus enabled them to simultaneously obtain several Pd or Pd alloy membrane samples, which were expected to have uniform properties. The H_2 permeance of their Pd-Ag membranes of thickness 11 μm was 1.2×10^{-6} mol $m^{-2}s^{-1}Pa^{-1}$ with a good H_2/N_2 selectivity of 2000.

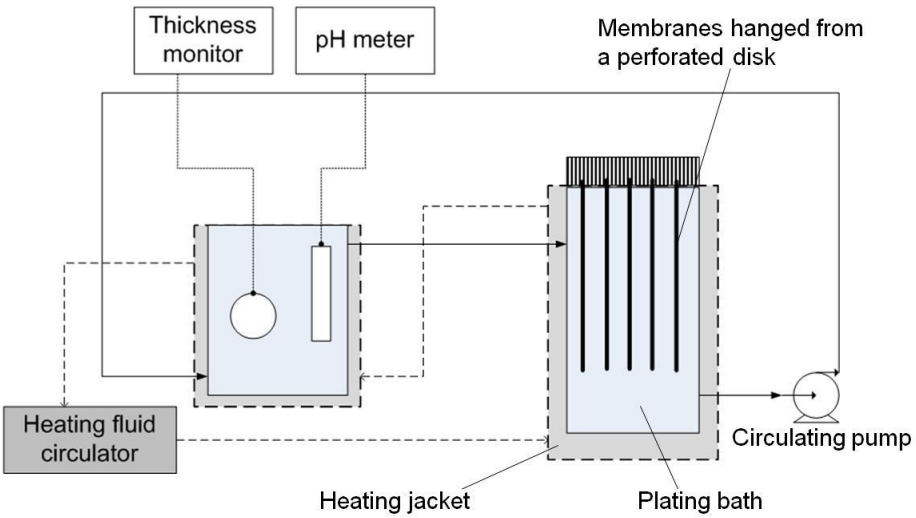

Figure 2.4. Schematic diagram for conducting electroless plating to obtain multiple palladium membranes with a uniform quality.

To address the problem of mechanical failure of composite membranes due to differences in thermal expansion coefficients between supporting materials (alumina, 6.7 × 10^{-6} K^{-1}) and the Pd layer (11.8 × 10^{-6} K^{-1}), several techniques were developed. For example, Zhao et al. [24] proposed a modified electroless plating method involving the use of an activated Pd(II)-modified boehmite sol prepared by a sol-gel process. They reported that this improved the adherence between the substrate layer and the selective layer. Their membrane had around 1μm thickness and showed high H_2 permeance of ~ 1× 10^{-6} mol $m^{-2}s^{-1}Pa^{-1}$ but only a H_2/N_2 selectivity of 23 at 723 K. The group of Harold prepared encapsulated Pd membranes by dip-coating γ-alumina layers on a thin Pd layer and then depositing Pd by an ELP technique to obtain a Pd selective layer which was formed in the pores of γ-alumina [25]. The Pd particles packed in the pores of the γ-alumina layer appeared to suppress the degradation of the selective layer during

temperature cycling. Their membrane had good thermal resistance with a high H_2/N_2 selectivity of 3000 but a low H_2 permeance of 4.84×10^{-7} mol $m^{-2}s^{-1}Pa^{-1}$ at 643 K due to blockage of pores or reduction of the pore size in the intermediate layers.

The group of Suzuki fabricated composite membranes packed with Pd nanoparticles employing an ELP technique under vacuum on γ-alumina layers beneath Pd seed layers with use of $Pd(OA_c)$ as a Pd precursor and hydrazine as a reducing agent (Fig. 2.5) [26]. The dispersion of fine Pd particles in the γ-alumina layer could prevent small defects from growing into large cracks and could suppress the stress associated with the α-β phase transition. Their membrane showed a high H_2 permeance of 1.36×10^{-6} mol $m^{-2}s^{-1}Pa^{-1}$ and a selectivity of 1000 at 573 K.

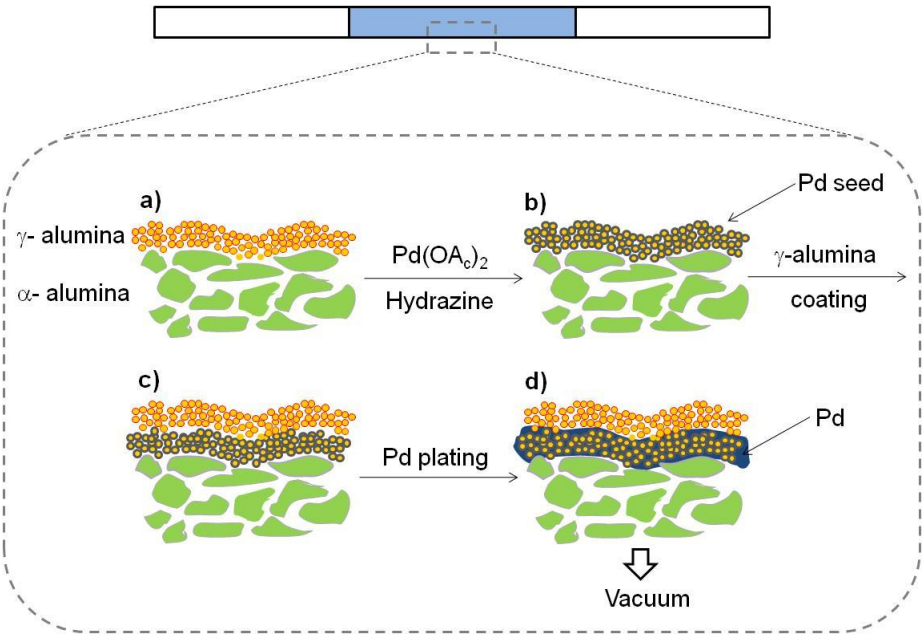

Figure 2.5. Preparation of composite Pd membrane by packed Pd into pore of γ-alumina layer.

Zhang and coworkers prepared stable Pd membranes by growing a Sil-1 zeolite intermediate layer on an α-alumina support and then depositing a 5 μm layer of Pd by ELP [27]. The best membrane had permeance of 1.8 x 10^{-6} mol $m^{-2}s^{-1}Pa^{-1}$ and a top H_2/N_2 selectivity of 1300 at 773 K with a Δp of 100 kPa and n = 1, Under long term gas cycling conditions the selectivity was 615 at 623 K and 506 at 473 K, but the membrane was stable for the 240 h duration of the measurements. Seshimo et al. prepared Pd membranes by ELP on an anodized alumina substrate using supercritical conditions with CO_2 and an emulsifier [28]. They report a membrane thickness of 1 μm, but the permeance was only 7.4 x 10^{-8} $m^{-2}s^{-1}Pa^{-1}$ and a H_2/N_2 selectivity of 200 at 673 K with a Δp of 101 kPa. The low permeance is probably due to the substrate, as a membrane prepared by conventional ELP showed similar hydrogen fluxes.

Alumina tubes are also available as hollow fibers, and these have been used as substrates. The hollow fibers are produced by an extrusion technique in which a polymer-inorganic composite is first formed and subsequently fired. The resulting fibers are typically of 0.7-2 mm OD and an average pore size of 0.1-0.5 μm.

Table 2.3. Palladium or palladium-alloy membranes supported on alumina for hydrogen separation

Layers on support	Method	L μm	T K	Δp kPa	n	P [a]	*P* [b]	$\alpha_{H2/N2}$	Ref
Pd/γ-Al_2O_3 with Pd/γ-Al_2O_3 [d]	ELP	6	753	100	1	26.0	46600	2100[c]	[7]
Pd	CVD	1	723	68	1	20.6	6100	780	[29]

Pd-Ni alloy	CVD	1	723	68	1	20.6	6100	317	[29]
Pd/γ-Al_2O_3[d]	CVD	1	573	-	1	2.0	600	200[e]	[21]
Pd	CVD	2	573	30	1	33.4	19900	5000	[30]
Pd/γ-Al_2O_3 packed with YSZ	ELP	5	723	280	0.5	12.5	18700	high	[10]
$Pd_{77}Ag_{23}$	ELP	12	623	50	0.5	12.0	43000	450	[19]
$Pd_{69}Ag_{30}Ru_1$	ELP	15	673	75	0.5	73.3	328000	-	[20]
$Pd_{70}Ag_{30}$	ELP	13	673	75	0.5	20.0	74600	-	[20]
Pd	ELP	6	673	75	0.5	6.67	11900	-	[20]
Pd/Polymer	ELP	5	773	100	1	33.3	49700	∞[e]	[22]
Pd/γ-Al_2O_3[d]	ELP	5	780	413	0.5	12.6	18800	600	[23]
$Pd_{88}Ag_{12}$/γ-Al_2O_3[d]	ELP	11	823	413	0.5	12.1	39700	2000	[23]
Pd/γ-Al_2O_3 with Pd	ELP	1	723	100	1	106	31600	23	[24]
Pd/γ-Al_2O_3 packed with Pd/γ-Al_2O_3[d]	ELP	2.6	643	413	0.5	4.84	3800	3000	[25]
γ-Al_2O_3/γ-Al_2O_3 packed with Pd/γ-Al_2O_3[d]	ELP	5	573	413	0.5	13.6	20300	1000	[26]
Pd/Sil-1	ELP	5	773	100	1	18	26800	1300	[27]
Pd/anodized alumina[f]	ELP	1	673	101	1	0.74	200	200	[28]

[a] P is H_2 permeance in the unit of 10^{-7}mol $m^{-2}s^{-1}Pa^{-1}$

[b] *P* is permeability in the unit of Barrer, 1Barrer = 3.35×10^{-16} mol $m^{-1}s^{-1}Pa^{-1}$

[c] H_2/Ar ratio, [d] intermediate layer , [e] H_2/He ratio, [f] Substrate

A recurring problem with Pd membranes is the occurrence of pinholes, which have the effect of reducing selectivity. A method of healing pinholes with ELP is the feeding of the palladium species and the reductant from opposite sides of the membrane [31]. This causes the deposition of metal precisely where the pinhole is found. However, the absence of reductant on the palladium side could result in overly thin membrane layers in some regions.

2.2.3. Porous metal supports

Porous metal supports are conductive substrates that can be formed into various shapes with average pore size of 0.2 ~ 100 μm. They are conventionally produced by a powder sintering or electrochemical deposition and are good candidates for support materials because their thermal expansion coefficient is similar to that of Pd compared to other materials (Table 2.4) [32,33]. In addition it is possible to obtain easy and sturdy sealing in industrial assemblies than with more fragile ceramic supports [34,35]. Among the porous metals, stainless steel is the most frequently used material due to its ease of fabrication, chemical resistance, and low cost.

Table 2.4. Thermal expansion coefficients of support materials and palladium at 293 K

Material	Linear thermal expansion coefficient (10^{-6} K^{-1})
Alumina	5.4 ~ 6.7
Borosilicate glass	3.3
Steel	11~13

Stainless steel	11 ~ 16
Palladium	11.8

The smallest pore size of commercially available stainless steel disks or tubes is 0.2 μm [1]. Rough surfaces from large pore sizes or non-uniform pore size distributions often result in defects or pinholes on the surface of thin Pd or Pd alloy membranes [7]. For this reason, porous metal supports require much thicker Pd films compared to ceramic supports to obtain defect-free selective layers. Shu et al. [36] reported that at least 15 μm of metal deposited by an ELP method is required to obtain a dense and defect-free film when using 0.2 μm porous stainless steel supports. Mardilovich et al. [37] showed that the Pd layer needs to be approximately three times as thick as the diameter of the largest pore to obtain a He-tight membrane.

The roughness and the defects from the macroporous metal supports can be minimized by shrinking the pore size by employing various methods such as mechanically altering the surface, abrading the surface, sintering at high temperature or depositing inexpensive metals such as Ni or Cu instead of Pd [38,39,40,41]. Jemaa et al. [40] prepared Pd membranes supported on porous stainless steel disks by an ELP method. They modified the metal substrate surface with 5-6 μm pore size openings by bombardment of iron shots (shot peening treatment) with an average diameter of less than 125 μm under a release pressure of 5.1×10^{5} Pa followed by a purge with air to reduce the pore openings on the metal surface. They claimed that the original pore openings were reduced to around 1 μm after a 300 s treatment. The H_2 permeance of their membranes was 5.8×10^{-7} mol $m^{-2}s^{-1}Pa^{-1}$, which indicated that gas permeance could be significantly

affected by the modification process. Nam et al. [38] fabricated Pd-Ni alloy composite membranes supported on a stainless steel disk by vacuum electrodeposition. They pretreated a 316L stainless steel substrate with average pore size of 500 nm by dispersing a submicron Ni powder on the substrate followed by sintering to make the substrate surface smooth and enhance adhesion between the top Pd-Ni alloy layer and the substrate. They claimed that defects or pin-holes were not observed on the surface of the pretreated membrane after deposition of 1 μm Pd-Ni, while macrospores on the surface of the unpretreated membranes still existed after deposition of 10 μm Pd-Ni. The H_2 permeance of their membranes was 6.76×10^{-6} mol $m^{-2}s^{-1}Pa^{-1}$ with a high H_2/N_2 selectivity of 3000 at 723 K. Membrane performances of recently published Pd or Pd alloy composite membranes supported on porous stainless steel with different preparation methods are summarized (Table 2.5).

Tong et al. [42] prepared Pd membranes with thickness of 2~3 μm by electroless plating of Pd or Pd/Ag layers with a thin diffusion barrier of silver by electro plating on a stainless steel substrate filled with aluminum hydroxide gel. They reported the hydroxide gel in the pores did not hinder hydrogen diffusion due to the significant shrinkage of the gels under thermal treatment up at 773 K. Their best membrane showed H_2 permeance of 1.7×10^{-6} mol $m^{-2}s^{-1}Pa^{-1}$ with no N_2 permeance at 673 K. The group of Huang produced Pd membranes employing a porous 310L stainless steel tube with a 0.5 μm pore size as a substrate [43]. They coated a porous yttria-stabilized zirconia (YSZ) layer by atmospheric plasma spray (APS) on the outside of the metal surface, conducted a MOCVD activation step using Pd(II)-hexafluoroacetyl-acetonate as a Pd precursor, and then made a selective Pd layer by an ELP method. They claimed that their MOCVD

activation technique was effective for obtaining nanometer-sized Pd particles evenly distributed on the support, which resulted in an impervious metal layer in the plating step. However, the H_2 permeance of their membrane was 7.5×10^{-7} mol $m^{-2}s^{-1}Pa^{-1}$ at 673 K with a H_2/N_2 selectivity of 700, which showed that defects or areas uncovered by Pd could be present due to the rough porous metal surface. The group of Nam prepared Pd-Cu alloy composite membranes by a vacuum assisted EPD using 316L stainless steel disks as supports [34]. They used a thin intermediate layer of silica prepared by a sol-gel method to smooth the surface of the mesoporous stainless steel supports and to improve the structural stability of the Pd alloy composite membranes. The H_2 permeance of their membranes was 4.9×10^{-6} mol $m^{-2}s^{-1}Pa^{-1}$ with a high H_2/N_2 selectivity of over 10000 at 623 K.

Various studies on factors such as preparation time, concentrations, and temperature of plating baths that can affect the compactness or grain and crystallite size of the Pd layers on porous metals have been conducted. For example, Shi et al. [44] reported the effect of concentration of $PdCl_2$ in a plating bath on Pd nanoparticles deposited on the surface of a 316L stainless steel plate and proposed a route to prepare Pd membranes with a very thin selective layer of around 400 nm thickness. The Pd particle size deposited on the surface was smaller with increasing concentration of $PdCl_2$ (Fig. 2.6) and the number of layers of the obtained Pd layer increased as to the crystallite size of Pd decreased. Their membrane which was prepared using 1.8~2 g/l of $PdCl_2$ concentration showed a H_2 permeance of 6.5×10^{-7} mol $m^{-2}s^{-1}Pa^{-1}$ at 773 K but did not mention the H_2 selectivity.

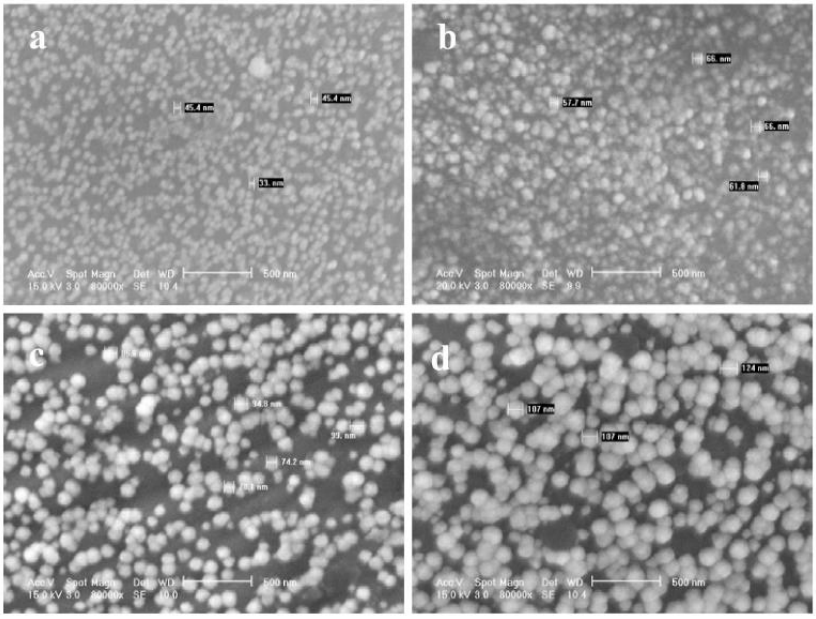

Figure 2.6. SEM images showing palladium nano paticles deposited on the stainless steel substrate at different concentrations of $PdCl_2$ a) 4.2 g/l, b) 3 g/l, c) 2.4 g/l, and d) 1.8~ 2 g/l.

Intermetallic diffusion can be a problem with Pd membranes on metallic substrates, and intermediate layers have been used as diffusion barriers [45,46,47]. The group of Ma reports that oxidation of a stainless steel (316) substrate produces a native layer of chromium oxide that serves as an effective diffusion barrier [48]. Their best membrane showed H_2 permeance of 3.5×10^{-7} mol m^{-2} $s^{-1}Pa^{-1}$ with a very high H_2/He selectivity at 723 K. Zhang et al. found that a layer of sol-gel derived yttria stabilized zirconia (YSZ) is a more effective barrier than such native oxide layers at temperatures above 600 ^oC (873 K) [49]. They reported that the minimum thickness of a Pd layer required for gas-tightness is 11 μm on an YSZ/PSS support, and 25 μm on an oxidized PSS support. Their Pd membrane with the YSZ layer as a diffusion barrier showed a

permeance of 9.8×10^{-7} mol m^{-2} $s^{-1}Pa^{-1}$ at 773 K with thermal stability to 923 K. Zahedi et al. report that WO_3 forms a good intermediary layer on stainless steel to produce a Pd membrane of thickness 12 μm by electroless plating [50]. The membrane has permeance of 2.1×10^{-8} mol m^{-2} $s^{-1}Pa^{0.5}$ with an exponent n = 0.5 and a N_2/H_2 selectivity of 10,000 at 723 K. Cornaglia and coworkers show that a NaA zeolite is an effective diffusion barrier to produce a Pd membrane of thickness 19 μm [51]. The membrane has permeance of 1.6×10^{-6} mol m^{-2} $s^{-1}Pa^{-1}$ with an exponent n = 0.5 and a N_2/H_2 selectivity of 608 at 723 K.

Table 2.5. Palladium or palladium-alloy membranes supported on porous metal for hydrogen separation

Layers on support	Method	L μm	T K	Δp kPa	n	P [a]	P [b]	$\alpha_{H2/N2}$	Ref
$PdNi_{0.2-0.3}$/Ni powder	CVD	1	723	68	1	22.1	6600	> 400	[29]
Pd-Ni alloy/Cu/Ni powder	EPD	2	723	55	1	67.6	40400	3000	[38]
Pd-Cu alloy/Silica/Ni powder	EPD	2	623	53	1	48.8	29100	10000	[34]
Pd	ELP	20	623	100	0.5	5.0	29900	5000	[35]
Pd	ELP	6	673	100	0.5	5.8	10400	-	[40]
Pd/filled with aluminum hydroxide gel/Ag	ELP	3	673	100	1	17.0	15200	c	[42]
Pd-Ag/3μm Pd/filled with aluminum hydroxide gel/Ag	ELP	2	673	100	1	15.0	13400	c	[42]

Pd/YSZ [d] by APS [e]	ELP	6	673	40	0.5	17.5	31300	100	[43]
Pd with MOCVD activation /YSZ by APS	ELP	7	673	40	0.5	7.5	15700	700	[43]
Pd	ELP	0.4	773	276	1	6.5	800	-	[44]
Pd/Cr_2O_3	ELP	32	723	300	0.5	3.5	38600	10^{6} [f]	[48]
Pd/YSZ	ELP	11	773	82	0.5	9.7	31900	-	[49]
Pd/WO_3	ELP	12	723	-	0.5	2.1[g]	-	10000	[50]
Pd/NaA	ELP	19	723	50	0.5	15.8	89600	608	[51]

[a] P is H_2 permeance in the unit of 10^{-7}mol $m^{-2}s^{-1}Pa^{-1}$

[b] *P* is permeability in the unit of Barrer, 1Barrer = 3.35×10^{-16} mol $m^{-1}s^{-1}Pa^{-1}$

[c] reported as a defect-free Pd or Pd-alloy layer in the literature, [d] yttria-stablized zirconia,

[e] atmospheric plasma spray, [f] H_2/He

[g] 10^{8} mol $m^{-2}s^{-1}Pa^{-0.5}$

2.3. Performance analysis of palladium membranes

Overall results are presented in this section to illustrate how the gas separation properties of these membranes depend on the fabrication methods and supporting materials. To determine the effect of the supporting materials used in the preparation of the Pd membranes, the H_2 permeance and H_2/N_2 selectivity was plotted as a function of separation layer thickness (Fig. 2.7).

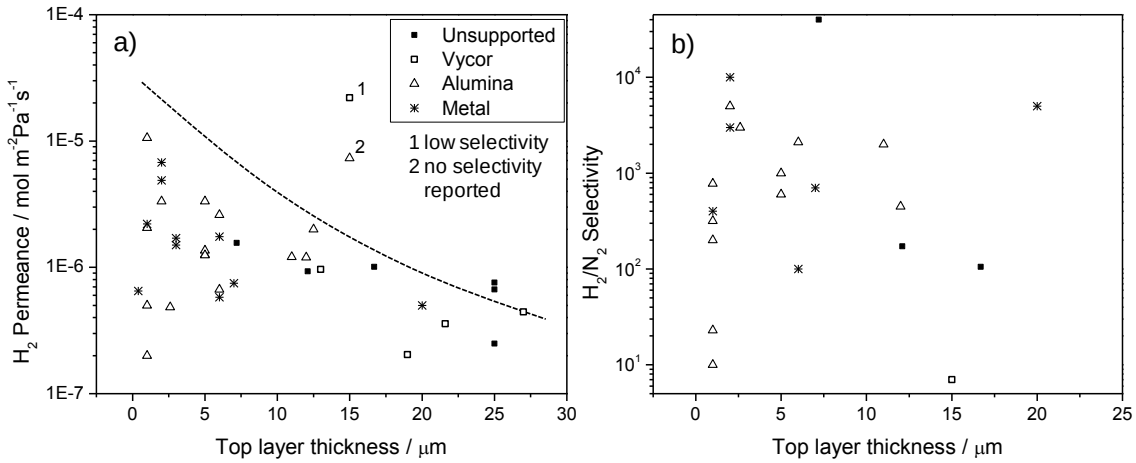

Figure 2.7. Performances of Pd membranes supported on different materials. a) H_2 permeance versus top layer thickness, b) H_2/N_2 selectivity versus top layer thickness.

As can be seen in Fig. 2.7 a), the H_2 permeance tends to decrease with increase in the selective top layer thickness for each support class, which favors the preparation of membranes with as thin a Pd layer as possible to obtain high H_2 permeance and low cost. The two systems which displayed unusually high H_2 permeance had either a very low H_2/N_2 selectivity or no selectivity was reported. The dashed line indicates a rough upper boundary to the permeance data, which highlights the general observation of decreasing permeance with increasing Pd thickness. Membranes with a top Pd layer thickness of less than 5 μm displayed a broad range of H_2 permeance from 1.1×10^{-7} to 1.0×10^{-5} mol $m^{-2}s^{-1}Pa^{-1}$. This indicates that the H_2 permeance does not depend only on the thickness of the Pd layer but also on the structure and thickness of both the Pd layer and the support. It is also noted that most unsupported membranes had a much higher thickness than the supported membranes which resulted in lower H_2 permeance for the former.

Fig. 2.7 b) shows that the H_2/N_2 selectivity dependence on the thickness of the separation layer is highly scattered. In Pd membranes, the selectivity can be infinite if the Pd layer does not have defects or pin-holes. The probability of obtaining these faultless membranes generally increases with the layer thickness because pinholes or other defects will be covered [22]. The selectivity was therefore expected to be proportional to the top layer thickness, but only a weak dependence is observed. The selectivity should be low in cases where the top Pd layer does not have a structural integrity regardless of the thickness of the selective layer, because the N_2 permeance through openings or other defects by Knudsen diffusion or viscous flow (Appendix A) is caused.

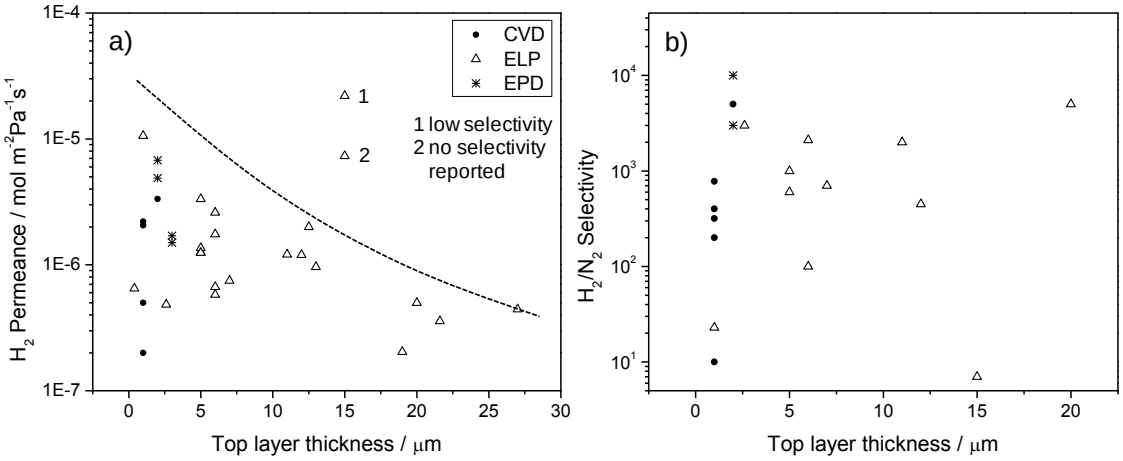

Figure 2.8. Performance of Pd membranes prepared by different fabrication methods. a) H_2 permeance versus top layer thickness, b) H_2/N_2 selectivity versus top layer thickness.

The effect of fabrication method is evaluated by plotting H_2 permeance and H_2/N_2 selectivity of Pd composite membranes prepared by different methods (Fig. 2.8). Regardless of the preparation method, the H_2 permeance is inversely proportional to the thickness of the Pd layer as obtained for the effect of support (Fig. 2.7). Palladium membranes prepared by EPD or CVD result in lower Pd thickness when compared to those prepared by ELP. Composite membranes prepared by EPD give superior H_2 separation performance when compared with the membranes prepared by other methods. However, the EPD method requires conductive supports and the CVD technique requires volatile and thermally stable Pd precursors, which limits the usefulness of these methods. For that reason, extensive efforts have been exerted on the development of composite membranes by ELP than by the other methods. A summary of the results of selectivity versus permeance for various methods of Pd membranes are presented in Fig. 2.9. Region A shows high selectivity and high permeance. Region B shows intermediate values running in a diagonal. Region C shows low selectivity and low permeance. Some of these systems demonstrate H_2 permeance of over 1×10^{-6} mol $m^{-2}s^{-1}Pa^{-1}$ with H_2/N_2 selectivity above 1000 (shaded area in Fig. 2.9), which could represent promising membranes for various commercial applications.

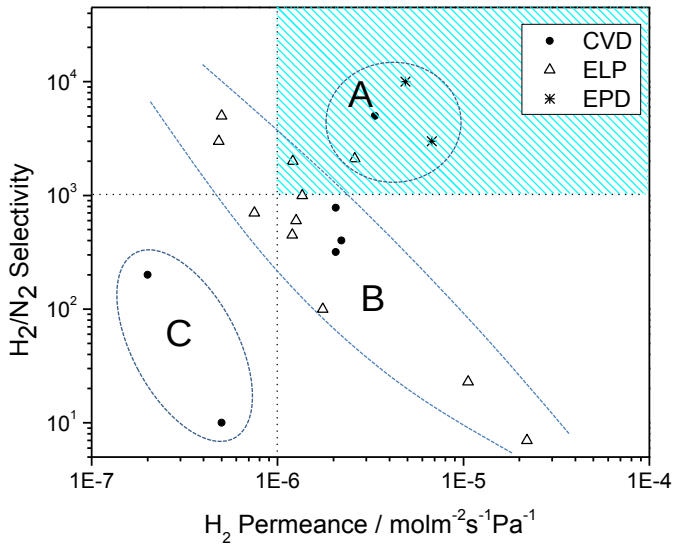

Figure 2.9. H_2/N_2 selectivity and H_2 permeance of Pd-based composite membranes with different fabrication methods.

For membranes in region (B) the H_2 selectivity is inversely proportional to the H_2 permeance. The H_2 permeance decreases with the top metal layer thickness when the structure and morphological properties of the selective layer and the supports are similar. The H_2 selectivity gradually increases as a function of the separation layer thickness until a non-porous Pd layer is developed on the substrate surface. Therefore, H_2 permeance generally decreases with H_2 selectivity increased up to the point where an impervious layer is obtained. Interestingly, two regions which show unusual behavior can be observed.

Membranes in region (A) with high H_2 selectivity and high permeance have a top layer thickness of less than 2 µm and thin intermediate layers of around 2 µm with an average sub nanometer pore size. The thin layers result in a low resistance to gas

permeation, which leads to high H_2 permeance. On the other hand, membranes in region (C) with low H_2 selectivity and low permeance have a thick support layer of around 2 mm with an average pore size of 4 – 6 nm or thick intermediate layers of around 10 μm. Thick supports and intermediate layers create a high resistance to permeation, which results in low H_2 permeance.

It is of interest to compare the performance of Pd membranes with that of polymeric membranes. It is found that regardless of the fabrication methods or support materials used for Pd membranes, the majority had performance well above the well-known trade-off line between the H_2/N_2 selectivity and H_2 permeation for polymeric membranes, which was reported by Robeson [52].A comparison of the permeation properties of Pd membranes surveyed in this study, polymeric membranes referred in the literature [52], and Robeson's upper boundary is given in Fig. 2.10.

Polymeric membrane systems generally show low H_2 permeances (below 1×10^{-8} mol m^{-2} s^{-1} Pa^{-1}) while Pd membranes show high permeances (above 1×10^{-7} mol m^{-2} s^{-1} Pa^{-1}). Polymeric membranes are generally non-porous and gas permeation occurs by the solution-diffusion mechanism [53]. Gas molecules diffuse from the feed side to the surface of polymeric membranes where they dissolve and permeate through free-volume elements (0.2 and 0.5 nm in size between the polymer chains) of the membrane by random molecular diffusion, followed by desorption and diffusion into the permeate side. Thus, polymeric membranes exhibit low H_2 permeance with moderate H_2/N_2 selectivity. Despite extensive research on gas separation, polymeric membranes have not been able to significantly advance beyond the upper bound of the Robeson plot (Fig. 2.10). This

general behavior demonstrates the limited performance of polymeric membranes for this gas system compared to that of Pd membranes.

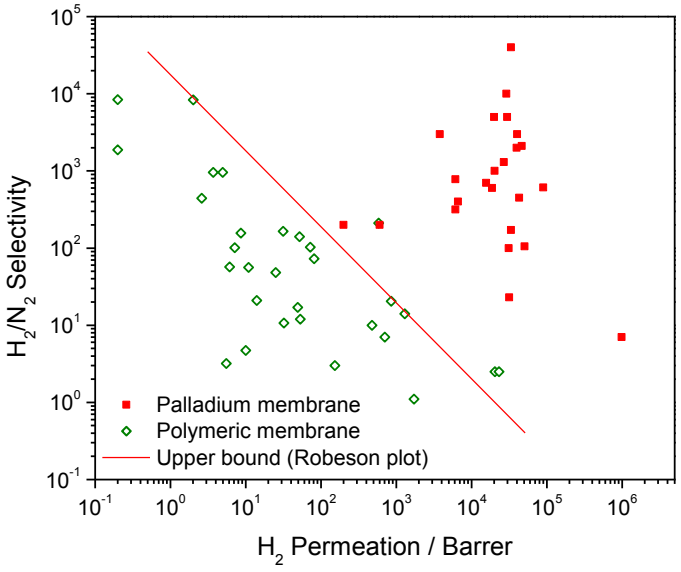

Figure 2.10. H_2/N_2 Selectivity as a function of H_2 permeation of different membrane categories.

2.4. Comparison of Pd membranes

For industrial H_2 separations, the Pd or Pd alloy layer thickness and H_2 permeance can be used for a rough estimate of the materials cost and production yield, respectively. Substrate material effects were assessed using the two factors (top layer thickness and H_2 permeance) for composite Pd membranes prepared by ELP (Table 2.6, Fig. 2.11). The

ELP method was considered because of its ease of application for any shape or substrate compared with other methods.

Table 2.6. H_2 permeance and top layer thickness of Pd composite membranes by ELP

Support material	Pd or Pd alloy layer (μm)	H_2 permeance (10^{7} mol $m^{-2}s^{-1}Pa^{-1}$)
Vycor glass	13 ~ 27	0.5 ~ 9.6
α-Alumina	1 ~ 15	2.0 ~ 33
Stainless steel	6 ~ 20	5.0 ~ 18

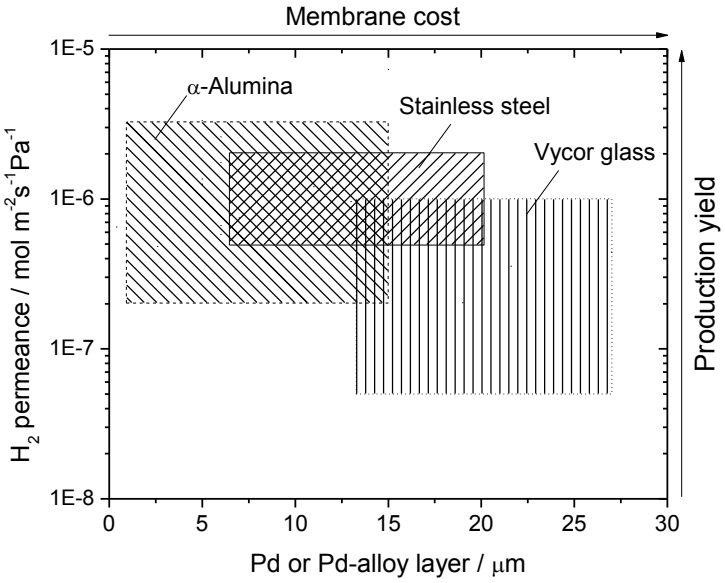

Figure 2.11. Assessment of economic feasibility of Pd membranes prepared by ELP.

Membranes using Vycor glass as a substrate require thicker separation layers to overcome the low mechanical stability of the glass and the difference in the thermal expansion coefficients of the materials. Membranes employing porous stainless steel also

need a thick Pd or Pd alloy layer to obtain a continuous separation layer due to the broad distribution of pore sizes and their large size in the metal substrate. Thick Pd or Pd alloy metal layers result in high membrane preparation cost with low H_2 production yield. It is concluded that the most desirable Pd membranes for practical applications should be prepared by the ELP technique on a porous alumina substrates. This does not consider the costs or ease of fabrication, which could still be substantial.

2.5. Summary

This chapter covers palladium-based membrane systems for H_2 separation prepared by the electroless plating (ELP), chemical vapor deposition (CVD) and electroplating (EPD) methods. The future of Pd membranes in the industry looks promising because several composite membranes surveyed here demonstrated good thermal and mechanical integrity with superior gas properties. The membranes can be classified into two groups, supported and unsupported membranes. The supported membranes were sub-divided into three general categories by the type of substrate employed, - Vycor glass, ceramic or metal.

Unsupported membranes are generally thick to have physical strength and for this reason exhibit inferior gas separation properties compared to supported membranes because of the associated high resistance to gas permeation for thick materials. Nevertheless they are important for the evaluation of the intrinsic properties of Pd membranes. Supported membranes prepared by both the CVD and EPD methods need

only thin selective Pd layers with high H_2 selectivity because of the structural strength provided by the support. However, the application of these methods is limited for practical applications. The CVD process requires volatile and thermally stable Pd precursors and that is limiting because commercially available Pd precursors are expensive or have very low vapor pressures. The EPD method requires conductive supports and this is problematic due to the surface roughness or non-uniform pore distribution of the available metal supports. Compared with other membrane preparation techniques, the ELP method allows the easy preparation of Pd membranes using simple equipment and any type of support.

Membrane structure has a significant effect on hydrogen permeance and selectivity of Pd membranes. As expected, the H_2 permeance is inversely proportional to the Pd layer thickness. The H_2 selectivity, however, showed no direct dependence on the top layer thickness but was affected by imperfections in the layer such as defects or pinholes on the surface, which are determined not by the thickness but by the quality of the top metal layer.

Current problems associated with the Pd membranes are H_2 embrittlement, poisoning and thermal and mechanical stability. These problems can be resolved by using Pd alloy layers and/or forming Pd layers with nano-sized crystalline particles. The durability problems associated with sulfur or carbon contamination still need to be addressed.

References

[1] S.N. Paglieri, J.D. Way, Innovations in palladium membrane research, Sep. Pur. Rev. 31 (2002) 1-169.

[2] B.R. Lanning, O. Ishteiwy, J.D. Way, D. Edlund, K. Coulter, Un-supported Pd alloy membranes for the production of hydrogen, In: A.C. Bose (Ed.), Inorganic Membranes for Energy and Environmental Application, Springer, New York, 2009, pp. 203-207.

[3] A.J. DeRosset, Diffusion of hydrogen through palladium membranes, Ind. Eng. Chem. 52 (1960) 525-528.

[4] D.L. McKinley, Method for hydrogen separation and purification, US Patent 3,439,474, Apr 22, 1969, Assigned to Union Carbide Corp.

[5] S.K. Gade, P.M. Thoen, J.D. Way, Unsupported palladium alloy foil membranes fabricated by electroless plating, J. Mem. Sci. 316 (2008) 112-118.

[6] B.D. Morreale, M.V. Ciocco, R.M. Enick, B.I. Morsi, B.H. Howard, A.V. Cugini, K.S. Rothenberger, The permeability of hydrogen in bulk palladium at elevated temperatures and pressures, J.Membr.Sci. 212 (2003) 87-97.

[7] X. Zhang, G. Xiong, W. Yang, A modified electroless plating technique for thin dense palladium composite membranes with enhanced stability, J. Membr. Sci. 314 (2008) 226-237.

[8] S. Uemiya, T. Matsuda, E. Kikuchi, Aromatization of propane assisted by palladium membrane reactor, Chem. Lett. (1990) 1335-1337.

[9] V.Z. Mordkovich, Y.K. Baichtock, M.H. Sosna, The large-scale production of hydrogen from gas mixtures: A use for ultra-thin palladium alloy membranes, Int. J. Hydrogen Energy, 18 (1993) 539-544.

[10] D. Tanaka, M. Tanco, T. Nagase, J. Okazaki, Y. Yakui, F. Mizukami, T. Suzuki, Preparation of "pore-fill" type Pd-YSZ-gamma-Al_2O_3 composite membrane supported on alpha-Al_2O_3 tube for hydrogen separation, J. Membr. Sci. 320 (2008) 436-441.

[11] I.O. Mazali1, A.G. Souza Filho, B.C. Viana, J. Mendes Filho and O.L. Alves, Size-controllable synthesis of nanosized-TiO2 anatase using porous Vycor glass as template, J. Nanopart. Res. 8 (2006) 141-148.

[12] S. Uemiya, N. Sato, H. Ando, Y. Kude, T. Matsuda, E. Kikuchi, Separation of hydrogen through Pd thin film supported on a porous glass tube, J. Membr. Sci. 56 (1991) 303-313.

[13] S. Uemiya, Y. Kude, K. Sugino, N. Sato, T. Matsuda, E. Kikuchi, A palladium/porous-glass composite membrane for hydrogen separation, Chem. Lett. (1988) 1687-1690.

[14] H. Masuda, K. Nishio, N. Baba, Preparation of microporous metal membrane using two-step replication of interconnected structure of porous glass, J. Mater. Sci. Lett. 13 (1994) 338-340.

[15] K. Kuraoka, H. Zhao, T. Yazawa, Pore-filled palladium-glass composite membranes for hydrogen separation by novel electroless plating technique, J. Mater. Sci. 39 (2004) 1879-1881.

[16] O. Altinisik, M. Dogan, G. Dogu, Preparation and characterization of Pd-plated porous glass for hydrogen enrichment, Catal. Today 105 (2005) 641-646.

[17] A.J. Burggraaf, Important characteristics of inorganic membranes, in: A.J. Burggraaf, L. Cot (Eds.), Fundamentals of Inorganic Membrane Science and Technology, Elsevier, Amsterdam, 1996, pp. 22-28.

[18] S.T. Oyama, Y. Gu, Hydrogen-Selective Silica-Based Membrane, US Patent 7,179,325, Feb 20, 2007, Assigned to Virginia Tech Intellectual Properties Inc.

[19] S. Abate, C. Cenovese, S. Perathoner, G. Centi, Performances and stability of a Pd-based supported thin film membrane prepared by EPD with a novel seeding procedure. Part 1-Behaviour in H_2:N_2 mixtures, Catal. Today 145 (2009) 63-71.

[20] L. Wang, R. Yoshiie, S. Uemiya, Fabrication of novel Pd-Ag-Ru/Al_2O_3 ternary alloy composite membrane with remarkably enhanced H_2 permeability, J. Membr. Sci. 306 (2007) 1-7.

[21] G. Xomeritakis, Y. Lin, CVD synthesis and gas permeation properties of thin Pd /alumina membranes, AIChE J. 44 (1998) 174-183.

[22] J. Tong, L. Su, K. Haraya, H. Suda, Thin and defect-free Pd-based composite membrane without any interlayer and substrate penetration by a combined organic and inorganic process, Chem. Commun. (2006) 1142-1144.

[23] B. Nair, J. Choi, M.P. Harold, Electroless plating and permeation features of Pd and Pd/Ag hollow fiber composite membranes, J. Membr. Sci. 288 (2007) 67-84.

[24] H. Zhao, K. Pflanz, J. Gu, A. Li, N. Stroh, H. Brunner, G. Xiong, Preparation of palladium composite membranes by modified electroless plating procedure, J. Membr. Sci. 142 (1998) 147-157.

[25] B. Nair, M.P. Harold, Pd encapsulated and nanopore hollow fiber membranes: Synthesis and permeation studies, J. Membr. Sci. 290 (2007) 182-195.

[26] D. Tanaka, M. Tanco, T. Nagase, J. Okazaki, Y. Yakui, F. Mizukami, T. Suzuki, Fabrication of hydrogen-permeable composite membranes packed with palladium nanoparticles, Adv. Mater. 18 (2006) 630-632.

[27] Y. Guo, X. Zhan, H. Deng, X. Wang, Y. Wang, J. Qiu, J. Wang, K. L. Yeung, A novel approach for the preparation of highly stable Pd membrane on macroporous α-Al_2O_3 tube, J. Membr. Sci. 362 (2010) 241-248.

[28] M. Seshimoa, T. Hirai, Md M. Rahman, M. Ozawa, M. Sone, M. Sakurai, Y. Higo, H. Kameyama, Functionally graded Pd/_-alumina composite membrane fabricated by electroless plating with emulsion of supercritical CO_2, J. Membr. Sci. 342 (2009) 321-326.

[29] C.-S. Jun, K.-H. Lee, Palladium and palladium alloy composite membranes prepared by metal-organic chemical vapor deposition method (cold-wall), J. Membr. Sci. 176 (2000) 121-130.

[30] N. Itoh, T. Akiha, T. Sato, Preparation of thin palladium composite membrane tube by a CVD technique and its hydrogen permselectivity, Catal. Today 104 (2005) 231-237.

[31] G. Zeng, A. Goldbach*, H. Xu, Defect sealing in Pd membranes via point plating, J. Membr. Sci. 328 (2009) 6-10.

[32] D.R. Askeland, The Science and Engineering of Materials, 3rd ed, PWS Publishing Company, Boston, 1994.

[33] D.R. Lide (Ed), CRC Handbook of Chemistry and Physics, 89th Edition. CRC Press. Boca Raton, Florida, 2008; Section 12, Properties of Solids; Thermal and Physical Properties of Pure Metals, 12-197.

[34] S.-E. Nam, K.-H. Lee, Hydrogen separation by Pd alloy composite membranes: introduction of diffusion barrier, J. Membr. Sci. 192 (2001) 177-185.

[35] I.P. Mardilovich, Y. She, Y.H. Ma, M.-H. Rei, Defect-free palladium membranes on porous stainless-steel support, AIChE J. 44 (1998) 310-322.

[36] J. Shu, A. Adnot, B.P.A. Grandjean, S. Kaliaguine, Structurally stable composite Pd-Ag alloy membranes: Introduction of a diffusion barrier, Thin Solid Films 286 (1996) 72-79.

[37] I.P. Mardilovich, E. Engwall, Y.H. Ma, Dependence of hydrogen flux on the pore size and plating surface topology of asymmetric Pd-porous stainless steel membranes, Desalination 144 (2002) 85-89.

[38] S.-E. Nam, K.-H. Lee, A study on the Pd/nickel composite membrane by vacuum electrodeposition, J. Membr. Sci. 170 (2000) 163.

[39] R.W. Pierce, Method for Making a Fine Porosity Filter Element, US Patent 3,241,298, Mar 22,1966.

[40] N. Jemaa, J. Shu, S. Kaliaguine, P.A. Grandjean, Thin palladium film formation on shot peening modified porous stainless steel substrates, Ind. Eng. Chem. Res. 35 (1996) 973-977.

[41] P. Quicker, V. Höllein, R. Dittmeyer, Catalytic dehydrogenation of hydrocarbons in palladium composite membrane reactors, Catal. Today 56 (2000) 21-34.

[42] J. Tong, R. Shirai, Y. Kashima, Y. Matsumura, Preparation of a pinhole-free Pd-Ag membrane on a porous metal support for pure hydrogen separation, J. Membr. Sci. 260 (2005) 84-89.

[43] Y. Huang, R. Dittmeyer, Preparation of thin palladium membranes on a porous support with rough surface, J. Membr. Sci. 302 (2007) 160-170.

[44] Z. Shi, J. Szpunar, Synthesis of an ultra-thin palladium membrane for hydrogen extraction, Rev. Adv. Mater. Sci. 15 (2007) 1-9.

[45] D. Yepes, L. M. Cornaglia, S. Irusta, E. A. Lombardo, Different oxides used as diffusion barriers in composite hydrogen permeable membranes. J. Membr. Sci. 274 (2006) 92-101.

[46] H. Y. Gao, Y. D. Li, J. Y. S. Lin, B. Q. Zhang, Characterization of zirconia modified porous stainless steel supports for Pd membranes. J. Porous Mater. 13 (2006) 419-426.

[47] M. Broglia, P. Pinacci, M. Radaelli, A. Bottino, G. Capannelli, A. Comite, G. Vanacore, M. Zani, Synthesis and characterization of Pd membranes on alumina-modified porous stainless steel supports, Desalination 245 (2009) 508-515.

[48] S. Samingprai, S. Tantayanon, Y.H. Ma, Chromium oxide intermetallic diffusion barrier for palladium membrane supported on porous stainless steel, J. Membr. Sci. 347 (2010) 8-16.

[49] K. Zhang, H. Gao, Z. Rui, P. Liu, Y. Li, Y. S. Lin, High-temperature stability of palladium membranes on porous metal supports with different intermediate layers, Ind. Eng. Chem. Res. 48 (2009) 1880-1886.

[50] M. Zahedia, B. Afraa, M. Dehghani-Mobarakea, M. Bahmani, Preparation of a Pd membrane on a WO_3 modified porous stainless steel for hydrogen separation, J. Membr. Sci. 333 (2009) 45-49.

[51] M.L. Bosko, F.Ojeda, E.A. Lombardo, L.M. Cornaglia, NaA zeolite as an effective diffusion barrier in composite Pd/PSS membranes, J. Membr. Sci. 331 (2009) 57-65.

[52] L.M. Robeson, The upper bound revisited, J. Membr. Sci. 320 (2008) 390-400.

[53] P. Scovazzo, J. Kieft, D.A. Finan, C. Koval, D. DuBois, R. Noble, Gas separation using non-hexafluorophosphate [PF_6^-] anion supported ionic liquid membranes, J. Membr. Sci. 238 (2004) 57-63.

Chapter 3 . Fabrication of Ultrathin Palladium Membranes by a Novel Electric-Field Assisted Activation Technique

3.1. Introduction

Membranes for hydrogen separation have received considerable attention due to the importance of hydrogen in the chemical and petroleum industries [1]. The two major types of membranes are ceramic (mostly silica) which generally operate at high temperature [2,3,4], and metallic (mostly palladium) which operate at low temperature [5,6]. Membranes made of palladium, and also nickel and platinum, which belong to group 10, and some metallic elements in groups 3-5 of the periodic table have the ability to dissociate and dissolve hydrogen. Considerable research has been carried out on the preparation of palladium-based membranes due to their high solubility of hydrogen in its bulk over a wide temperature range and a fast surface reaction on the metal surface [5,7,8]. For practical applications, in addition to high hydrogen flux and selectivity, and a steady performance over a long period of time, the membranes must have a low cost, and hence a thin Pd layer (< 2 μm) [9,10,11,12,13].

Among Pd membranes composite materials with a thin metal layer on a porous alumina support have the best performance reported to date [14,15,16]. However, when the membranes are too thin, mechanical instability of the Pd-based membranes arising from the different thermal expansion coefficients between the palladium layer ($11.8 \times 10^{-}$

^{6} K^{-1}) [17] and the alumina support (6.7×10^{-6} K^{-1}) [18] can be a significant problem. In addition, pinholes and other defects in the thin selective layers are hard to avoid when the substrate surface contains macro sized pores [8]. Intermediate layers with nano-sized pores can be used to alleviate defects but these may cause a decrease in hydrogen permeance.

The most widely used preparation method for palladium membranes is the electroless plating (ELP) technique due to its ease of coating on any material of arbitrary shape, low cost and use of simple equipment [19,20]. In many cases it has been found that a minimum thickness of 5 μm of Pd is required for obtaining a flawless selective layer by ELP [8,12,21,22], however, there are reported membranes of thickness of 3 μm or even less [23,24]. A drawback of the conventional ELP method is that it requires a complicated and time-consuming activation and sensitization process before final plating of the desired metal can be carried out. Sensitization and activation is usually executed by dipping the substrate into a $SnCl_2$ solution and a $PdCl_2$ solution sequentially with washing and drying after each immersion. These processes are usually conducted several times to deposit uniform Pd seeds [13]. Another problem with this sensitization-activation process is the contamination of the Pd film with Sn, which may degrade membrane stability at high temperatures (> 573 K) [25]. The group of Way eliminated Sn from the activation process by utilizing a solution of Pd acetate in chloroform [26,30]. The membranes using Pd acetate were reported to be more stable than those using $SnCl_2$/$PdCl_2$. However, the Pd layer thickness was measured to be 9 ~ 20 μm.

For these reasons the development of a fabrication method of Pd composite membranes with a selective layer of less than 2 μm by a simple electroless plating

technique would be significant for practical applications. We report here a novel activation technique using electric field assisted deposition which results in a narrow sized range of Pd nanoparticles restricted to the outer surface region of an α-alumina support material. The final layer of Pd of the membranes is very thin (800 nm ~ 1μm) but largely impermeable to any other gases except hydrogen. The selective layer also shows improved thermal stability compared with a membrane prepared using the conventional activation method. The method reported here uses an electric field to cause migration of palladium ions to a region where they encounter a reductant. From a broad standpoint the method is related to the opposing reactants technique for forming palladium membranes [27,28].

3.2. Experimental

3.2.1. Preparation of the membranes

Asymmetric porous α-Al_2O_3 tubes provided by NOK, Japan, were used as membrane supports. The tube had an outside diameter (OD) of 2.9 mm, an inside diameter (ID) of 2.2 mm and an average pore size of 150 nm. The alumina support was cut into 3-4 cm lengths and was connected to dense alumina tubing using a glass glaze (Duncan) which was fused at 1153 K. The glass glaze was reapplied to ensure a leak-free connection. After connection, a novel activation step was conducted using a simple experimental setup consisting of a hollow fiber tube held vertically in a holder with a thin platinum wire threaded in the interior (Fig. 3.1). A cylindrical platinum tube was placed

on the outside and served as the cathode, while the platinum wire inside the hollow fiber served as the anode, with a variable potential of 0-6 V established between them. A circulation pump allowed feeding of liquid reagents to the inside of the hollow fiber tube in an upward direction. First, an aqueous Pd solution (pH: 11.0 ~ 11.2) containing 0.2 wt% (0.01 M) palladium chloride (II), 2.5 wt% ammonium hydroxide, 2 wt% disodium ethylenediamine tetraacetate (NaEDTA) and 0.24 wt% sodium hydroxide was fed into the inside tube using the pump at a volumetric flow rate of 5 cm^3/min. Second, the thin Pt wire was inserted rotated at ~ 250 rpm with the aid of a dc motor to minimize variations of electric field. Third, a reducing agent aqueous solution (pH:12.0 ~ 12.2) containing 0.018 wt% hydrazine and 0.24 wt% sodium hydroxide was introduced to the shell side of the system. Palladium complex ions were favorably reduced to Pd particles in basic condition [29]. The sodium hydroxide was added to maintain the pH at a high value to stabilize the ions. The solution in the shell side and the tube side were separated by the hollow fiber wall. Under the influence of the electric field the Pd complex ions migrated from the tube side to the shell side through the hollow fiber, and were reduced to Pd metal by the reducing agent in the outer surface region. The electric field was applied immediately on the introduction of the reducing agent solution and the whole process was carried out for 10 min at room temperature. Depending on the experiment an electric potential of 0 ~ 6V was applied. After the deposition the tube was washed with deionized water, dried at 353 K, calcined at 773 K for 3 h under forced air flow at a heating rate of 1K/min, slowly cooled to 723 K, treated with H_2 flow for 2 h at 723 K, and cooled to room temperature under Ar flow at a cooling rate of 1K/min. This tube was then used for electroless plating at 323 K for 1 h at a reduced pressure of 34 kPa on

the shell side of the tube with the tube blocked by a rubber stopper (Fig. 3.2). The composition of the Pd plating bath was the same as the Pd solution used in the activation step except for the addition of 10 ppm of 1M hydrazine. The plating solution was injected 10 min later after the shell side pressure set. The plated membrane then was heated to 723 K, held for 3 h, and cooled to 623 K under an Ar stream for permeance measurements.

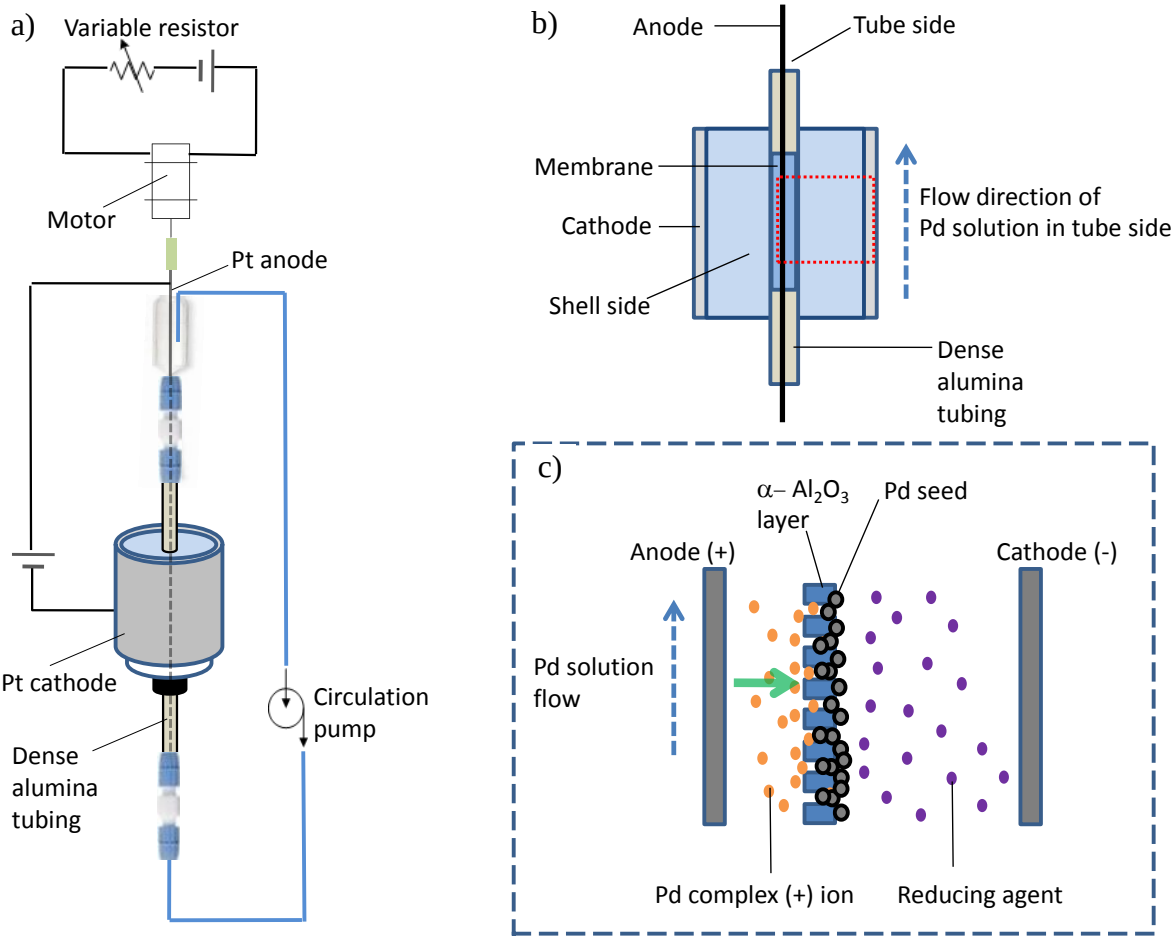

Figure 3.1. Schematic diagram of electric-field assisted deposition of Pd nanoparticles: a) experimental setup, b) description of the electrical system, c) magnification of dotted area in b): schematic depiction of Pd metal deposition assisted by an electric field.

The conventional activation method was carried out by dip-coat with palladium acetate solution (0.05 M), as described elsewhere [22], after which the tube was dried at 353 K, calcined at 773 K for 3 h under forced air flow at a heating rate of 1K/min, slowly cooled to 723 K, treated with H_2 flow for 2 h at 723 K, and cooled to room temperature under Ar flow at a cooling rate of 1K/min.

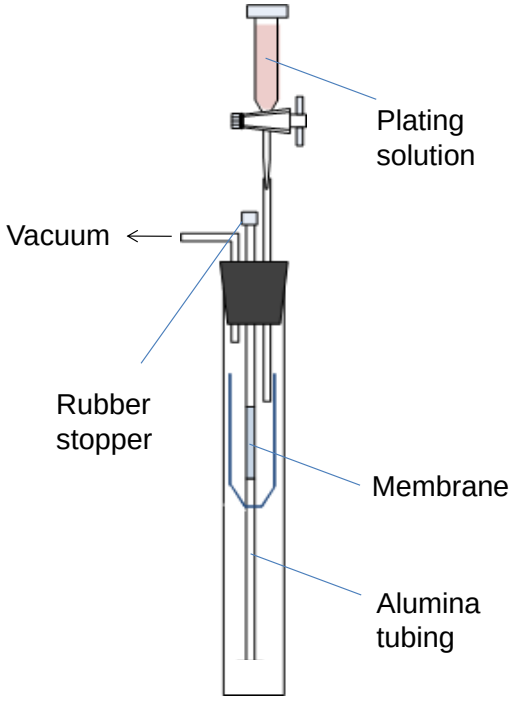

Figure 3.2. Schematic of an apparatus for electroless plating.

3.2.2. Characterization of the membranes

The gas permeance of the membranes was evaluated at 733K at a pressure difference of 105 kPa using a shell and tube apparatus (Fig. 3.3) with pure N_2 or H_2 by measuring the flow rate of the gases passing through the membrane with a bubble flow meter. For the Scanning electron microscope-energy dispersive spectroscopy (SEM-EDS) analysis the membranes were cooled to room temperature under Ar flow and were introduced into the scanning electron microscope (SEM). The surface images and SEM-EDS analysis were obtained using a LEO 1550 (Zeiss) instrument equipped with a back scattered electron detector. X-ray mapping images and line scan analysis were measured using a FEI Quanta 600 FEG.

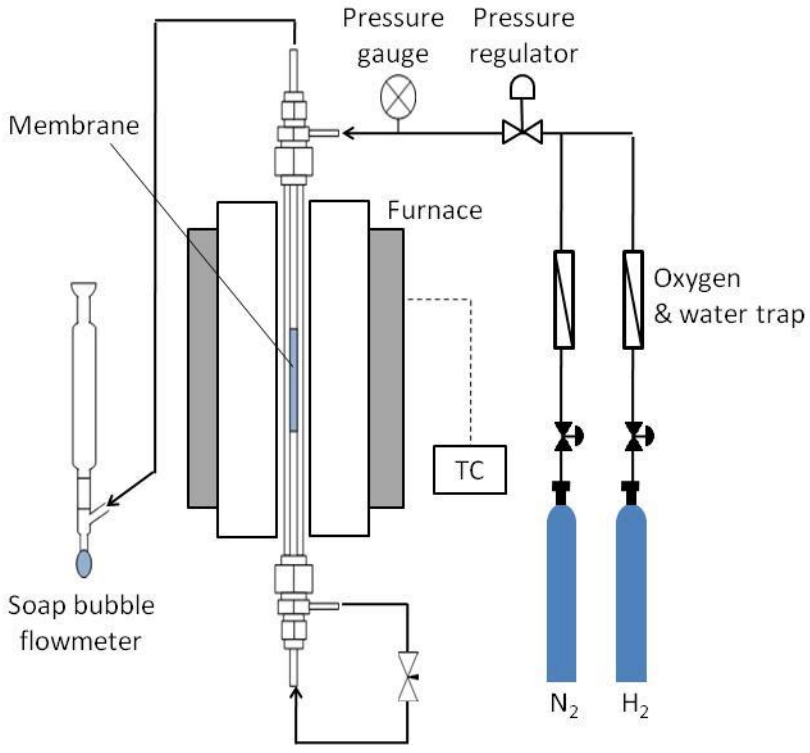

Figure 3.3. Schematic of a tube-shell type apparatus for gas permeation of the Pd membranes

3.3. Results and discussion

3.3.1. Formation of thin and defect-less palladium membrane

For activation, the membrane support was placed in the plating apparatus (Fig. 3.1a). The palladium complex ions on the tube side migrated through the support layer under the influence of the electric field and were then reduced to palladium metal as they came in contact with the reducing agent supplied to the outer membrane surface (Fig. 3.1b,c). Palladium nanoparticles were formed according to the following auto-catalytic reaction [7,30].

$$2Pd(NH_3)_4^{2+} + N_2H_4 + 4OH^- \rightarrow 2Pd^0 + 8NH_3 + N_2 + 4H_2O \quad (3.1)$$

During the activation process, bubbles around both electrodes appeared due to electrolysis according to the following reactions: On the cathode, $2H^+ + 2e^- \rightarrow H_2$, on the anode: $4OH^- \rightarrow O_2 + 2H_2O + 4e^-$. The bubbles were not in contact with the deposited Pd particles.

The process resulted in the formation of Pd nanoparticles with a narrow particle distribution in a limited region of the surface of the substrate. Optical photographs of the membranes (Fig. 3.4, left inserts) showed that the activated surface prepared by the new method was much darker than the surface obtained by the classic method using Pd acetate, visually indicating that more Pd seeds were formed on the surface of the support material. The photographs also show that the Pd is deposited exclusively in the region of the porous support, so no wasteful deposition occurs on the solid alumina tubes.

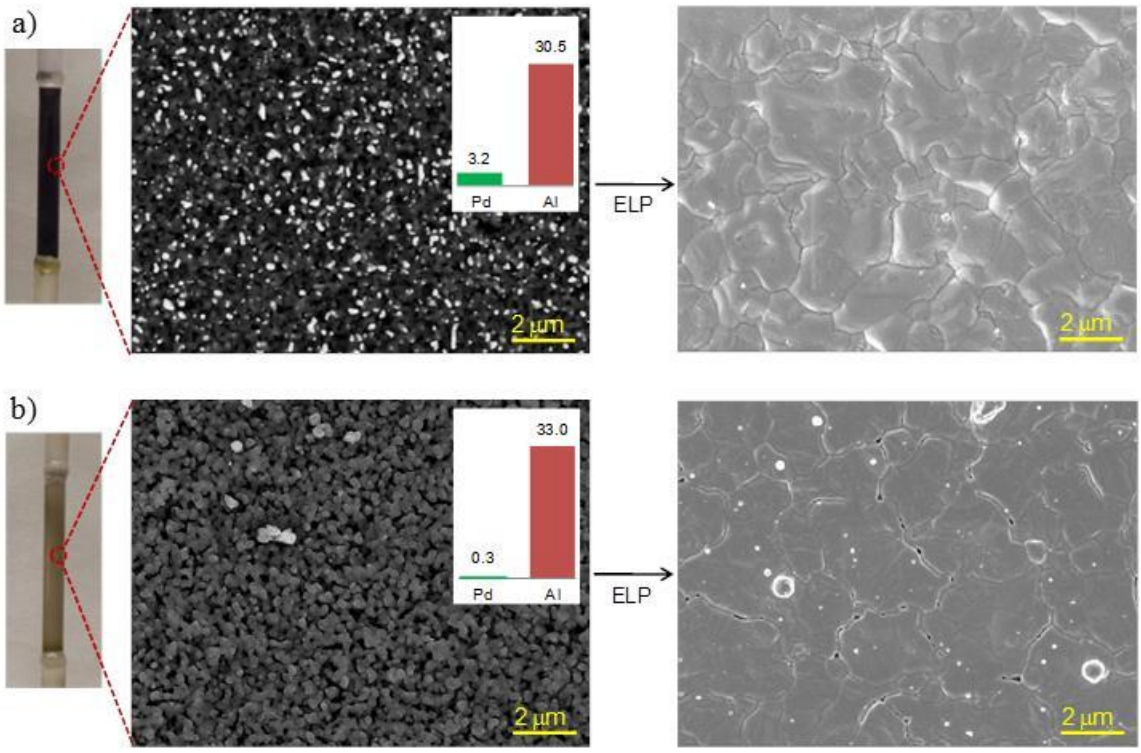

Figure 3.4. Photos, SEM images, and atomic analysis (by SEM-EDS, atomic %) of activated surface and SEM images of Pd selective layer after stability test: a) by the new activation technique with a potential of 4.0 V, b) by the classic activation method with Pd acetate solution.

Scanning electron microscopy (SEM) images and elemental analysis results of the activated surface by energy dispersive spectroscopy (SEM-EDS) provide a more detailed picture of the membrane surface (Fig. 3.4, middle panels). Elements with high atomic numbers backscatter electrons more strongly than light elements, so Pd particles with heavier atomic weight than alumina appear brighter in the image [31]. In the SEM images of the activated surfaces, the electric field assisted activation method produced Pd nanoparticles of similar size uniformly distributed on the surface of the alumina support,

while the classic activation technique with Pd acetate formed irregular Pd particles in much smaller amounts (Fig. 3.4, middle panels). A quantitative analysis of the surface composition was conducted by SEM-EDS. It was confirmed that the new method deposited around ten times more Pd than the classic method (3.2 vs 0.3 atom %). After electroless Pd plating and stability testing, SEM shows that the new method produces a top selective layer with a continuously smooth surface morphology while at the same conditions the classical method resulted in small pinhole defects around the metal grains (Fig. 3.4, right panels).

If a control experiment were attempted to try to deposit the same amount of Pd on the surface, the classical method would also deposit more Pd in the interior because it is nonselective, and would result in an extremely thick membrane of lower permeance. In fact, our method of synthesis was carried out with 5 times less Pd concentration (0.01 M compared to 0.05 M) than the standard method, and yet resulted in a high concentration of Pd on the surface. This was the result of the transport of the Pd to the reductant side under the action of the electric field potential.

The location of the Pd particles deposited by the electric-field assisted activation method was determined by x-ray mapping and line scanning with SEM-EDS. The X-ray mapping image of the membrane cross section after activation prepared by the new method showed a narrow and distinct Pd layer formed on the outer surface with Pd particles deposited in the pores of the support a few μm from the top surface (Fig. 3.5a) while the image of the membrane cross section after activation by the conventional technique demonstrated that most Pd seeds were formed on top of the surface (Fig. 3.5c). The X-ray mapping image after electroless plating and a quantitative analysis of the cross

section also demonstrate that the deposited Pd was packed in the narrow region where the palladium seeds were formed in the activation step (Fig. 3.5b). A cross sectional micrograph of the Pd membrane prepared with the new activation technique shows that the top Pd layer is uniform and thin with a thickness of around 900 nm (Fig. 3.6). Beneath the Pd layer, a graded Pd/α-Al_2O_3 layer whose thickness is around 3 μm is observed. This is probably formed because the diffusion front where the Pd ions and reductant meet is not sharp. The graded Pd layer likely minimizes peeling of the Pd layer from the support by formation of a strong bond between the selective layer and the support layer as also conjectured earlier [13]. The Pd in the graded layer probably does not fill the pores. Compared with the H_2 permeance of the membrane by Nair and Harold [10], which had 2.6 μm of Pd completely filling the pores, our permeance is almost 10 times higher even though the Pd layer is only half as thick.

The total amount of Pd cannot easily be measured gravimetrically, as a 900 nm layer of Pd over a membrane length of 1 cm corresponds to a weight of 0.0013 g, and the sensitivity of our balance is only 0.0001 g, resulting in considerable error. The SEM-EDS scan shows that the amount of Pd in the pores is likely to be much smaller (Fig. 3.5), so it is likely that the effective membrane thickness is 0.9 μm (900 nm) as shown by the SEM cross-sectional image (Fig. 3.6). As will be discussed, the permeance of our membrane is consistent with this thickness.

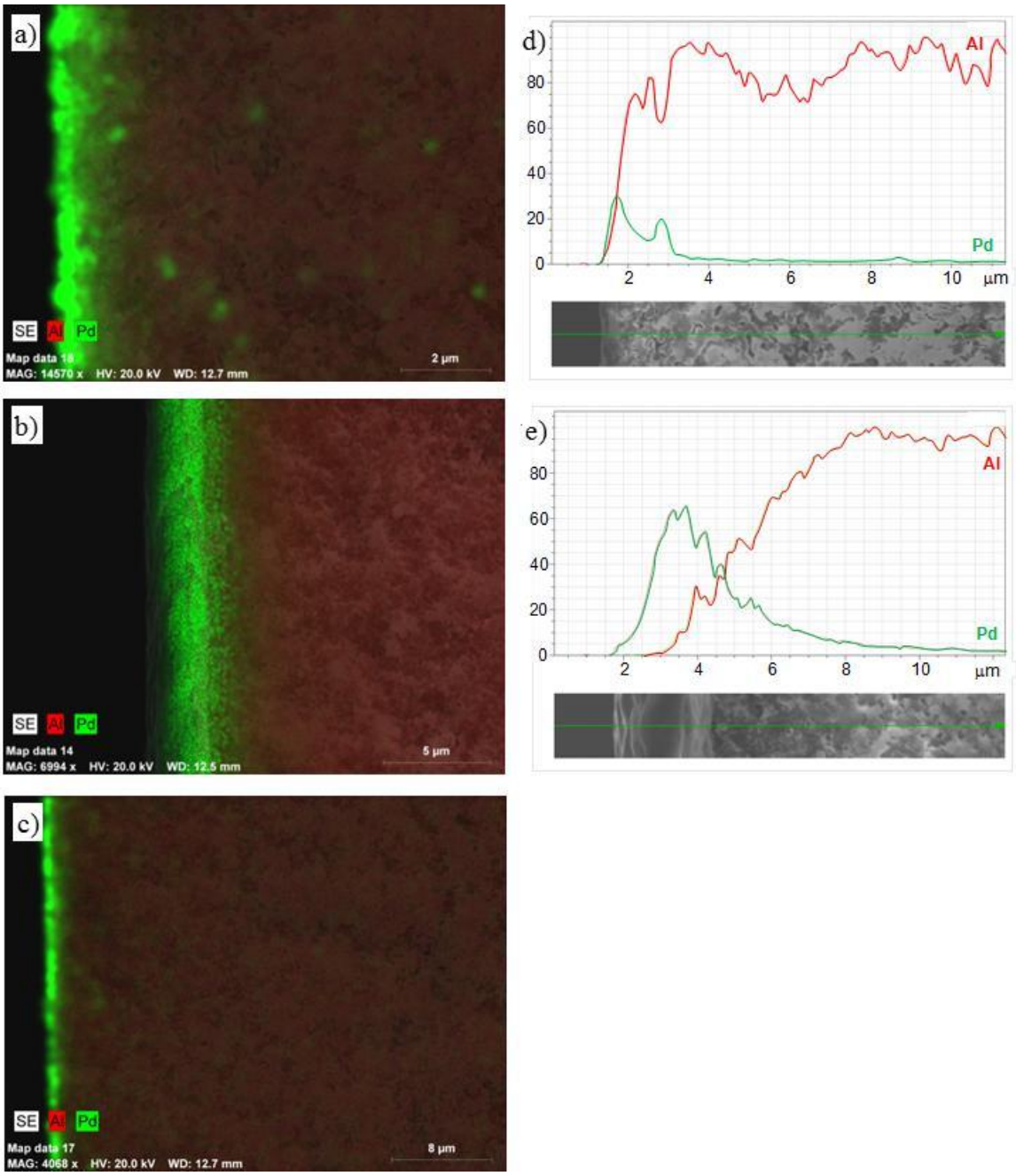

Figure 3.5. X-ray mapping images of crosectional membranes after new activation technique with a potential of 4.0 V (a), after Pd plating on the activated surface prepared by the new technique (b), and after conventional activation method (c) and composition

analysis of the SEM-EDS image after new activation technique (d) and after Pd plating following the new activation technique (e).

The key factors for producing a thin, defect-free and sustainable separation layer are the formation of an even nanoparticle distribution of Pd and the incorporation of Pd into the support. The uniform distribution of Pd seeds lead to a dense and flawless Pd layer with uniform quality in the following plating step. The formation of additional Pd metal deeper in the pores of the support also provides anchoring points that enhance adhesion and gives the top layer thermal and mechanical stability.

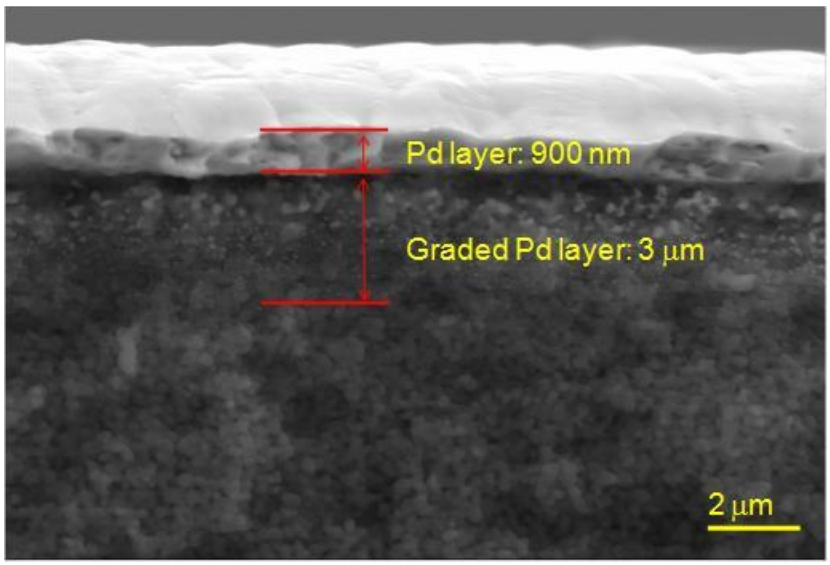

Figure 3.6. SEM image of the cross section showing thin Pd layer and graded Pd layer of the membrane prepared by the new activation with a potential of 4.0 V (Top white layer is not cross-sectional Pd layer but the surface of Pd layer).

3.3.2. Gas permeation characteristics of the thin palladium membranes

The hydrogen flux of the Pd membrane prepared by the novel electric-field assisted activation was measured at 613-733K. According to Sievert's law [32], when the rate controlling step is bulk diffusion through the palladium layer, the value of n is 0.5 because the diffusion rate is proportional to the concentration of hydrogen atoms on opposite sides of the metal surface and this hydrogen concentration is proportional to the square root of the hydrogen pressure. When transport to and from the surface or adsorption or desorption of hydrogen molecules is rate determining, the value of *n* is 1 since there processes depend linearly on the concentration of hydrogen. As shown in Fig. 3.7a, hydrogen flux is linearly proportional to the pressure difference across the membrane at the temperature range, which demonstrates that surface process is the rate-determining step rather than bulk diffusion for hydrogen permeation through the Pd layer. This is a consequence of having a very thin material and is in a good agreement with previous reports for thin Pd membranes in the literature [12, 16,33].

This linear relationship between hydrogen flux and pressure was observed in the membrane prepared by the conventional activation due to its thin nature. It is expected that a thick membrane would show square root pressure dependence.

From data of Morreale, et al. [34] the hydrogen flux for a free-standing Pd film of thickness 1 mm at 673 K for a pressure difference of 100 kPa ($\Delta p^{½}$ = 316 $Pa^{½}$) is 0.006 mol $m^{-2}s^{-1}$, which corresponds to a permeance of 6 x 10^{-8} mol $m^{-2}Pa^{-1}s^{-1}$. This is much smaller than the permeance of thin Pd membranes, where the transport through the Pd is so fast that external transport or surface reaction is limiting. If a linear correction for the

thickness is applied the corresponding permeance for a 1 μm Pd membrane would be 6 $\times 10^{-5}$ mol $m^{-2}Pa^{-1}s^{-1}$, which, as expected, is higher than observed.

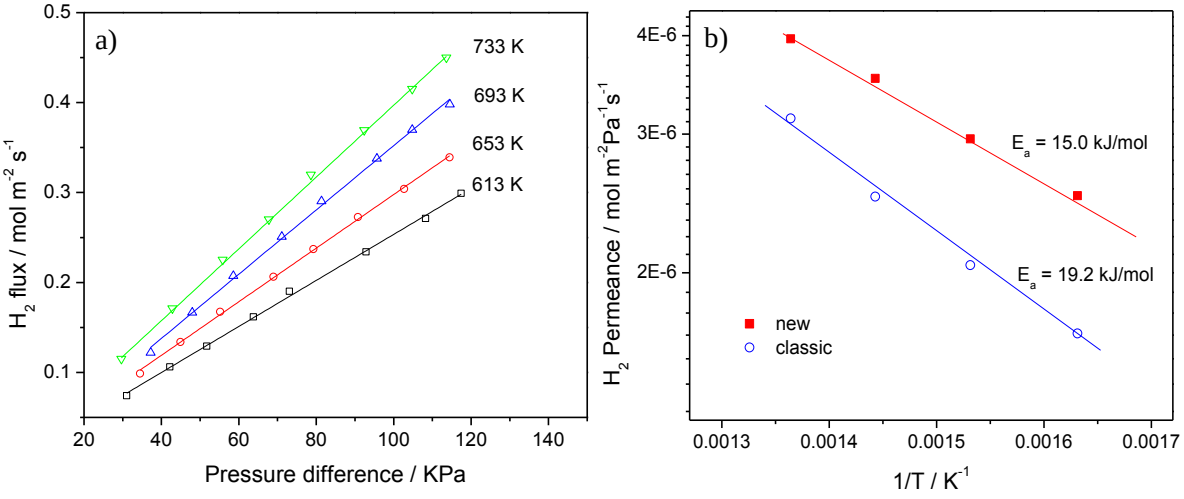

Figure 3.7. Pd membrane prepared by the new activation method with a potential of 4.0 V showing a) linear dependence of H_2 flux for hydrogen pressure difference at 613-733 K and b) linear relation of H_2 permeance (in logarithmic scale) for reciprocal temperature at hydrogen pressure difference of 105 kPa.

The hydrogen permeance could be described by the following Arrhenius-type equation:

$$P = P_0 \exp(-E_a/RT) \quad (3.2)$$

where P is hydrogen permeance, P_0 is pre-exponential factor (mol $m^{-2}Pa^{-1}s^{-1}$) and E_a is activation energy (J mol^{-1}) for hydrogen permeation through Pd membrane. The hydrogen permeance data of the Pd membranes fit the equation well and give estimates of the activation energy (Fig. 3.7b), calculated to be 15.0 kJ mol^{-1} and 19.2 kJ mol^{-1} for the

membranes prepared by the new method and the classic method, respectively. These fall well in the range of 10-22 kJ mol^{-1} for Pd membranes reported previously [14,35,36]. The activation energy can be affected by such factors as the thickness of the Pd layer, the preparation method, the grain microstructure of the layers, and experimental conditions such as temperature and pressure [26,37]. The higher activation energy in the case of the classic method can be attributed to lattice defects around metal grain which act as traps resulting in slow hydrogen permeation [26,38].

3.3.3. Evaluation/Discussion of membrane performance

The performance of the membranes as function of activation method was evaluated by hydrogen permeance and H_2/N_2 selectivity measurements. The thickness of the Pd layer was measured to be ~ 900 nm regardless of activation method. Comparison of the hydrogen permeance and H_2/N_2 selectivity shows that the membrane prepared by the electric field assisted method is superior to that prepared by the traditional method (Fig. 3.8). The measurements were carried out at 733 K after a heat-treatment with H_2 at 733 K for 3 h. After 150 h the membrane prepared with the electric field had a high hydrogen permeance of 5.0×10^{-6} mol $m^{-2}s^{-1}Pa^{-1}$ while the membrane prepared conventionally had a slightly lower permeance of 4.0×10^{-6} mol $m^{-2}s^{-1}Pa^{-1}$. The corresponding selectivities were 6500 and 200, with that of the membrane prepared with the electric field remaining constant for the duration of the measurements, while that of the membrane prepared conventionally declining steadily. The decline in selectivity is

probably due to growth in the size of the defects with time. This result is in a good agreement with the surface measurement by SEM (Fig.3.4).

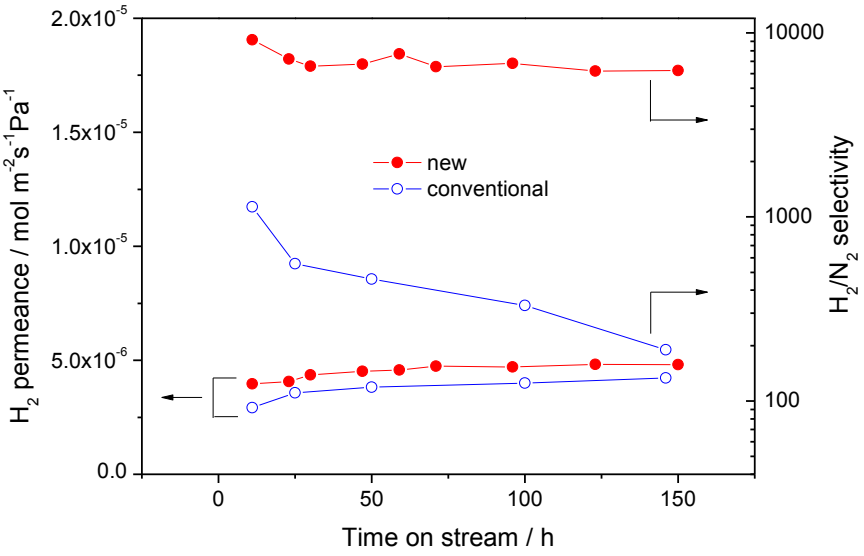

Figure 3.8. H_2 permeance and H_2/N_2 selectivity of Pd membranes (red dot: membrane prepared by the new activation with a potential of 4.0 V, blue circle: membrane prepared by the classic activation) at 733K as a function of activation method.

To investigate the effect of the electric field, different voltages were applied during the activation step (Fig. 3.9). The current density increased with electric potential while the total system resistance declined with the intensity of electric current. At potentials below 4.0 V (< 130 mA cm^{-2}) the H_2/N_2 selectivity increased steadily from low values of 15-20 with zero potential to 6000-9000. At potentials above 4.0 V the H_2/N_2 selectivity declined slowly to the 3000-7000 level. The membranes showed good stability with modest decrease in selectivity after 5 days. The hydrogen permeance of

these membranes was uniformly high, in the range of 4.0-5.0×10^{-6} mol $m^{-2}s^{-1}Pa^{-1}$. Optimal electric potential range for obtaining uniform Pd seeds deposited on the substrate in the new activation method seems to exist but further research should be addressed.

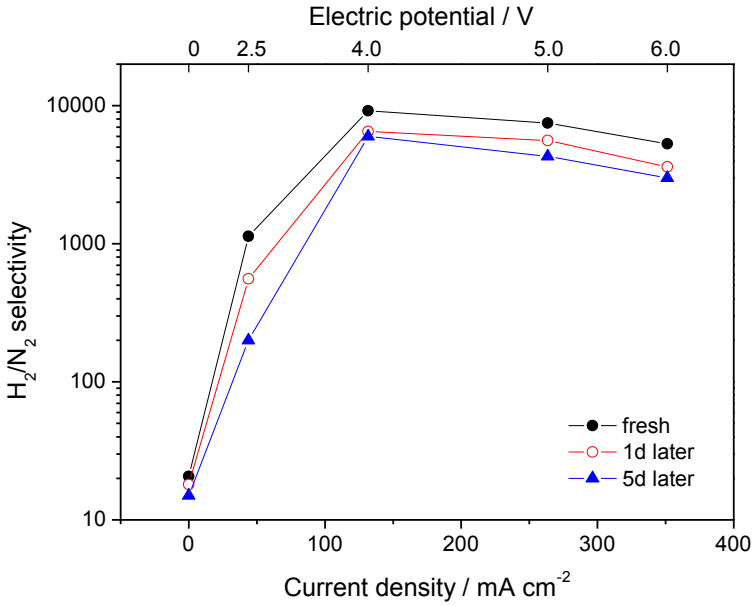

Figure 3.9. H_2 permeance and H_2/N_2 selectivity of Pd membranes at 733K as a function of electric field intensity in the novel activation.

The Pd membrane developed here shows a better performance in H_2 permeance and selectivity compared with other composite membranes reported in the literature assessed under similar, but not exactly the same, conditions (Fig. 3.10, Table 3.1). Although for accurate comparison the hydrogen permeance of the membranes should be measured at the same temperature, the activation energy is generally low so the error introduced is small. The permeance values from the literature have been converted into the unit of mol $m^{-2}s^{-1}Pa^{-1}$ using the thickness of separation layer and the hydrogen partial

pressure difference so that reported values can be compared. Several studies that have achieved very thin Pd layers (< 2 μm) with high hydrogen selectivity use more cumbersome preparation methods, but a couple use the same ELP method.

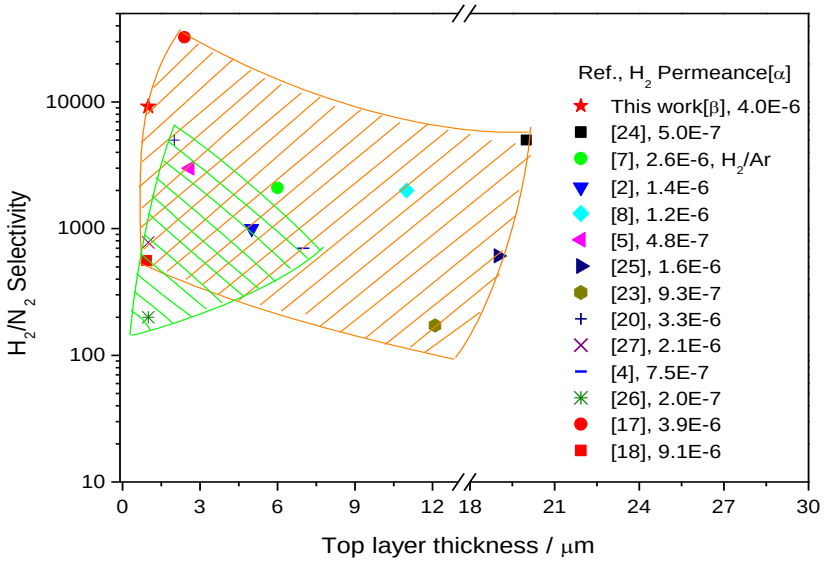

Figure 3.10. Comparison with other Pd membranes prepared by electroless plating (solid symbols) or chemical vapor deposition (point symbols) published in the literature. [α] The permeance values from the literature were converted into units of mol $m^{-2}s^{-1}Pa^{-1}$ using partial pressure difference of hydrogen so that reported values can be compared. [β] Electric-filed assisted activation with electric density of 130 mA cm^{-2}.

Studies that use more complex methods are discussed first. Itoh et al. prepared tubular palladium composite membranes supported on α-alumina by means of forced-flow chemical vapor deposition (CVD) [39]. Their palladium membrane with a top layer

of ~ 2 μm showed a H_2/N_2 selectivity of 5000 and a H_2 permeance of ~ 3.4×10^{-6} mol m^{-2} s^{-1} Pa^{-1} at 573K Nam et al. fabricated disk-type Pd-Cu alloy composite membranes supported on stainless steel by a vacuum electrodeposition (EPD) method using a thin intermediate layer of silica by a sol-gel method [40]. Their membranes had a thin Pd layer of ~2 μm and showed H_2/N_2 selectivity of ~ 10000 along with a H_2 permeance of ~ 4.9×10^{-6} mol m^{-2} s^{-1} Pa^{-1} at 623K. However, the CVD technique requires volatile and thermally stable Pd precursors [41] and the EPD method requires conductive supports, which limits the usefulness of these methods.

Studies that use the classical ELP method are discussed next. Li et al. prepared Pd membranes on a 13 mm OD alumina tube using electroless deposition after activation with $SnCl_2$ and $PdCl_2$ solutions. They obtained a membrane of thickness 2.4 μm and permeance of 3.9 x 10^{-6} mol m^{-2} s^{-1} Pa^{-1} and H_2/N_2 selectivity of 32,500 (red circle in Fig. 8). Compared to our membrane of thickness 0.8 μm (red star in Fig. 8), which had a permeance of 4.0 x 10^{-6} mol m^{-2} s^{-1} Pa^{-1} and H_2/N_2 selectivity of 9200, the membrane of Li et al. has similar permeance but higher selectivity. The higher selectivity can be explained by the thicker Pd layer, and the high permeance from the use of a higher temperature (773 K vs. 733 K), so the results are comparable. Hatlevik et al. report a Pd membrane supported on a stainless steel support with an yttria-stabilized zirconia diffusion barrier prepared by electroless plating using a Pd acetate activation method. The membrane had a thickness 0.93 μm and at 673 K had a permeance of 9.1 x 10^{-6} mol m^{-2} s^{-1} Pa^{-1} and H_2/N_2 selectivity of 560 (red square point in Fig. 8). Here the thickness is comparable to our membrane, but the permeance is higher and the selectivity considerably lower, consistent with a material with some defects. Overall, compared to

other materials reported in the literature, our membrane performance represents the current state-of-the-art among Pd membranes.

Table 3.1. Comparison of the permeance and selectivity results of different composite Pd membranes.

Layers on support	Support	Method	L [a] μm	T K	Δp kPa	P [b]	α_{H_2/N_2}	Ref
Pd/ γ-Al_2O_3	Alumina	ELP	2.4	773	101	39	32,500	[23]
$Pd_{88}Ag_{12}$/γ-Al_2O_3	Alumina	ELP	11	823	413	12	2000	[13]
Pd/γ-Al_2O_3 with Pd/γ-Al_2O_3	Alumina	ELP	6	753	100	26	2100 [c]	[12]
Pd/γ-Al_2O_3 packed with Pd/γ-Al_2O_3	Alumina	ELP	2.6	643	413	4.8	3000	[10]
γ-Al_2O_3/γ-Al_2O_3 packed with Pd/γ-Al_2O_3	Alumina	ELP	5	573	413	14	1000	[7]
Pd/Polymer	Alumina	ELP	5	773	100	33	∞ [d]	[17]
Pd-Cu alloy/Silica/Ni powder	Stainless steel [e]	EPD	2	623	53	45	10000	[40]
Pd	Alumina	CVD	2	573	30	33	5000	[39]
Pd disk	Self	ELP	12.1	673	120	9.3	172	[42]
Pd59Cu41 disk	Self	ELP	16.7	673	120	10	105	[42]
Pd/γ-Al_2O_3 with Pd	Alumina	ELP	1	673	75	6.7	23	[43]
Pd	Stainless steel	ELP	20	623	100	5	5000	[35]
Pd/YSZ by APS	Stainless steel	ELP	6	673	40	18	100	[9]

Pd/YSZ	Stainless steel	ELP	0.93	673	140	9.1	560	[24]
Pd with MOCVD activation/YSZ by APS [f]	Stainless steel	ELP	7	673	40	7.5	700	[9]
Pd/NaA zeolite	Stainless steel	ELP	19	723	50	16	608	[44]
Pd/γ-Al_2O_3	Alumina	CVD	1	573		2	200	[45]
Pd	Alumina	CVD	1	723	68	21	780	[46]
Pd-Ni alloy	Alumina	CVD	1	723	68	21	317	[46]
$PdNi_{0.2-0.3}$/Ni powder	Stainless steel	CVD	1	723	68	22	400	[46]
Pd-Ni alloy/Cu/Ni powder	Stainless steel [e]	EPD	2	723	55	68	3000	[47]
Pd	Alumina	ELP	0.9	733	105	40	9200	[g]
Pd	Alumina	ELP	0.9	733	103	31	1200	[h]

[a] Top layer (selective layer) thickness,
[b] P is H_2 permeance in the unit of 10^{-7}mol $m^{-2}s^{-1}Pa^{-1}$
[c] H_2/Ar selectivity, [d] H_2/He selectivity, [e] disk type, [f] APS: atmospheric plasma spray
[g] This work prepared by the electric-field assisted activaton with electric current density of 130 mA cm^{-2}, [h] This work prepared by a conventional activation with a Pd acetate solution

3.4. Conclusions

In this chapter, a new method for ultrathin (< 1μm) and defect-less Pd membranes was developed. The prepared membranes showed higher H_2 permeance properties and better thermal stability compared with Pd membranes prepared by a conventional method. The hydrogen permeance of the Pd membranes prepared by a new electric-field

assisted activation technique at the electric potential range of 4.0-6.0 V was measured to be 4.0-5.0×10^{-6} mol $m^{-2}s^{-1}Pa^{-1}$ with H_2/N_2 selectivity 3000-9000 at 733 K. This level of performance stands among the best reported for comparable membranes prepared by electroless plating. The thermal stability and high hydrogen permeance of the Pd membranes prepared by the method reported here can be attributed to the concentrated distribution of Pd nanoparticles in the surface region of the support. Unlike competing techniques, which are limited in usable substrate geometry and material characteristics, this method is generally applicable. It can directly produce thin and defect-free Pd film on porous substrates of any shape without an intermediate layer because Pd seeds are formed with a uniform distribution on the outer surface at high concentration. This method is expected not only to minimize the preparation time for Pd membranes due to its simplicity but also to reduce the membrane cost and improve the permeability with a high separation factor because of a thin and flawless Pd layer.

References

[1] S. T. Oyama, S. M. Stagg-Williams, Eds., Correlations in Membrane Science, Elsevier, Amsterdam, 2011.

[2] D. Lee, L. Zhang, S. T. Oyama, S. Niu, R. F. Saraf, Synthesis, characterization, and gas permeation properties of a hydrogen permeable silica membrane supported on porous alumina, J. Membr. Sci. 231 (2004) 117.

[3] S. T. Oyama, D. Lee, P. Hacarlioglu, R. F. Saraf, Theory of hydrogen permeability in nonporous silica membranes, J. Membr. Sci. 244 (2004) 45.

[4] Y. Gu, S. T. Oyama, Ultrathin, hydrogen-selective silica membranes deposited on alumina-graded structures prepared from size-controlled boehmite sols, J. Membr. Sci. 306 (2007) 216.

[5] Y.H. Ma, Composite Pd and Pd/alloy membranes, in: A.C. Bose (Ed.), Inorganic Membranes for Energy and Environmental Applications, Springer, New York, 2009, pp. 241-254.

[6] A. Basile, F. Gallucci, S. Tosti, Synthesis, characterization and applications of palladium membranes, in: R. Mallada, M. Menéndez (Eds.), Membrane Science and Technology, Elsevier, 2008, pp. 255-323.

[7] D.A.P. Tanaka, M.A.L. Tanco, T.N.J. Okazaki, Y. Wakui, F. Mizukami, T.M. Suzuki, Fabrication of hydrogen-permeable composite membranes packed with palladium nanoparticles. Adv. Mater. 18 (2006) 630-632.

[8] J. Tong, L. Su, K. Haraya, H. Suda, Thin and defect-free Pd-based composite membrane without any interlayer and substrate penetration by a combined organic and inorganic process. Chem. Commun. (2006) 1142-1144.

[9] Y. Huang, R. Dittmeyer, Preparation of thin palladium membranes on a porous support with rough surface. J. Membr. Sci. 302 (2007) 160-170.

[10] B. Nair, M.P. Harold, Pd encapsulated and nanopore hollow fiber membranes: Synthesis and permeation studies. J. Membr. Sci. 290 (2007) 182-195.

[11] K. Aasberg-Petersen, C.S. Nielsen, S.L. Jørgensen, Membrane reforming for hydrogen. Catal. Today 46 (1998) 193-201.

[12] X. Zhang, G. Xiong, W. Yang, A modified electroless plating technique for thin dense palladium composite membranes with enhanced stability. J. Membr. Sci. 314 (2008) 226-237.

[13] B. Nair, J. Choi, M.P. Harold, Electroless plating and permeation features of Pd and Pd/Ag hollow fiber composite membranes. J. Membr. Sci. 288 (2007) 67-84.

[14] X.L. Pan, G.X. Xiong, S.S. Sheng, N. Stroh, H. Brunner, Thin dense Pd membranes supported on α-Al2O3 hollow fibers. Chem. Commun. (2001) 2536-2537.

[15] F. Roa, J.D. Way, Influence of alloy composition and membrane fabrication on the pressure dependence of the hydrogen flux of palladium-copper membranes. Ind. Eng. Chem. Res. 42 (2003) 5827-5835.

[16] J.H. Tong, Y. Matsumura, Thin Pd membrane prepared on macroporous stainless steel tube filter by an in-situ multi-dimensional plating mechanism. Chem. Commun. (2004) 2460-2461.

[17] In: D.R. Lide, Editor, CRC Handbook of Chemistry and Physics, 89th ed., CRC Press. Boca Raton, Florida, 2008, p. 12-197

[18] D.R. Askeland, The Science and Engineering of Materials, 3rd ed., PWS Publishing, Boston, 1994, p. 705.

[19] O. Altinisik, M. Dogan, G. Dogu, Preparation and characterization of palladium-plated porous glass for hydrogen enrichment. Catal. Today 105 (2005) 641-646.

[20] S. Yun, S.T. Oyama, Correlations in palladium membranes for hydrogen separation: J. Membr. Sci., in revision.

[21] V. Höllein, M. Thornton, P. Quicker, R. Dittmeyer, Preparation and characterization of palladium composite membranes for hydrogen removal in hydrocarbon dehydrogenation membrane reactors. Catal. Today 67 (2001) 33-42.

[22] F. Roa, J. D. Way, R. L. McCormick, S. N. Paglieri, Preparation and characterization of Pd-Cu composite membranes for hydrogen separation. Chem. Eng. J. 93 (2003) 11-22.

[23] H. Li, A. Goldbach, W. Li, H. Xu, PdC formation in ultra-thin Pd membranes during separation of H2/CO mixtures, J. Membr. Sci. 299 (2007) 130-137.

[24] Ø . Hatlevik, S. K. Gade, M. K. Keeling, P. M. Thoen, A.P. Davidson, J. D. Way, Palladium and palladium alloy membranes for hydrogen separation and production: History, fabrication strategies, and current performance, Sep. Purif. Technol. 73 (2010) 59-64.

[25] A. Li, G. Xiong, J. Gu, L. Zheng, Preparation of Pd/ceramic composite membrane 1. Improvement of the conventional preparation technique. J. Membr. Sci. 110 (1996) 257-260.

[26] S.N. Paglieri, K.Y. Foo, J.D. Way, A new preparation technique for Pd alumina membranes with enhanced high-temperature stability. Ind. Eng. Chem. Res. 38 (1999) 1925-1936.

[27] M. Tsapatsis, S. Kim, S. W. Nam, G. Gavalas, Synthesis of Hydrogen Permselective SiO2, TiO2, A12O3, and B2O3 Membranes from the Chloride Precursors, Ind. Eng. Chem. Res. 30 (1991) 2152-2159.

[28] Y. Gu, S. T. Oyama, Permeation properties and hydrothermal stability of silica-titania membranes supported on porous alumina substrates, J. Membr. Sci. 345 (2009) 267–275.

[29] C.K. Lai, Y.Y. Wang, C. C. Wan, A study of the reduction of chelated palladium on mercury electrode, Bull. Chem. Soc. Jpn. 64 (1991) 635-640.

[30] S.N. Paglieri, J.D. Way, Innovations in palladium membrane research. Sep. Pur. Rev. 31 (2002) 1-169.

[31] J. Goldstein, D. Newbury, D. Joy, P. Echlin, C. Lyman, E. Lifshin, L. Sawyer. J. Michael, Scanning Electron Microscopy and X-ray Microanalysis, 3rd ed, Springer, New York, 2003, pp. 25-30.

[32] R. C. Hurlbert, J. O. Konecny, Diffusion of hydrogen through palladium, J. Chem. Phys. 34 (1961) 655.

[33] H. Chen, C. Chu, T. Huang, Comprehensive characterization and permeation analysis of thin Pd/Al2O3 composite membranes prepared by suction-assisted electroless deposition, Sep. Sci. Technol. 39 (2004) 1461-1483.

[34] B. D. Morreale, M. V. Ciocco, R. M. Enick, B. I. Morsi, B. H. Howard, A. V. Cugini, K. S. Rothenberger, The permeability of hydrogen in bulk palladium at elevated temperatures and pressures, J. Membr. Sci. 212 (2003) 87-97.

[35] P.P. Mardilovich, Y. She, Y.H. Ma, M.-H. Rei, Defect-free palladium membranes on porous stainless-steel support. AIChE J. 44 (1998) 310-322.

[36] H.-I. Chen, C.-Y. Chu, T.-C. Huang, Comprehensive characterization and permeation analysis of thin Pd/Al2O3 composite membranes prepared by suction-assisted electroless deposition, Sep. Sci. Technol. 39 (2004) 1461-1483.

[37] F.C. Gielens, H.D. Tong, M.A.G. Vorstman, J.T.F. Keurentjes, Measurement and modeling of hydrogen transport through high-flux Pd membranes, J. Membr. Sci. 289 (2007) 15-25.

[38] R.V. Bucur, N.O. Ersson, X.Q. Tong, Solubility and diffusivity of hydrogen in palladium and Pd77Ag23 containing lattice defects. J. Less-Common Met. 748 (1991) 172-174.

[39] N. Itoh, T. Akiha, T. Sato, Preparation of thin palladium composite membrane tube by a CVD technique and its hydrogen permselectivity. Catal. Today 104 (2005) 231-237.

[40] S.-E. Nam, K.-H. Lee, Hydrogen separation by Pd alloy composite membranes: introduction of diffusion barrier. J. Membr. Sci. 192 (2001) 177-185.

[41] G. Xomeritakis, Y. S. Lin, Fabrication of thin metallic membranes by MOCVD and sputtering, J. Membr.Sci.120 (1996) 217-230.

[42] S.K. Gade, P.M. Theon, J.D. Way, Unsupported palladium alloy foil membranes fabricated by electroless plating. J. Membr. Sci. 316 (2008) 112-118.

[43] H.-B. Zhao, K. Pflanz, J.-H. Gu, A.-W. Li, N. Stroh, H. Brunner, G.-X. Xiong, Preparation of palladium composite membranes by modified electroless plating procedure. J. Membr. Sci. 142 (1998) 147-157.

[44] M.L. Bosko, F. Ojeda, E.A. Lombardo, L.M. Cornaglia, NaA zeolite as an effective diffusion barrier in composite Pd/PSS membranes, J. Membr. Sci. 331 (2009) 57-65.

[45] G. Xomeritakis, Y. Lin, CVD synthesis and gas permeation properties of thin palladium/alumina membranes. AIChE J. 44 (1998) 174-183.

[46] C.-S. Jun, K.-H. Lee, Palladium and palladium alloy composite membranes prepared by metal-organic chemical vapor deposition method (cold-wall). J. Membr. Sci. 176 (2000) 121-130.

[47] S.-E. Nam, K.-H. Lee, A study on the palladium/nickel composite membrane by vacuum electrodeposition. J. Membr. Sci. 170 (2000) 91-99.

Chapter 4 . Ethanol Steam Reforming in a Membrane Reactor

4.1. Introduction

Hydrogen is commonly produced by the methane steam reforming (Me SR), coal gasification, oil or natural gas partial oxidation, and water electrolysis as discussed in chapter 1. Recently, much work has been reported for the ethanol steam reforming (EtOH SR), because there have been significant advances in its production from biomass, increasing the supply [1,2,3,4]. Compared to methane, this bio-ethanol can be reformed at a much lower temperature and is a CO_2-neutral energy source. The overall reaction of EtOH SR is as follows:

$$C_2H_5OH + 3H_2O \rightleftharpoons 6H_2 + 2CO_2 \qquad \Delta H^o_{298} = 174 \text{ kJ mol}^{-1} \qquad (4.1)$$

Ethanol reacts with water and produces hydrogen and carbon dioxide in a 3:1 ratio. It is expected that the highest ethanol conversion will be obtained at high temperature and low pressure because the reaction is endothermic and volume-increasing reactions. There are other possible reactions occurring with the main transformation [5]. These reactions are the water gas shift (eq. 4.2), ethanol decomposition (eq. 4.3), ethanol dehydrogenation (eq. 4.4), ethanol dehydration (eq. 4.5), acetaldehyde steam reforming (eq. 4.6), and acetaldehyde decomposition (eq. 4.7).

$$CO + H_2O \rightleftharpoons H_2 + CO_2 \qquad \Delta H^o_{298} = -41 \text{ kJ mol}^{-1} \qquad (4.2)$$

$$C_2H_5OH \rightleftharpoons CO + CH_4 + H_2 \qquad \Delta H^o_{298} = 50 \text{ kJ mol}^{-1} \qquad (4.3)$$

$$C_2H_5OH \rightleftharpoons CH_3CHO + H_2 \qquad \Delta H^o_{298} = 69 \text{ kJ mol}^{-1} \qquad (4.4)$$

$$C_2H_5OH \rightleftharpoons C_2H_4 + H_2O \qquad \Delta H^o_{298} = 46 \text{ kJ mol}^{-1} \qquad (4.5)$$

$$CH_3CHO + 3H_2O \rightleftharpoons 5H_2 + 2CO_2 \qquad \Delta H^o_{298} = 105 \text{ kJ mol}^{-1} \qquad (4.6)$$

$$CH_3CHO \rightleftharpoons CH_4 + CO \qquad \Delta H^o_{298} = -19 \text{ kJ mol}^{-1} \qquad (4.7)$$

Several studies report significant advances in high activity catalysts for the EtOH SR at relatively low temperatures in the range 573-673 K. Marino et al. [6] reported that the EtOH SR over a Cu-Ni-K/γ-Al_2O_3 catalyst produced substantial amounts of hydrogen at 100 kPa and 573 K at a gas hourly space velocity (GHSV) of 1500 h^{-1}. The highest ethanol conversion was found to be 82 % and the main products were H_2, CO, CH_4, CH_3CHO, and CH_3COOH. They claimed that nickel addition increased the gas yield and reduced by-products such as acetaldehyde and acetic acid. Llorca et al. [7] reported that a Co-Na/ZnO catalyst showed very stable activity over 240 h with the major products being H_2 and CO_2 together with small amounts of CH_4 and CO. They used a higher water-to-ethanol molar ratio (13:1) than stoichiometric (3:1) in the study, and found that the ethanol conversion was 100 % at a GHSV of 5000 h^{-1} at temperatures higher than 623 K. Diagne et al. [8] reported that a Rh/CeO_2-ZrO_2 catalyst at 573 K at a GHSV of 15,400 h^{-1} had high activity and selectivity for hydrogen, producing H_2, CO_2, CH_4 and CO with complete ethanol conversion. Sun et al. [9] reported that Ni nano-particles supported on Y_2O_3 gave an ethanol conversion was 98 % with products of H_2, CH_4, CO_2, CO, and CH_3CHO without deactivation of the catalyst for 66 h at 573 K at a GHSV of 1400 h^{-1}. Batista et al. [10] investigated the reaction with Co-based catalysts using SiO_2 or Al_2O_3 as support materials at 673 K at a GHSV of 17,400 h^{-1} and found an ethanol conversion

higher than 70 % with main products of H_2, CO_2, CH_4 and CO. They claimed that higher cobalt content led to the reduction of undesirable liquid products.

The development of membranes has led to numerous studies in the field because of the considerable potential advantages that MRs provide such as higher conversion and product yield, cost reduction for plant equipment and maintenance, and the opportunities of simplified separation and heat management [11,12]. Prabhu and Oyama [13] performed methane dry reforming (Me DR) with a 1 % Rh/Al_2O_3 catalyst at 848-973 K in a MR using a modified Vycor glass membrane. Higher conversions of CH_4 were achieved in the MR compared with a packed-bed reactor (PBR). Irusta et al. [14] carried out the Me DR with Rh/La_2O_3 and Rh/La_2O_3-SiO_2 catalysts at 823 K in a MR employing a commercial Pd-Ag alloy membrane. Conversion enhancement in CH_4 and CO_2 was observed exceeding equilibrium by more than 40 %. Tsuru et al. [15] conducted Me SR over a Ni catalyst at 773 K in a MR equipped with a microporous silica membrane, which had a H_2/N_2 selectivity ratio of 30-100. Increase in methane conversion from 44 to 80% by the use of the MR was reported. Tong et al. [16] investigated the Me SR over a Ni/Al_2O_3 catalyst at 773 K in a MR containing a Pd-Ag membrane prepared by a combination of electroless plating and electroplating. It was found that the CH_4 conversion in the MR was more than 3 times higher than in a traditional reactor. Basile et al. [17] investigated the methanol steam reforming (MeOH SR) reaction with a $CuO/ZnO/Al_2O_3$ catalyst at 523 K in a MR fitted with a dense Pd-Ag membrane. It was claimed that the use of the MR resulted in a methanol conversion enhancement from 45 to 50 % compared to a traditional reactor. A correlation between hydrogen permeation rate and hydrogen formation rate in a MR was presented by Oyama and Lim [18]. They

suggested that an operability level coefficient (OLC), defined as the ratio of product permeation and product formation rates, related to the inverse combination of the Damköhler unmber and the Peclet number (1/DaPe), could be a useful tool for estimating performances of membrane reactors operating as separators in equilibrium-limited reactions.

Despite the many studies of MRs, few studies have applied these for the EtOH SR. Lim et al. [1] found that in the EtOH SR over Co-Na/ZnO with a reactor equipped with a silica-alumina composite membrane the acetaldehyde product was suppressed whereas CO, CO_2 and CH_4 were enhanced. The different behavior occurred because acetaldehyde was a primary product, while the other specieswere secondary products, and this was confirmed by contact time studies. Tosti et al. [2] carried out a kinetic study of the EtOH SR over Ru, Pt, and Ni based catalysts equipped with a Pd-Ag membrane and analyzed the results using a power-rate law model. They presented an optimization of the membrane reformer based on a Damkohler-Peclet number analysis. Yu et al. [3] carried out the EtOH SR with a Pt-impregnated Knudsen membrane and the performance in the MR was compared to that in a conventional reactor. They reported that ethanol conversion and hydrogen yield was higher in the MR by 7-14 % and 4-10 %, respectively.

In this chapter, a study of the EtOH SR was carried out over a Co-Na/ZnO catalyst both in a packed bed reactor (PBR) and MRs equipped with ultrathin Pd or Pd-Cu membranes with different H_2 permeability. It was observed that, for all studies, ethanol conversion and hydrogen yield in the MRs were significantly higher than in the PBR. However a significant contamination of the Pd membrane by CO or carbon compounds adsorption was observed resulting in low enhancements of ethanol

conversion and hydrogen yield compared to the Pd-Cu membrane. A one-dimensional model for the EtOH SR was developed using a simplified power law model and predicted values matched experimental data with only minor deviations.

4.2. Experimental

4.2.1. Synthesis and characterization of Co-based catalysts

The Co-Na/ZnO catalysts were prepared by a co-precipitation method described elsewhere [7]. An aqueous solution of 0.1M Na_2CO_3 was added to a mixed aqueous solution of 0.1 M $Co(NO_3)_2 \cdot 6H_2O$ and 0.4 M $Zn(NO_3)_2 \cdot 6H_2O$ under vigorous stirring at 313 K for 1.5 h with a controlled pH of 8-9 using NH_4OH. The precipitated solution was then filtered and washed with water (volumetric ratio of precipitated catalyst to water = 1:2) to control the Na content. The filtered catalyst was dried for 12 h at 363 K and calcined for 12 h at 673 K. The calcined catalyst was ground, pressed, and sieved to a particle size of 0.85-1.18 mm (20/16 mesh). The prepared catalysts were characterized by elemental analysis, surface area determinations, and CO uptake measurements. Elemental analysis was carried out by inductively coupled plasma-atomic emission spectroscopy (ICP-AES, Spectroflame Model FTMO A85D). The BET surface area of the catalysts was observed in a volumetric adsorption apparatus (Micrometrics model ASAP2010). The irreversible CO uptake was carried out to count the metallic active sites on the surface of the catalyst in a pulse flow system equipped with a mass spectrometer (Dycor/Ametek Model MA 100) by monitoring CO^+ (m/e = 28) signal

resulting from the injection of pulses from a calibrated volume (19.6 µm). Before uptake measurements, all catalysts were reduced under H_2 flow for 2 h at 723 K and cooled to room temperature. X-ray diffraction (XRD) patterns of reduced catalysts were obtained using a PANalytical X'Pert powder diffractometer operated at 45kV and 40mA with Cu monochromatized radiation (wave length of the X-ray radiation (λ) = 0.154 nm) at a scan rate of 0.017 ^{o} s^{-1}

4.2.2. Preparation of the membranes

Pd and Pd-Cu alloy membranes were used in the MR study. The Pd membrane was prepared by an electric-field assisted activation technique followed by electroless plating, as described in our previous study [19]. In the case of the Pd-Cu membrane, the same technique used in the preparation of Pd membrane was applied for the activation, but a sequential electroless plating method described elsewhere [20] was carried out for the fabrication of the selective Pd-Cu layer using plating solutions of Pd and Cu (Table 4.1).

Table 4.1. Composition of plating solutions of palladium and copper

	Component	Concentration
Pd plating bath (1h, 333 K)	$PdCl_2$	4.0 g l^{-1}
	NH_4OH (28 wt %)	198ml l^{-1}
	Na_2EDTA	40g l^{-1}
	N_2H_4 (1.0 M) *	6.0 ml l^{-1}
Cu plating bath	$CuSO_4 \cdot 5H_2O$	30g l^{-1}

(40min, 298 K)	Na_2EDTA	60g l^{-1}
	HCHO (37 wt %) *	25ml l^{-1}
	NaOH	20g l^{-1}
	Tritron X-100	25 mg l^{-1}
	2.2-bipyridyl	5 mg l^{-1}

* added just before the use of each solution

4.2.3. Ethanol steam reforming (EtOH SR) reaction

The prepared catalysts were used for the EtOH SR reaction at atmospheric pressure in a PBR and a MR. Fig. 4.1 presents a schematic of the reactor system. The catalyst was placed in the shell side around the membrane to achieve sufficient heat transfer. In the case of the PBR, a dense alumina tube instead of the membrane was used to keep the geometry the same. The volume of catalyst bed was around 1 cm^3 and consisted of 0.57 g of catalyst with 0.64 g of quartz chips for dilution, in which a particle size of 0.85-1.18 mm was used for both the catalyst and the quartz chips. Quartz wool was placed at both ends of the catalyst bed to hold the catalyst securely in place. In all experiments, catalysts were reduced under H_2 with a flow rate of 20 cm^3 (NTP) min^{-1}) for 2 h at 723 K before reaction. A thermal couple was placed on the surface of the reactor around catalyst bed and was connected with a temperature controller to govern the reaction temperature.

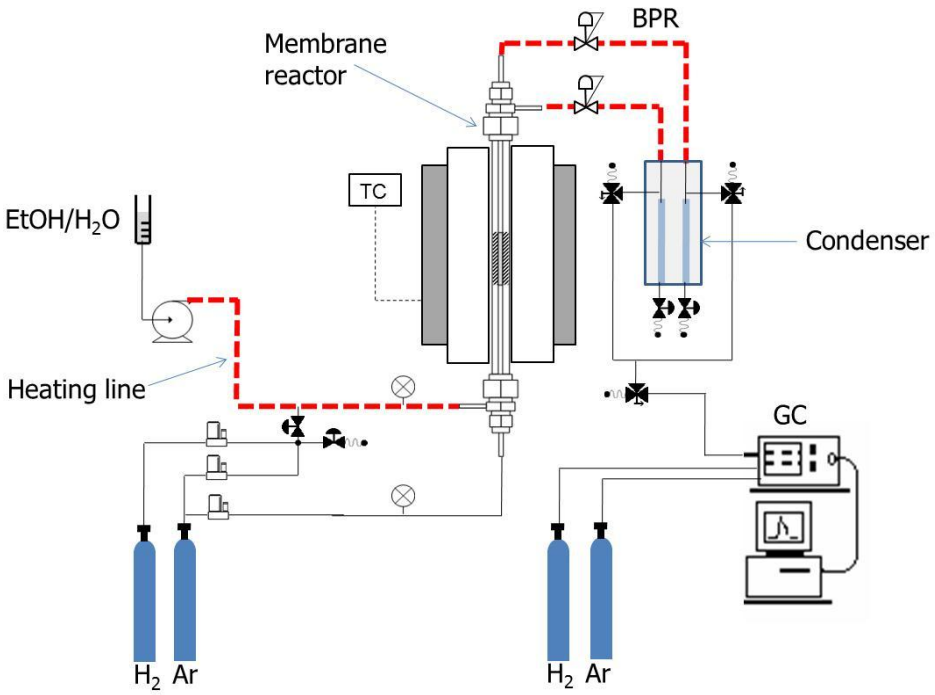

Figure 4.1. Schematic of the experimental system for EtOH SR reaction.

After reduction, the reactor was set to the desired reaction temperature, and a mixture of EtOH:H_2O = 1:4 in volume ratio (EtOH:H_2O = 1:13 molar basis) was supplied by a liquid pump (Lab Alliance Series I), vaporized at 423 K, and diluted with Ar before being introduced to the shell side of the reactor. During the reaction, liquid products were collected in a condensate trap filled with ice, sampled, and injected to a gas chromatography (SRI 8610C) and gas products were introduced online by the GC equipped with an automated injection valve. The composition of liquid products were measured with an AT ^{TM}-1000 column (1/8" OD × 6 ft) attached to a flame ionization detector (FID) and gas products were analyzed with a Carbosphere column (1/8" OD × 6 ft) connected to a thermal conductivity detector (TCD). The ethanol conversion was calculated from the ratio of ethanol consumed and ethanol fed into the reactor. Product

selectivity was calculated from the moles of each molecule divided by the total moles of all product molecules produced.

4.3. Results and discussion

4.3.1. Properties of Co-Na/ZnO catalysts

The properties of the catalyst are summarized in Table 2, which includes elemental analysis, BET surface area, CO uptake and dispersion percentage of the Co (D). The dispersion of the Co metal on the catalyst was calculated based on the CO uptake (eq. 4.8)

$$D\ (\%) = \frac{Co\ atoms\ at\ the\ surface}{total\ Co\ atoms} = \frac{(CO\ uptake)(MW_{Co})}{Co\ wt\ \%} \times 100 \qquad (4.8)$$

Table 4.2. Properties of the Na-Co/ZnO catalyst

	Na / wt%	Co / wt%	BET / $m^2\ g^{-1}$	CO uptake / $\mu mol\ g^{-1}$	D / %
Catalyst	2	17	41	20	0.68

X-ray diffraction (XRD) patterns of the reduced catalysts are shown in Fig. 4.2.
The XRD patterns of reduced catalysts are compared with those of standards from the Powder Diffraction File (PDF) [21] and show the presence of metallic cobalt (44.2^{o}) and ZnO phases.

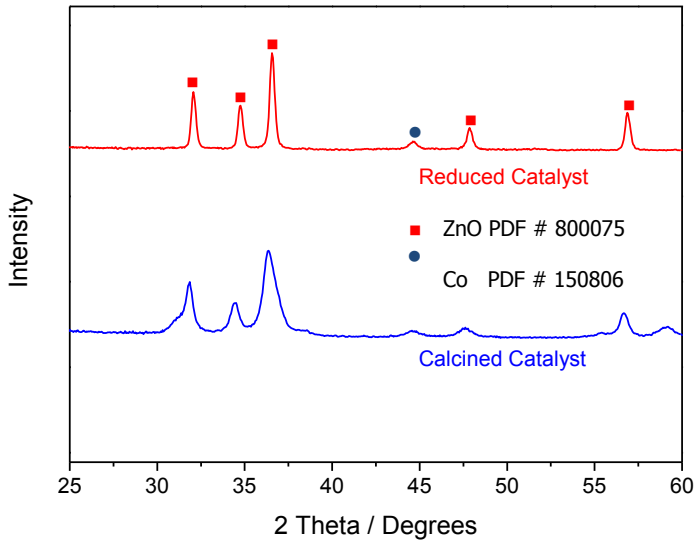

Figure 4.2. X-ray diffraction patterns of calcined and reduced Na-Co/ZnO catalyst.

4.3.2. Studies of the EtOH SR reaction in PBR

To investigate the effects of temperature and space velocity (SV) on the EtOH SR reaction, the catalyst was first studied in the PBR. The thermodynamic equilibrium conversion was found to be 99 % at 623 K (Appendix B). Ethanol conversion, selectivity, and SV were calculated from the following equations.

$$Ethanol\ conversion\ [\%] = \frac{Mol\ ethanol\ in\ feed - Mol\ ethanol\ in\ product}{Mol\ ethanol\ in\ feed} \times 100 \quad (4.9)$$

$$Selectivity\ of\ product\ i\ [\%] = \frac{Mol\ of\ product\ i}{Mol\ of\ total\ products} \times 100 \quad (4.10)$$

$$SV\ [h^{-1}] = \frac{Volumetric\ flow\ rate\ of\ feed\ and\ Ar\ at\ NTP\ [cm^3 h^{-1}]}{Catalyst\ volume\ [cm^3]} \quad (4.11)$$

The ethanol conversion at different temperatures in the SV range of 6000 – 12500 is shown in Fig. 4.3. Ethanol conversion was proportional to temperature and inversely proportional to space velocity. For example, increasing the temperature from 623 to 693 K at a fixed space velocity of 9800 increased the ethanol conversion from 35 to 88 % and decreasing SV from 12,600 to 6400 increased the conversion from 30 to 60 % at 623 K. The H_2 and CO_2 selectivity were around 69 and 24 %, respectively, which indicates that the ratio of H_2/CO_2 is close to a stoichiometric ratio of 3 in the overall reaction ($C_2H_5OH + 3H_2O \rightleftharpoons 6H_2 + 2CO_2$).

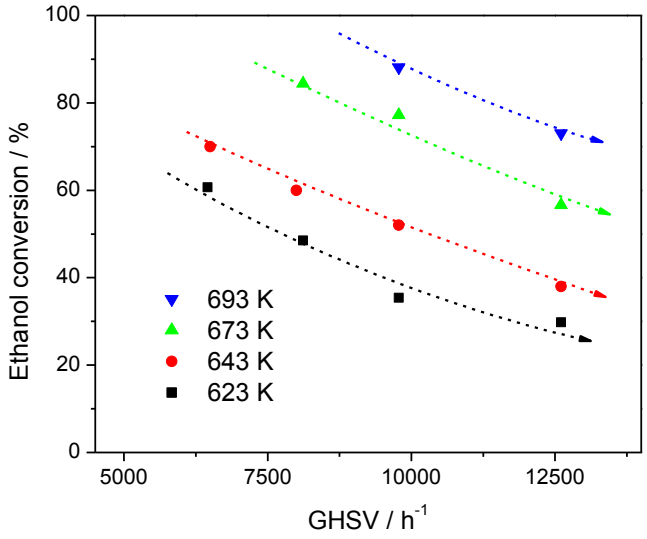

Figure 4.3. Ethanol conversion with different SVs and temperatures in the PBR.

The effect of temperature on product selectivity was evaluated at the same space velocity of 9800 and at 1 atm (Fig. 4.4a). The amount of the main products H_2 and CO_2 was found not to be highly dependent on the temperature but the selectivity to minor products such as CO and CH_4 steadily increased while the selectivity of CH_3CHO

continuously decreased as temperature was raised, which is in agreement with the results of a previous study [1]. The reduced selectivity of CH_3CHO and the favored selectivity to CO and CH_4 with increasing temperature can be attributed to the acceleration of acetaldehyde decomposition ($CH_3CHO \rightleftharpoons CO + CH_4$) at high temperatures. However, the effect of temperature on CH_4 selectivity is contrary to the results of Mas et al. [22]. They found that selectivity to CH_4 decreased with increasing temperature and attributed this to Me SR becoming important at high temperature. This may have been due to their use of a Ni catalyst. The effect of SV on the product selectivity was also examined at 623 K and at 1atm (Fig. 4.4b). The selectivity to the main products H_2 and CO_2 slightly decreased from 70 to 67 % and 25 to 23 % as SV increased. The selectivity to the minor products CO, CH_4, and CH_3CHO increased from 1.0 to 1.7 %, 2.6 to 4.0 %, and 1.8 to 4.7 %, respectively, with increasing SV.

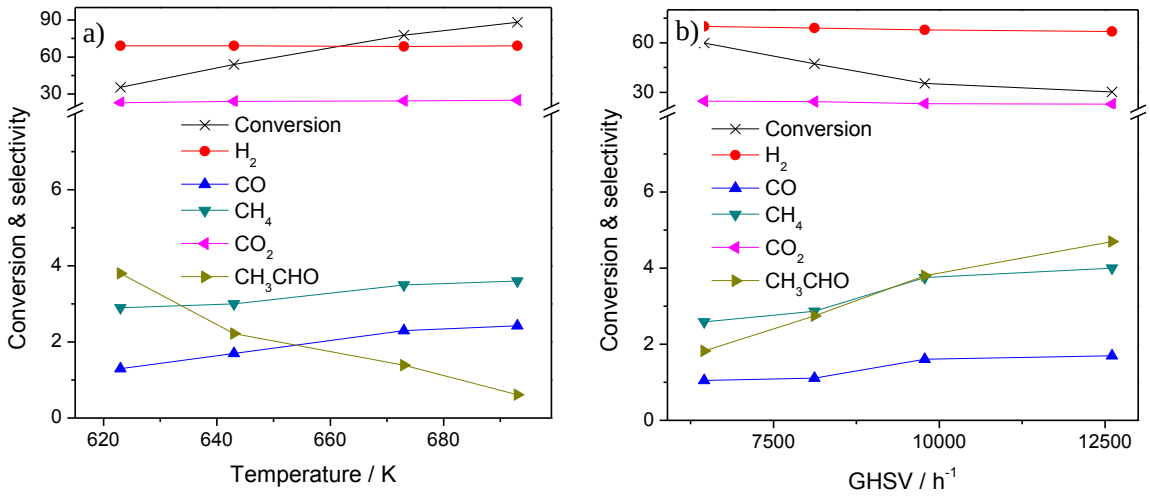

Figure 4.4. Conversion and selectivity versus a) temperature and b) space velocity.

4.3.3. Studies of the EtOH SR reaction in MR

To evaluate the benefit of using a membrane in the production of H_2, the reaction was carried out in the MR using Pd or Pd-Cu membranes and the results were compared with those from the PBR. The membrane properties used in this study are summarized in Table 4.3.

Table 4.3. Properties of Pd or Pd-Cu membranes used in the MR measured at 733 K and 105 kPa

Membrane	Thickness µm	Permeance [1] mol $m^{-2}Pa^{-1}s^{-1}$	Selectivity H_2/N_2	Permeance [2] mol $m^{-2}Pa^{-1}s^{-1}$	Selectivity [3] H_2/N_2
Pd	1.3	4.0×10^{-6}	5500	8.0×10^{-7}	> 160
Pd-Cu (20 wt% Cu)	2	2.5×10^{-6}	970	1.5×10^{-6}	> 220

[1] Before reaction [2] After reaction [3] Lower limit estimated from gas-chromatographic sensitivity

Respective H_2 permeances of 4.0×10^{-6} and 2.5×10^{-6} mol $m^{-2}s^{-1}$ Pa^{-1} at 733 K were obtained with respective H_2/N_2 selectivities of 5500 and 970 for Pd and Pd-Cu membranes. It was found that H_2 permeance of the Pd and Pd-Cu membranes was proportional to temperature before use in the reaction (Fig. 4.5).

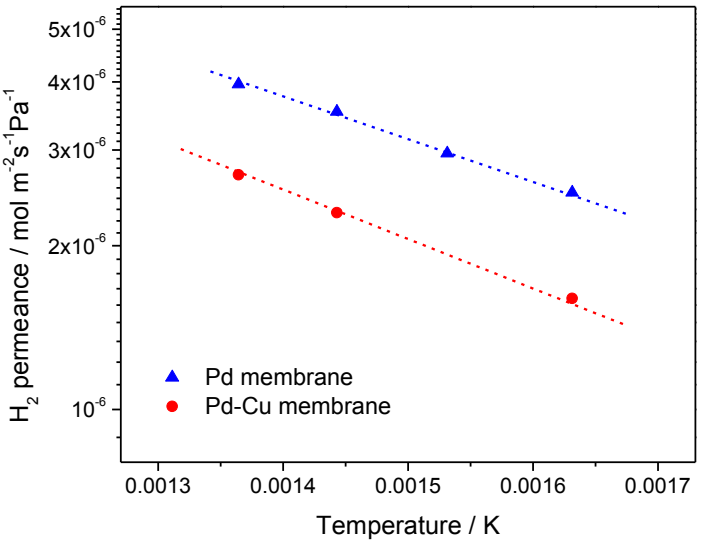

Figure 4.5. H_2 permeance of Pd and Pd-Cu membranes as a function of temperature.

The thickness of the Pd and Pd-Cu layers was measured to be ~ 1.3 and ~ 2 µm, respectively by SEM (Fig. 4.6a,b) and the Cu composition in the Pd-Cu layer was found to be 20 wt% by SEM-EDS. An X-ray mapping image of the surface of the Pd-Cu layer after heat treatment with Ar flow at 773 K for 6 h showed that a homogeneous Pd-Cu alloy layer was formed (Fig 4.6c).

For comparison, the same experimental conditions were used in the EtOH SR reactions described in Table. 4.4. To minimize pressure drop in the catalyst bed, the catalyst was pressed and sieved to a narrow particle size of 0.85-1.18 mm. The enhancement of ethanol conversion and H_2 yield were calculated as follows:

$$\textit{Conversion enhancement } (\Delta X, \%) = \frac{Conversion\ in\ MR - Conversion\ in\ PBR}{Conversion\ in\ PBR} \times 100 \qquad (4.12)$$

$$\textit{H}_2\textit{ yield enhancement } (\Delta H_2, \%) = \frac{H_2\ molar\ flow\ in\ MR - H_2\ molar\ flow\ in\ PBR}{H_2\ molar\ flow\ in\ PBR} \times 100 \qquad (4.13)$$

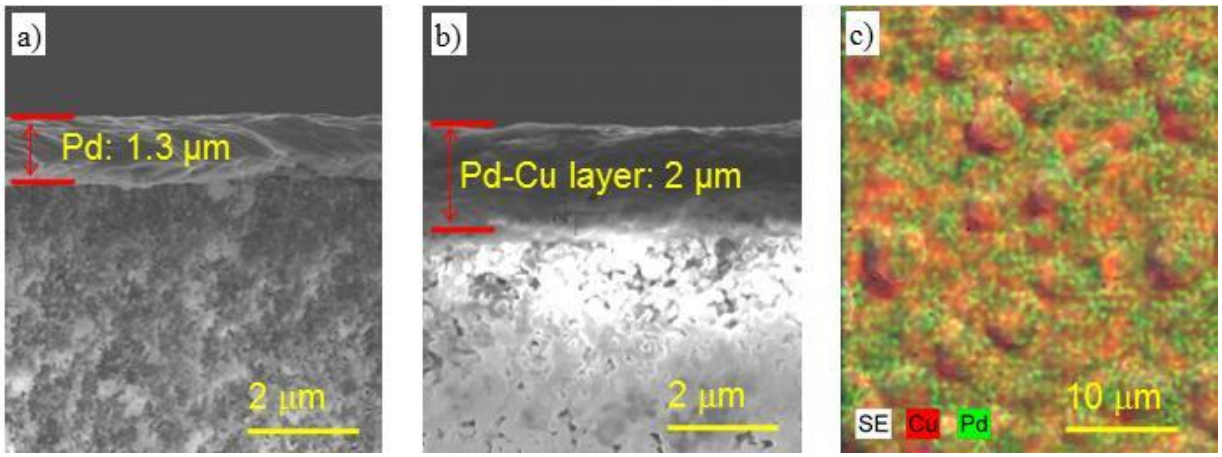

Figure 4.6. SEM images of the cross section of the Pd membrane (a) and the Pd-Cu membrane (b), respectively and X-ray mapping image of the surface of the Pd-Cu layer (c).

Table 4.4. Reaction conditions in the MR and PBR

	Condition	Comments
H_2O/EtOH	13	Mol ratio
Ar	20 cm^3 (NTP) min^{-1}	For dilution
Total feed rate	6.2×10^{-4} mol min^{-1}	-
GHSV	5100 h^{-1}	-
Catalyst	0.56 g	-
Quartz chips	0.66 g	For dilution of catalytic bed
Catalyst/quartz chip	1	Volume ratio
Temperature	553 – 633 K	Increase with time [a]
Pressure	1 atm	-
Ar sweep gas	20 cm^3 (NTP) min^{-1}	For MRs

[a] Order of experiments:553 K (15 h) → 573 K (5 h) → 593 K (15 h) → 613 K (5 h) → 633 K (5 h)

As shown in Fig. 4.7, for all studies, both ethanol conversion and H_2 molar flow were found to be proportional to temperature. Increasing the temperature from 553 to 633 K increased the ethanol conversion from 23 to 53 %, 26 to 58 %, and 31 to 74 % for the PBR, the Pd MR, and the Pd-Cu MR, respectively. As temperature was raised the product H_2 molar flow also grew from 0.4 to 2.0 µmol s^{-1} for the PBR, 0.5 to 2.3 µmol s^{-1} for the Pd MR, and 0.4 to 2.5 µmol s^{-1} for the Pd-Cu MR. However, in the case of the MRs, ethanol conversion and H_2 molar flow were higher compared with the values in the PBR. It was found that the average ethanol conversion enhancements and H_2 yield enrichment were 12 % and 11 % in the Pd MR and 22 % and 19 % in the Pd-Cu MR, respectively.

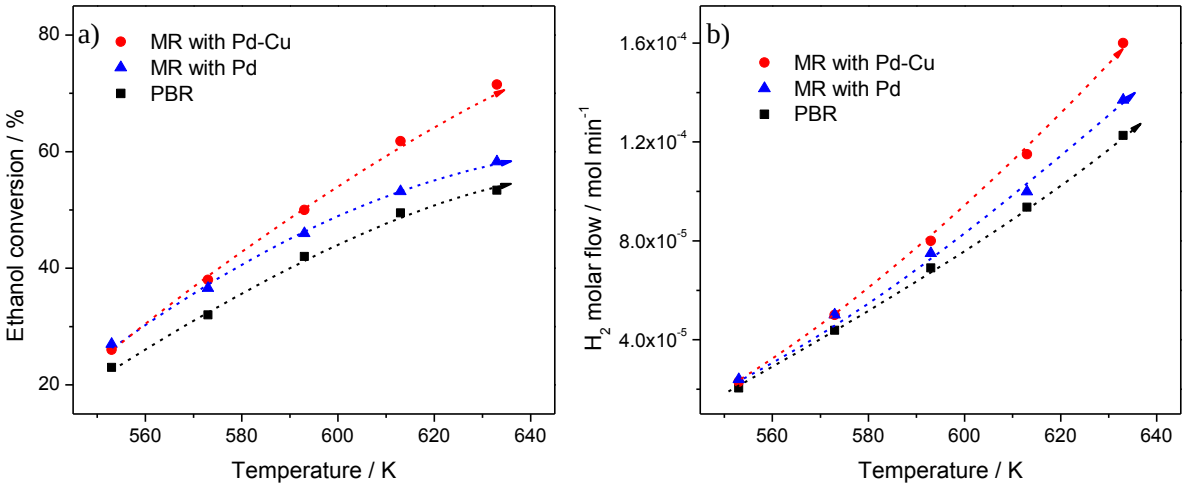

Figure 4.7. Ethanol conversion a) and H_2 molar flow rate b) in PBR and MRs at 1 atm.

The enhanced ethanol conversion and H_2 yield for the MRs are shown as a function of temperature (Fig. 4. 8). The enhancement is attributed to the shift of the reaction equilibrium to the right by removal of the product H_2 through the Pd or Pd-Cu

membrane [18]. It is reasonable for the enhancement to be proportional to the temperature because of the accompanying increase in H_2 permeance. The enhanced values in the Pd MR should have been higher than those in the Pd-Cu MR due to the higher H_2 permeance of the Pd membrane. The enhanced values grew with increasing temperature for the Pd-Cu MR, while such dependence was not observed for the Pd MR. In addition, the values were higher in the Pd-Cu membrane than in the Pd membrane. The low enhancement in the Pd MR compared with in the Pd-Cu MR can be attributed to the catalytic poisoning of the Pd surface by CO adsorption or carbon compound deposition during the reaction, which decreases the actual permeation rate of the Pd membrane [23,24].

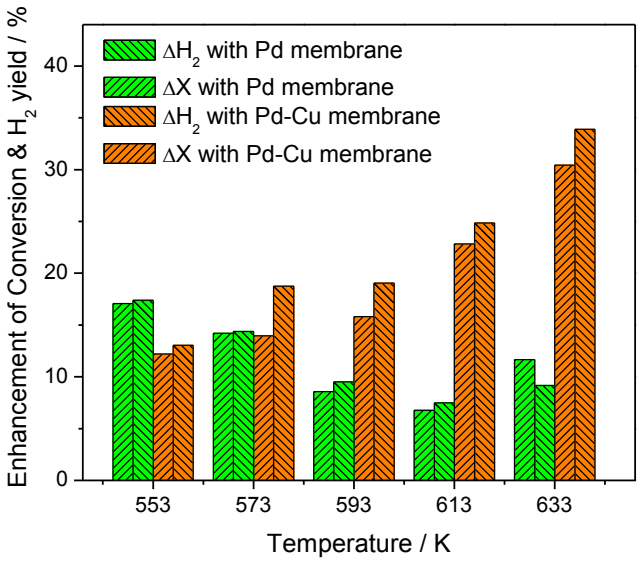

Figure 4.8. Enhanced conversion and H_2 yield in the Pd and the Pd-Cu MRs.

Compared to the poisoning effect of CO in Pd membrane, the propensity of decreasing H_2 permeability can be suppressed in Pd-Cu membranes [25]. Adsorption of CO or

carbon compounds on the surface of a Pd-Cu layer is different from that on a pure Pd surface due to the difference in surface reactivity and electronic structure between pure metal and alloy materials [25].

Hydrogen permeances of the Pd and the Pd-Cu membranes during the reaction were measured using hydrogen partial pressure difference between the retentate side and permeate side at the reaction temperature. The degree of deterioration of the permeance at a given temperature was expressed (Fig. 4.9) using the active H_2 permeance, which was defined as follows:

$$\text{Active } H_2 \text{ permeance (\%)} = \frac{H_2 \text{ permeance in the course of reaction}}{H_2 \text{ permeance before the reaction}} \times 100 \qquad (4.14)$$

As seen in Fig. 4.9, both the H_2 permeance of the Pd and the Pd-Cu layers were rapidly reduced after an initial time period of about 6 h. However, the H_2 permeance of the Pd membrane steadily decreased to 20% of the fresh layer with time, while the value of the Pd-Cu membrane was maintained at around 60 % of the fresh layer after the initial rapid drop. The initial decrease of H_2 permeance of the Pd-Cu layer could be the result of the adsorption of water vapor on the surface of the layer [26,27,28]. In spite of the high H_2 permeance of the Pd membrane compared to that of the Pd-Cu membrane before reaction, the H_2 permeance was found to be lower in the Pd MR than in the Pd-Cu MR; the permeance in the Pd MR was 5.5×10^{-7} mol $m^{-2}s^{-1}Pa^{-1}$ and that in the Pd-Cu MR was 1.0×10^{-6} mol $m^{-2}s^{-1}Pa^{-1}$ at 633 K during the reaction. This observation in the MRs is consistent with comparative low enhancements of ethanol conversion and H_2 yield for the Pd MR.

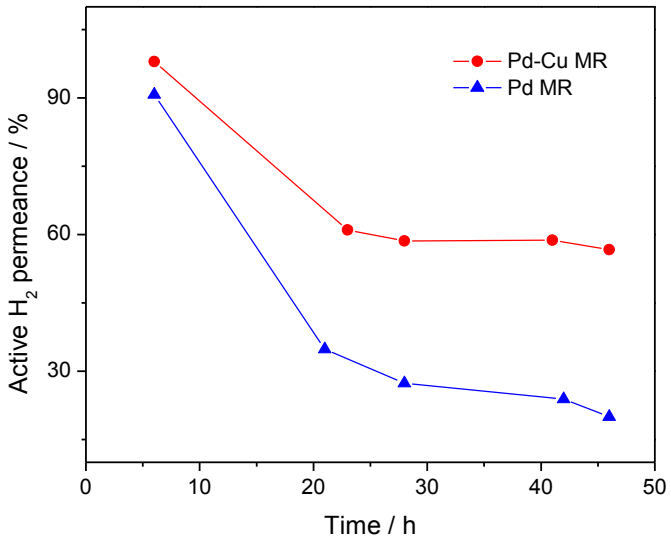

Figure 4.9. Active H_2 permeance of the Pd and the Pd-Cu membranes in the MRs as a function of time.

A different deterioration of the Pd and the Pd-Cu layer was also observed by measuring SEM for each layer before and after reaction (Fig. 4.10). Defects or pin-holes were not observed in both the Pd and the Pd-Cu layer before the reaction even though the surface of the Pd-Cu layer was slightly rougher than that of the Pd layer. However, significant defects around the metal grains were detected after reaction in the case of the Pd layer while a few openings were observed in the case of the Pd-Cu layer. These imperfections were probably restricted to the surface as gas chromatographic analysis of the permeate during reaction revealed only the presence of hydrogen, indicating that both Pd and Pd-Cu membranes retained their bulk integrity.

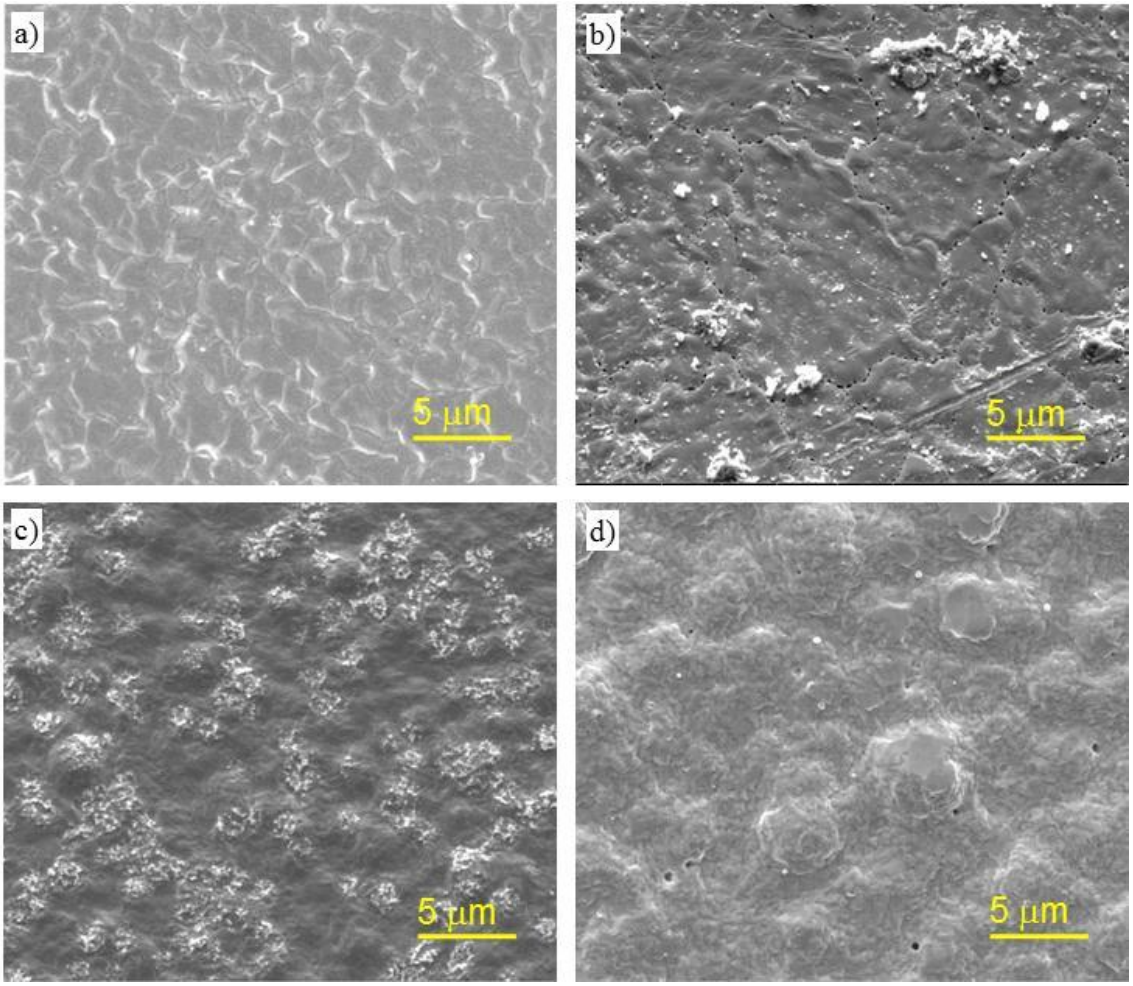

Figure 4.10. Comparison between the Pd layer before a) and after b) use in the EtOH SR reaction and the Pd-Cu layer before c) and after d) use in the same reaction.

The effect of temperature on product selectivity of the Pd and Pd-Cu membrane reactor was revealed in Fig. 4.11 and was found to be the same as in the PBR. The main products H_2 and CO_2 slightly decreased but the selectivity to minor products such as CO and CH_4 steadily increased while the selectivity to CH_3CHO continuously decreased as temperature increased. The reduced selectivity of CH_3CHO and the increasing selectivity to CO and CH_4 with increasing temperature can be attributed to the

acceleration of the acetaldehyde decomposition ($CH_3CHO \rightleftharpoons CO + CH_4$) as discussed earlier.

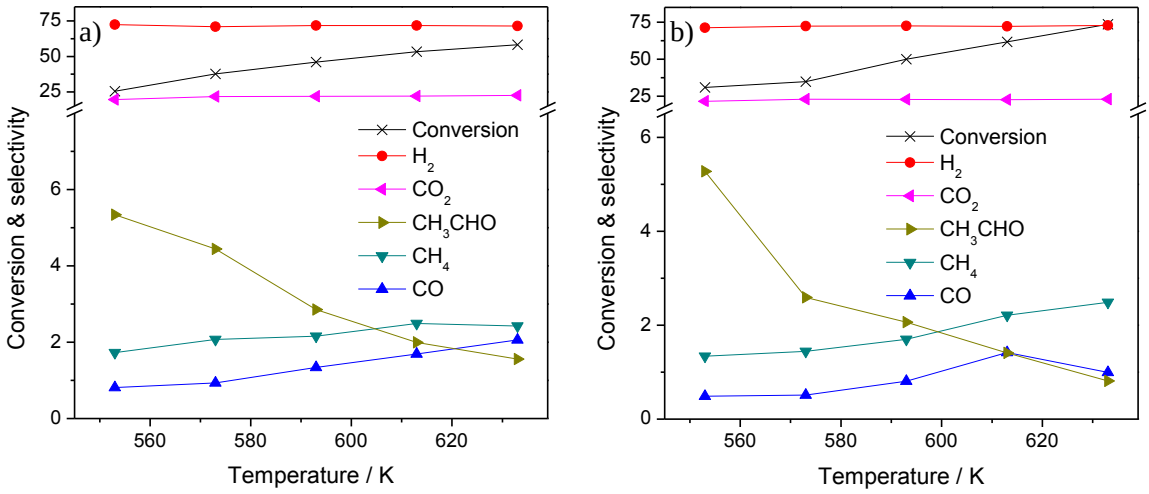

Figure 4.11. Effect of temperature on the ethanol conversion and product selectivity in the MR with a) the Pd membrane b) the Pd-Cu membrane.

4.3.4. Kinetic Analysis of EtOH SR Reaction

In a packed bed reactor, the rate of ethanol consumed can be described as follows:

$$r_{EtOH}[\text{mol gcat}^{-1}\text{s}^{-1}] = F_{EtOH0}[\text{mol s}^{-1}]\frac{dX}{dW} \quad (4.15)$$

The overall reaction rate of EtOH SR (r_{EtOH}) can be expressed as a turnover frequency (TOF) based on active sites measured by the chemisorption of CO. The dependence of the rate or TOF on partial pressure can be described by a power-rate law expression (eq. 4.18).

$$r_{EtOH} = TOF_{EtOH}\, D\, \frac{1}{MW_{Co}}\, \frac{\%\, Co}{100} \quad (4.16)$$

$$TOF = \frac{Flow\ rate\ of\ reactant\ [mol\ s^{-1}] \times Conversion of\ the\ reactant}{Quantity\ of\ active\ sites\ on\ the\ catalyst\ surface\ [mol\ g^{-1}] \times Catalyst\ weight\ [g]} \quad (4.17)$$

$$TOF = k_0 e^{-\frac{E_a}{RT}} (p_{EtOH})^{\alpha} (p_{water})^{\beta} \quad (4.18)$$

In these expressions k_0 is the frequency factor, E_a is the activation energy, R is the gas constant, T is the temperature, p_{EtOH} and p_{water} are the partial pressure of ethanol and water, and α and β are the orders with respect to ethanol and water partial pressure, respectively. In particular, several kinetic studies reported that the reaction rate could be described as depending only on the ethanol partial pressure (eq. 4.19) when water was in excess [2,4,29]. In this study the ethanol/water fed molar ratio was13, which satisfies the condition.

$$TOF = k e^{-\frac{E_a}{RT}} (p_{EtOH})^{\alpha} \quad (4.19)$$

where k [$Pa^{-\alpha}\ s^{-1}$] is lumped constant ($k_0 (p_{water})^{\beta}$)

The rate expression for ethanol conversion was determined by nonlinear least squares regression analysis (Levenberg-Marquardt algorithm with Polymath 5.1) of the experimental kinetic data (Fig. 4.3) measured in the PBR. The method minimizes the sum of squares of the errors between the empirical and the estimated values. The rate of ethanol conversion using all the data was found to be:

$$TOF\ (EtOH) = 0.351 exp(-\frac{45810}{RT}) {p_{EtOH}}^{0.86} \quad (4.20)$$

$$r_{EtOH} = 7.1 \times 10^{-6} exp(-\frac{45810}{RT}) {p_{EtOH}}^{0.86} \quad (4.21)$$

The fitting analysis resulted in a R^2 degree of fit and variance values of 0.92 and 3.57×10^{-5}, respectively. The reaction order with respect to ethanol and apparent activation

energy were found to be 0.86 ± 0.3 and 46 ± 4 kJ mol^{-1}, respectively. The exponent for the ethanol partial pressure is consistent with values of 0.5 – 1.0 described in the literature [2,4,29] and the activation energy is similar to a reported value [1]. The comparison between predicted ethanol conversion and experimental results as a function of SV at various temperatures is shown in Fig. 4.12. The experimental values fall along the predicted line for the range of conditions.

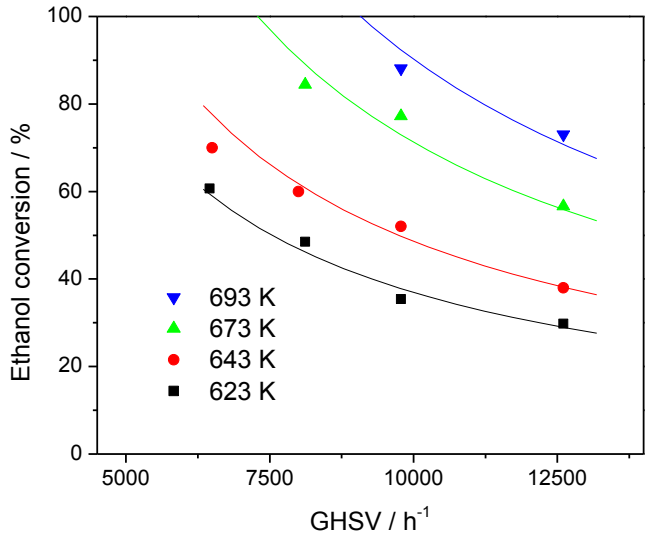

Figure 4.12. Experimental (symbol) and simulated (solid line) results for ethanol conversion vs. SV at various temperatures for a PBR.

In a membrane reactor, the rate of permeation of species *i* can be described as follows:

$$R_i = \frac{P_i A}{W}(p_i - p_i^{sweep}) \quad (4.22)$$

where P_i is the permeance of species i, A is the membrane area, and p_i and p_i^{sweep} are the partial pressure in the retentate (bed) and permeate (sweep) sides. Assuming that only H_2 can permeate through the membrane leads to the following mass balance equations:

$$\frac{dF_{EtOH}}{dw} = -r_{EtOH} \tag{4.23}$$

$$\frac{dF_{H_2}}{dw} = 6r_{EtOH} - R_{H_2} \tag{4.24}$$

$$\frac{dF_{CO_2}}{dw} = 2r_{EtOH} \tag{4.25}$$

$$\frac{dF_{H_2O}}{dw} = -3r_{EtOH} \tag{4.26}$$

$$\frac{dF_{H_2^{sweep}}}{dw} = R_{H_2} \tag{4.27}$$

It should be noted that these equations were derived with the following assumptions: the reaction operated at steady state conditions, pressure losses were negligible through the catalyst bed, no radial concentration gradients existed, and the permeation rate was linear in pressure difference.

A one-dimensional reaction model for a MR was developed using the parameters measured and reaction rate obtained from the PBR (Table 4.5). It was found that the developed model could be used to estimate the conversion and H_2 molar flow for the Pd and the Pd-Cu MRs. To take into account the H_2 permeance of the membranes exposed to ethanol reformate, the final active H_2 permeances were used.

Table 4.5. Parameter values and rate expressions used in one-dimensional membrane reactor model.

Parameters/ reaction rates	
r_{EtOH} [mol gcat^{-1}s^{-1}]	$7.1 \times 10^{-6} exp(-\frac{45810}{RT}) {p_{EtOH}}^{0.86}$
R_{H_2} [mol gcat^{-1}s^{-1}]	$\frac{P_{H_2} A}{W}(p_{H_2} - p_{H_2}^{sweep})$
P_{H_2} [mol m^{-2}s^{-1}Pa^{-1}] for Pd	0.2 × (1.2×10^{-8} T [K] – 5.1×10^{-6}) [a]
P_{H_2} [mol m^{-2}s^{-1}Pa^{-1}] for Pd-Cu	0.6 × (9.0×10^{-9} T [K] – 4.0×10^{-6}) [b]
A [m^{-2}]	2.3 × 10^{-4}
W [g]	0.57

[a] 20 % of the values obtained by a regression of permeance data of the Pd membrane in Fig. 4.5

[b] 60 % of the values obtained by a regression of permeance data of the Pd-Cu membrane in Fig. 4.5

Ethanol conversions in a PBR and a MR at various temperatures were predicted using the developed reactor model and compared with the experimental data (Fig. 4.13a). For the range of experiments, calculated values from the model were in agreement with the measured values with only a minor deviation. As expected, the ethanol conversion predicted from the model increased with increasing temperature but decreased with increasing SV. However, the enhancement of ethanol conversion and H_2 yield in the MR interestingly increased both with temperature and with SV. Again, the higher conversion in MR at all temperatures can be explained by the continuous removal of hydrogen during the reactions resulted in a shift of equilibria to the products. The hydrogen removal rate increased due to the increasing permeability with increasing temperature,

which is in a good agreement with the enhancement of conversion and H_2 yield with increasing temperature (Fig. 4.13b). The enhancements with SV were also reasonable because the decrease of conversion in a MR with increasing SV is less than that in a PBR. At conditions with the same molar ratio of ethanol/water and the same flow rate of Ar regardless of SV, the conversion both in the PBR and the MRs decreased with increasing SV due to the increasing partial pressure of ethanol. However, the increase in ethanol partial pressure in the MR is relatively less than that in a PBR as SV increased because the hydrogen removal rate is linearly proportional to hydrogen partial pressure difference that increases with increasing SV.

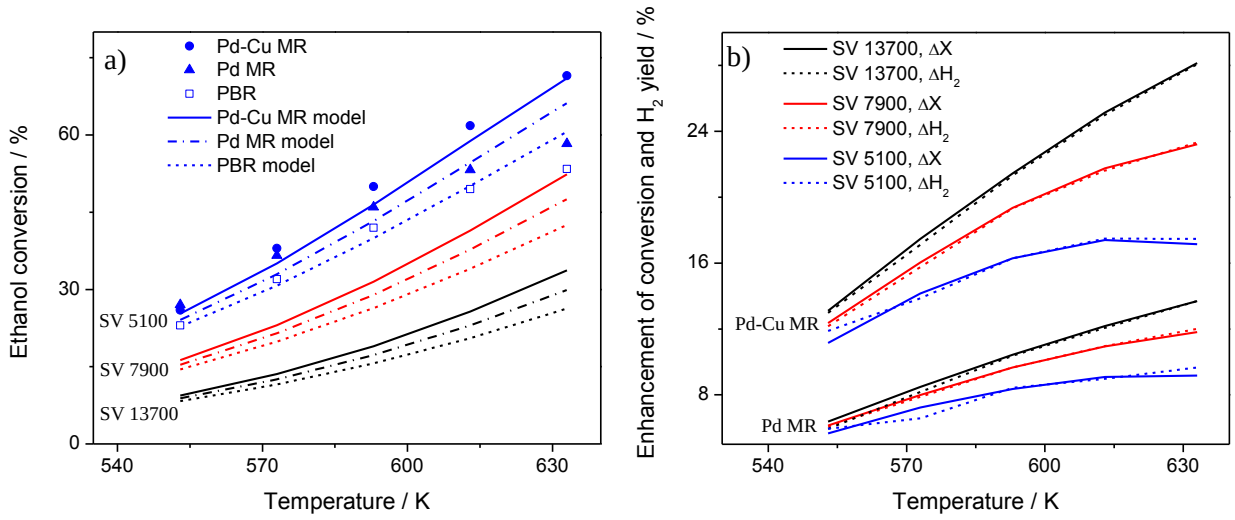

Figure 4.13. Experimental (symbol) and predicted values (solid or dashed line) a) ethanol conversion and b) enhancement of ethanol conversion and hydrogen yield.

4.4. Conclusions

The Pd (1.3 μm) and Pd-Cu (2 μm) membranes prepared by the electric-field assisted activation followed by electroless plating on a hollow-fiber α-alumina support were combined with a fixed bed reactor to carry out the EtOH SR reaction over a Co-Na/ZnO catalyst prepared by a co-precipitation method. The performance of these Pd and Pd-Cu MRs was compared to that of a PBR under identical conditions. According to the shift in equilibria to the products during the reaction by the consecutive removal of H_2 through the membranes, the average ethanol conversion increased by around 12 % in the Pd MR and 22 % in the Pd-Cu MR. The average H_2 yields for the Pd MR and the Pd-Cu MR were 11% and 19 % higher, respectively, compared to that for the PBR. In spite of a higher H_2 permeance of the Pd membrane compared to the Pd-Cu membrane, the low enhancement in the Pd MR was attributed to the significant deterioration of the Pd layer by CO or carbon compound adsorption on the membrane surface, which was suppressed on the Pd-Cu alloy surface. The ethanol conversion and hydrogen yield both in the MRs and the PBR were also compared with the predicted values from a one-dimensional reactor model developed using a power law model. The estimated values from the developed model were well matched with experimental data both in the PBR and the MRs. The predicted conversion and H_2 yield enhancement was found to increase with increasing SV, which can be explained by the different ethanol partial pressures in the MRs and the PBR.

References

[1] H. Lim, Y. Gu, S. T. Oyama, Reaction of primary and secondary products in a membrane reactor: Studies of ethanol steam reforming with a silica–alumina composite membrane, J. Membr. Sci. 351 (2010) 149-159.

[2] S. Tosti, A. Basile, R. Borelli, F. Borgognoni, S. Castelli, M. Fabbricino, F. Gallucci, C. Licusati, Ethanol steam reforming kinetics of a Pd–Ag membrane reactor, Int. J. Hydrogen Energy 34 (2009) 4747-4754.

[3] C.-Y. Yu, D.-W. Lee, S.-J. Park, K.-Y. Lee, K.-H. Lee, Ethanol steam reforming in a membrane reactor with Pt-impregnated Knudsen membranes, Appl. Catal. B: Environ. 86 (2009) 121-126.

[4] M. Veronica, B. Graciela, A. Norma, L. Miguel, Ethanol steam reforming using Ni(II)-Al(III) layered double hydroxide as catalyst precursor kinetic study, Chem. Eng. J. 138 (2008) 602-607.

[5] J. M. Guil, N. Homs, J. Llorca, P. R. de la Piscina, Microcalorimetric and infrared studies of ethanol and acetaldehyde adsorption to investigate the ethanol steam reforming on supported cobalt catalysts, J. Phys, Chem. B 109 (2005) 10813-10819.

[6] F. Marino, M. Boveri, G. Baronetti, M. Laborde, Hydrogen production from steam reforming of bioethanol using Cu/Ni/K/γ-Al_2O_3 catalysts. Effect of Ni, Int. J. Hydrogen Energy 26 (2001) 665-668.

[7] J. Llorca, N. Homs, J. Sales, J.L.G. Fierro, P.R. de la Piscina, Effect of sodium addition on the performance of Co-ZnO based catalysts for hydrogen production from bioethanol, J. Catal. 222 (2004) 470-480.

[8] C. Diane, H. Idriss, A. kiennemann, Hydrogen production by ethanol reforming over Rh/CeO_2-ZrO_2 catalysts, Catal. Commun. 3 (2002) 565-571.

[9] J. Sun, X. Qiu, F. Wu, W. Zhu, W. Wang, S. Hao, Hydrogen from steam reforming of ethanol in low and middle temperature range for fuel cell application, Int. J. Hydrogen Energy 29 (2004) 1075-1081.

[10] M.S. Batista, R.K.S. Santos, E.M. Assaf, J.M. Assaf, E.A. Ticianelli, High efficiency steam reforming of ethanol by cobalt-based catalysts, J. Power Sources 134 (2004) 27-32.

[11] P. Quicker, V. Höllein, R. Dittmeyer, Catalytic dehydrogenation of hydrocarbons in palladium composite membrane reactors, Catal. Today 56 (2000) 21-34.

[12] H. Lim, Ph.D. Dissertaiton; Virginia Polytechnic Institute and State University; Blacksburg, Virginia, US, 2007.

[13] A.K. Prabhu, S.T. Oyama, Highly hydrogen selective ceramic membranes: application to the transformation of greenhouse gases, J. Membr. Sci. 176 (2000) 233-248.

[14] S. Irusta, J. Munera, C. Carrara, E.A. Lombardo, L.M. Cornaglia, A stable, novel catalyst improves hydrogen production in a membrane reactor, Appl. Catal. A: General 287 (2005) 147-158.

[15] T. Tsuru, K. Yamaguchi, T. Yoshioka, M. Asaeda, Methane steam reforming by microporous catalytic membrane reactors, AIChE J. 50 (2004) 2794-2805.

[16] J. Tong, L. Su, Y. Kashima, R. Shirai, H. Suda, Y. Matsumura, Simultaneously depositing Pd−Ag thin membrane on asymmetric porous stainless steel tube and application to produce hydrogen from steam reforming of methane, Ind. Eng. Chem. Res. 45 (2006) 648-655.

[17] A. Basile, F. Gallucci, L. Paturzo, A dense Pd/Ag membrane reactor for methanol steam reforming: Experimental study, Catal. Today 104 (2005) 244-250.

[18] S. T. Oyama, H. Lim, An operability level coefficient (OLC) as a useful tool for correlating the performance of membrane reactors, Chem. Eng. J. 151 (2009) 351-358.

[19] S. Yun, J.H. Ko, S.T. Oyama, Ultrathin palladium membranes prepared by a novel electric filed assisted activation, J. Membr. Sci. 369 (2011) 482-489.

[20] Y.H. Ma, I.P. Mardilovich, E.E. Engwall, Thin composite palladium and palladium/alloy membranes for hydrogen separation, Ann. N.Y. Acad. Sci. 984 (2003) 346-360.

[21] "Powder Diffraction Data Files" JCPDS International Center for Diffraction Data, swathmore, PA, 1992.

[22] V. Mas, M.L. Bergamini, G. Baronetti, N. Amadeo, M. Laborde, A kinetic study of ethanol steam reforming using a nickel based catalyst, Top. Catal. 51 (2008) 39-48.

[23] F. Gallucci, F. Chiaravalloti, S. Tosti, E. Drioli, A. Basile, The effect of mixture gas on hydrogen permeation through a palladium membrane: Experimental study and theoretical approach, Int. J. Hydrogen Energy 32 (2007) 1837-1845.

[24] A. Li, W. Liang, R. Hughes, The effect of carbon monoxide and steam on the hydrogen permeability of a Pd/stainless steel membrane, J. Membr. Sci. 165 (2000) 135-141.

[25] H. Gao, Y.S. Lin, Y. Li, B. Zhang, Chemical stability and its improvement of palladium-based metallic membranes, Ind. Eng. Chem. Res. 43 (2004) 6920-6930.

[26] M.A. Henderson, The interaction of water with solid surfaces: fundamental aspects revisited. Surf. Sci. Rep. 46 (2002) 1-308.

[27] A. Li, W. Liang, R. Hughes, The effect of carbon monoxide and steam on the hydrogen permeability of a Pd/stainless steel membrane, J. Membr. Sci. 165 (2000) 135-141.

[28] S.H. Jung, K. Kusakabe, S. Morooka, S.-D. Kim, Effects of co-existing hydrocarbons on hydrogen permeation through a palladium membrane, J. Membr. Sci. 170 (2000) 53-60.

[29] P.D. Vaidya, A.E. Rodrigues, Kinetics of steam reforming of ethanol over a Ru/Al_2O_3 Catalyst, Ind. Eng. Chem. Res. 45 (2006) 6614-6618.

Chapter 5 . Conclusions

Thin and defect-free palladium and palladium-copper alloy membranes were successfully prepared on a hollow fiber α-alumina substrate by a novel electric-field assisted activation followed by electroless plating of Pd or consecutive electroless plating of Pd and Cu. The Pd membranes prepared at the electric potential range of 4.0-6.0 V in the activation were found to have high and stable hydrogen over nitrogen selectivity of 3000- 9000 with high hydrogen permeance of 4.0-5.0 × 10^{-6} mol $m^{-2}s^{-1}Pa^{-1}$ at 733K. The Pd-Cu membrane showed a hydrogen selectivity of 970 with a hydrogen permeance of 2.5 × 10^{-6} mol $m^{-2}s^{-1}Pa^{-1}$.

Compared to the Pd membrane prepared by a conventional method, the high hydrogen permeance and robust thermal stability of the Pd membranes in this work can be attributed to the well distributed Pd nanoparticles in a limited region on the surface of the support. Another benefit given by this technique is general application unlike competing techniques, which are limited in support geometry and material characteristics, because it can directly produce Pd seeds formed with a uniform distribution on porous substrates of any shape without intermediate layer.

Studies of the ethanol steam reforming (EtOH SR) reaction were carried out in a packed bed reactor (PBR) employing a Co-Na/ZnO catalyst in temperature range of 623-693K and space velocity of 6000-12000 h^{-1} at atmospheric pressure. The ethanol conversion was proportional to temperature and inversely proportional to space velocity. Negligible temperature dependence was observed for the selectivity of main products of H_2 and CO_2. However, the selectivity of CO and CH_4 steadily increased and the selectivity of CH_3CHO

continuously decreased as temperature increased, which can be described by the favorable reaction of acetaldehyde decomposition.

Combining the Pd and Pd-Cu membranes in a fixed bed reactor with the Co-Na/ZnO catalyst for EtOH SR reaction showed enhancement ethanol conversion and hydrogen yield compared with a reaction study in a PBR because of the equilibria shift to the products by continuous removal of hydrogen in membrane reactors (MRs). Average ethanol conversion and hydrogen yield enhancement were found to be around 11% in a MR equipped with the Pd membrane and around 20 % in a MR equipped with the Pd-Cu membrane. Relative high enhancements in the Pd-Cu MR despite lower hydrogen permeance compared to that of the Pd MR can be explained by a significant contamination of Pd membrane by CO adsorption and carbon compound deposition on the surface during the reaction, which reduces the ability of hydrogen transportation through the membrane.

A one dimensional reactor model of EtOH SR both in the MR and the PBR was developed using a power law model to predict the conversion and hydrogen yield at various conditions and the obtained values from the model study were compared with the experimental data. The predicted values were found to match the experimental values with minor deviations. The kinetic study showed that the enhancements of ethanol conversion and hydrogen yield increased with increasing space velocity, which can be attributed to the different ethanol pressures in the MRs and the PBR.

Chapter 6 . Recommendations for Future Work

In the present work, Pd and Pd-Cu membranes were prepared by a new activation technique followed by electroless plating of Pd or sequential electroless plating of Pd and Cu. The membranes were employed to enhance the ethanol steam reforming reaction by the shift of equilibria through the simultaneous formation and separation of hydrogen. In the course of reaction, a significant drop in H_2 permeance of the Pd layer was observed due to catalytic poisoning by CO adsorption or carbon deposition on the surface. This decrease in H_2 permeance was suppressed in the Pd-Cu membrane because Cu reduces the surface reactivity of Pd. This Pd-Cu alloy is reported to be among the best material for hydrogen production because of the resistance to the corrosion of the layers by CO or hydrocarbon compounds without H_2 permeance loss [1]. This membrane should thus be effective in use with reactions such as ethanol steam reforming, methanol steam reforming, and methane steam reforming.

An even greater problem than CO or carbonatious contamination is poisoning of Pd or Pd alloy materials by sulfur compounds. This is a critical problem in H_2 production by the gasification of fossil fuels, because they contain significant amounts of sulfur [1,2]. The current tolerance of Pd alloy materials for sulfur is around 20 ppmv, while the tolerance target set by the U.S. Department of Energy is more than 100 ppmv by 2015 (Table 6.1) [3].

Table 6.1. Hydrogen separation membrane technical targets of the U.S. Department of Energy.

Performance Criteria	Units	Current Status (Pd-alloy)	2010 Target	2015 Target
Flux	mol $m^{-2}s^{-1}$	< 0.83	< 0.76	1.13
Temperature	^{o}C	300 - 400	300 - 600	250 - 500
S Tolerance	ppmv	~20 ppmv	20	> 100
Cost	$\$/m^2$	< 2200	1100	< 1100
WGS Activity	-	N/A	Yes	Yes
ΔP Operating Capability	kPa (bar)	6900 (69) (tested)	Up to 2800 (28)	Up to 5500 (55) to 6900 (69)
Carbon Monoxide Tolerance	-	Yes	Yes	Yes
Hydrogen Purity	%	>99.999	99.5	99.99
Stability/Durability	years	0.9 (tested)	3	5

An extensive research has been conducted to improve the sulfur resistance of Pd-based membranes by alloying with Cu, Fe, Au, and Ag [4,5,6,7]. Considerable work has been done with Pd-Cu and Pd-Au alloys because unlike Pd, they do not suffer H_2 embrittlement problems at low temperatures. In addition they have similar or higher H_2 permeability compared to pure Pd [4,8]. Nevertheless, it has been reported that small amount of sulfur compounds in the feeds can lead to deactivation of these materials during operation [9].

To develop effective membranes which meet the specific technical targets above, it is recommended to fundamentally understand surface and transport phenomena associated with hydrogen separation from coal-derived syngas. Based on this understanding, new composite materials could be designed by alloying Pd with elements which are known to be sulfur resistant. It is then recommended that promising

compositions from the design are synthesized and fabricated into membranes for the evaluation of their performance.

References

[1] B.D. Morreale, M.V. Ciocco, B.H. Howard, R.P. Killmeyer, A.V. Cugini, R.M. Enick, Effect of hydrogen-sulfide on the hydrogen permeance of palladium-copper alloys at elevated temperatures. J. Membr.Sci. 241 (2004) 219-224.

[2] J.B. Miller, B.D. Morreale, A.J. Gellman, The effect of adsorbed sulfur on surface segregation in a polycrystalline $Pd_{70}Cu_{30}$ alloy, Surf. Sci. 602 (2008) 1819-1825.

[3] Hydrogen from Coal Program, RD&D Plan, External Draft, U.S. Department of Energy, Office of Fossil Energy, NETL, September 2010.

[4] D.L. McKinley, Method for hydrogen separation and purification, US Patent 3,439,474, Apr 22, 1969, Assigned to Union Carbide Corp.

[5] K. J. Bryden, J. Y. Ying, Nanostructured palladium-iron membranes for hydrogen separation and membrane hydrogenation reactions, J. Membr. Sci. 203 (2002) 29-42.

[6] N. Pomerantz, Y.H. Ma, Effect of H_2S on the Performance and long-term stability of Pd/Cu membranes, Ind. Eng. Chem. Res. 48 (2009) 4030-4039.

[7] L. Shi, A. Goldbach, G. Zeng, H. Xu, Preparation and performance of thin-layer PdAu/ceramic composite membranes, Int. J. Hydrogen Energy 35 (2010) 4201-4208.

[8] A. Kulprathipanja, G.O. Alptekin, J. L. Falconer, J. D. Way, Pd and Pd-Cu membranes: inhibition of H_2 permeation by H_2S. J. Membr. Sci. 254 (2005) 49-62.

[9] J.F. Gabitto, C. Tsouris, Sulfur poisoning of metal membranes for hydrogen separation, Int. Rev. Chem. Eng. 1 (2009) 394-411.

Appendices

A. Hydrogen permeation equation

The flux of hydrogen (mol/m^2 s) by diffusion through dense metals is described by Ficks' first law (eq A.1)

$$J_{H_2} = -D_{H_2} \nabla C_{H_2} \quad \text{(A.1)}$$

where, D_{H_2} is the diffusion coefficient ($m^2 s^{-1}$) and ∇C is the gradient in concentration (mol m^{-4}).

For one dimensional diffusion,

$$J_{H_2} = -D_{H_2} \frac{\Delta C_{H_2}}{L} \quad \text{(A.2)}$$

where, L is the thickness of the metal layer

When surface reaction or mass transport is rate controlling step, Henry's law (eq. A.3) can be used.

$$S_H = \frac{C_{H_2}}{p_{H_2}} \quad \text{(A.3)}$$

where, S_H is Henry's law constant, which depends on the solute, the solvent and the temperature. When the concentration in Henry's law is substituted into Ficks' first law the result is:

$$J_{H_2} = -D_{H_2} S_H \frac{\Delta p_{H_2}}{L} = P \frac{p_{H_2,h} - p_{H_2,l}}{L} \quad \text{(A.4)}$$

where, P is the permeance and $p_{H_2,h}$ and $p_{H_2,l}$ are the partial pressures of hydrogen on the high pressure (feed) side and the low pressure (permeate) side, respectively. When diffusion through the bulk metal is rate determining step, Sieverts' law (eq. A.5) can be applied. In this case, H_2 molecule is dissociated to two hydrogen atoms prior to the diffusion through the membrane layer.

$$S_H = \frac{C_{H_2}}{p_{H_2}^{1/2}} \tag{A.5}$$

where, S_H is the Sieverts' law constant or solubility.

The concentration in Sieverts' law is substituted into Ficks' first law;

$$J_{H_2} = -D_{H_2} S_H \frac{\Delta p_{H_2}^{1/2}}{L} = P \frac{p_{H_2,h}^{1/2} - p_{H_2,l}^{1/2}}{L} \tag{A.6}$$

For the case of Knudsen and Hagen-Pouiselle flow the flux is proportional to $\Delta p_{H_2} = p_{H_{2,h}} - p_{H_{2,l}}$. The Knudsen flux is given by,

$$J_{H_2}^K = \frac{\varepsilon d_p}{\tau L} \left(\frac{8}{9\pi MRT}\right)^{1/2} \Delta p_{H_2} \tag{A.7}$$

where L is the thickness of the membrane, ε is the porosity of the membrane, d_p is the pore diameter, τ is the tortuosity, R is the gas constant and M is molecular weight of the diffusing gas.

The viscous flow Hagen-Pouiselle equation is

$$J_{H_2}^{HP} = \frac{R^2}{8\eta L P_0} P_{ave} \Delta p_{H_2} \tag{A.8}$$

When these mechanisms occur in conjunction with bulk permeance through palladium the overall hydrogen flux becomes,

$$J_{H_2}^{Total} = \frac{1}{\frac{1}{J_{H_2}} + \frac{1}{J_{H_2}^K} + \frac{1}{J_{H_2}^{HP}}} \tag{A.9}$$

Then the overall order in hydrogen can be between 0.5 and 1.

B. Thermodynamic analysis

Among the several reactions occurring during the EtOH SR (eq. 4.1-4.7), the overall reaction is steam reforming (eq. 4.1). From the relationship between the equilibrium constant (*K*) and Gibbs free energy change (Δ*G*) for the overall reaction,

$$RTlnK = -\Delta G,\ K = \frac{a_{H_2}^6 a_{CO_2}^2}{a_{C_2H_5OH}^1 a_{H_2O}^3} \quad \text{(A.10)}$$

where a_i is the activity species i

$$a_i = \frac{f_i}{f_i^v} = \gamma_i p_i \quad \text{(A.11)}$$

where $f_i =$ fugacity of species i, $f_i^v =$ fugacity of standard state, and $\gamma_i$is the activity coefficient

$$K = \frac{\gamma_{H_2}^6 \gamma_{CO_2}^2}{\gamma_{C_2H_5OH}^1 \gamma_{H_2O}^3} \cdot \frac{p_{H_2}^6 p_{CO_2}^2}{p_{C_2H_5OH}^1 p_{H_2O}^3} = K_\gamma K_P \quad \text{(A.12)}$$

where p_i is partial pressure of species i

At high temperature and low pressure, $K \approx K_P$

$$K = \frac{p_{H_2}^6 p_{CO_2}^2}{p_{C_2H_5OH}^1 p_{H_2O}^3} = \frac{y_{H_2}^6 y_{CO_2}^2}{y_{C_2H_5OH}^1 y_{H_2O}^3} \cdot p^4 \quad \text{(A.13)}$$

where y_i is mole fraction of species i and p is total pressure

The equilibrium composition can be described with the equilibrium conversion *X* at GHSV of 6000 with the same feed composition used in the reaction (Table A.1).

Table A.1. Chemical equilibrium of overall reaction of the EtOH SR

	species				
	C_2H_5OH	H_2O	H_2	CO_2	Ar (inert)
moles in the feed	a	$13a$	0	0	$18a$
moles reacted or produced	$-aX$	$-3aX$	$6aX$	$2aX$	0
moles at equilibrium	$a(1-X)$	$a(1-X)$	$6aX$	$2aX$	$18a$
mol fraction at equilibrium	$\frac{a(1-X)}{32a+4aX}$	$\frac{a(13-3X)}{32a+4aX}$	$\frac{6aX}{32a+4aX}$	$\frac{2aX}{32a+4aX}$	$\frac{18a}{32a+4aX}$

$$K = \frac{(6X)^6(2X)^2}{(1-X)(13-3X)^3} \cdot \frac{1}{(32+4X)^4} \quad \text{(A.14)}$$

The relationship between ΔG and temperature can be obtained by regression of tabulated data in the temperature range of 473 ~ 773 K (Fig. A.1a).

$$\Delta G\ [kJ/mol] = -0.4093T + 193.02,\ K = exp\left(\frac{0.4093T-193.02}{8.314\times10^{-3}\cdot T}\right) \quad \text{(A.1)}$$

The equilibrium conversion X at a given temperature can be calculated by solving the below equation

$$exp\left(\frac{0.4093T-193.02}{8.314\times10^{-3}\cdot T}\right) = \frac{(6X)^6(2X)^2}{(1-X)(13-3X)^3} \cdot \frac{1}{(32+4X)^4} \quad \text{(A.2)}$$

and is plotted (Fig. A.1b).

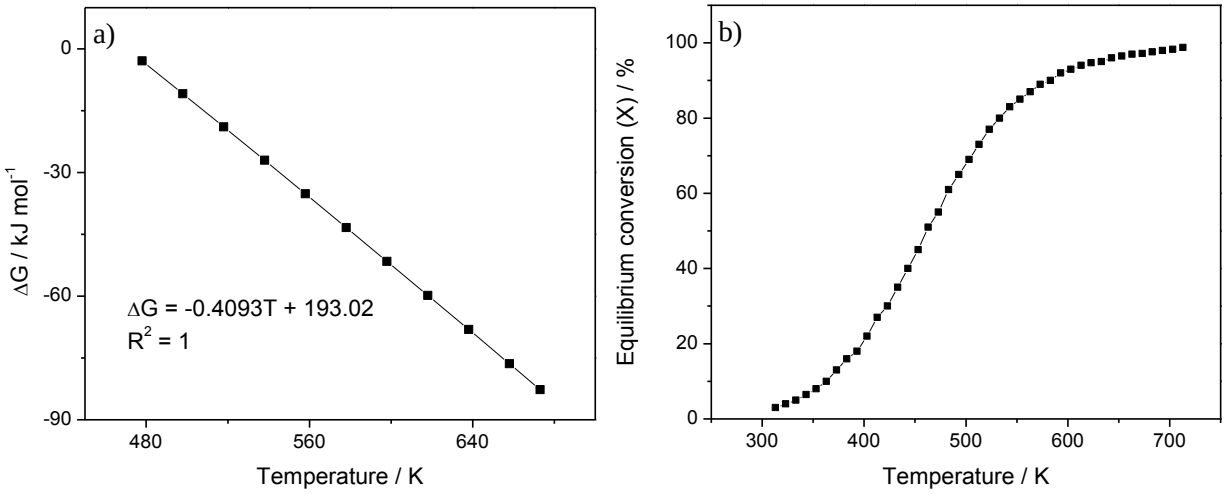

Figure A. 1. Gibbs free energy change as a function of temperature (a) and equilibrium conversion as a function of temperature (b).

Nomenclature

J	Hydrogen flux [mol $m^{-2}s^{-1}$]
P	Hydrogen permeance [mol $m^{-2}s^{-1}Pa^{-1}$] or
	Hydrogen permeability [mol $m^{-1}s^{-1}Pa^{-1}$]
L	Thickness of layer [m]
p_h	Hydrogen partial pressure on the feed (catalyst bed) side [Pa]
p_l	Hydrogen partial pressure on the permeate (sweep) side [Pa]
p_i	Partial pressure of species *i* [Pa]
n	Pressure exponent [-]
E_a	Activation energy [J mol^{-1}]
Δp	Pressure difference between feed and permeate side [Pa]
$\alpha_{H2/N2}$	Hydrogen over nitrogen selectivity [-]
P_0	Pre-exponential factor [mol $m^{-2}Pa^{-1}s^{-1}$]
ΔH	Enthalpy change of formation [J mol^{-1}]
ΔX	Ethanol conversion enhancement [%]
ΔH_2	Hydrogen yield enhancement [%]
r_i	Reaction rate of species *i* [mol $gcat^{-1}s^{-1}$]
F_i	Molar flow rate of species *i* [mol s^{-1}]
D	Dispersion of Co metal [%]
d	Particle size of Co metal [nm]
W	Weight of catalyst [g]

R	Gas constant [J $mol^{-1}K^{-1}$]
A	Membrane surface area [m^2]
D_{H_2}	Diffusion coefficient [m^2 s^{-1}]
ΔC	Gradient in concentration [mol m^{-4}]
S_H	Sieverts' law constant or Henry's law constant [-]
ε	Porosity of membrane [-]
d_p	Pore diameter [m]
M	Molecular weight of diffusing gas [g mol^{-1}]
a_i	Activity of species *i* [-]
f_i	Fugacity of species *i* [Pa]
K	Equilibrium constant [-]
ΔG	Gibbs free energy change [J mol^{-1}]
T	Reactor temperature [K]